

# The Effect of Electrolyte Composition on Lithium Plating During Low Temperature Charging of Li-Ion Cells

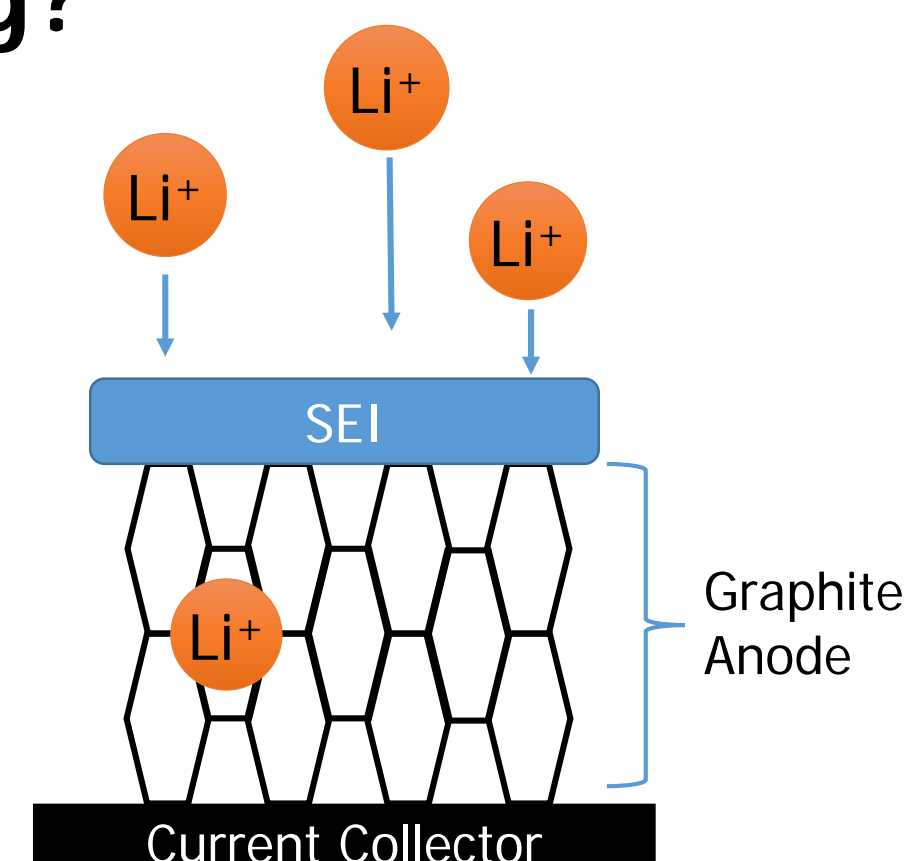
Authors: John-Paul Jones (346), Marshall C. Smart (346), Frederick C. Krause (346), Bugga V. Ratnakumar (346) and Erik Brandon (346)

## Introduction

- Low temperature operation is critical for possible missions to the surface of Europa
- Long term missions will require a primary power source (photovoltaic, radioisotope, etc.) coupled with energy storage
- Li-ion batteries can lose capacity and may potentially fail when charged at low temperature
- Lithium metal forms on the anode during charging at low temperature and high rate
  - Metallic lithium reacts with electrolyte, reducing capacity
  - Can lead to abrupt cell failure
- Electrolyte composition and film forming additives influence plating characteristics
- Can we find an electrolyte formulation that allows charging at low temperatures without plating?**

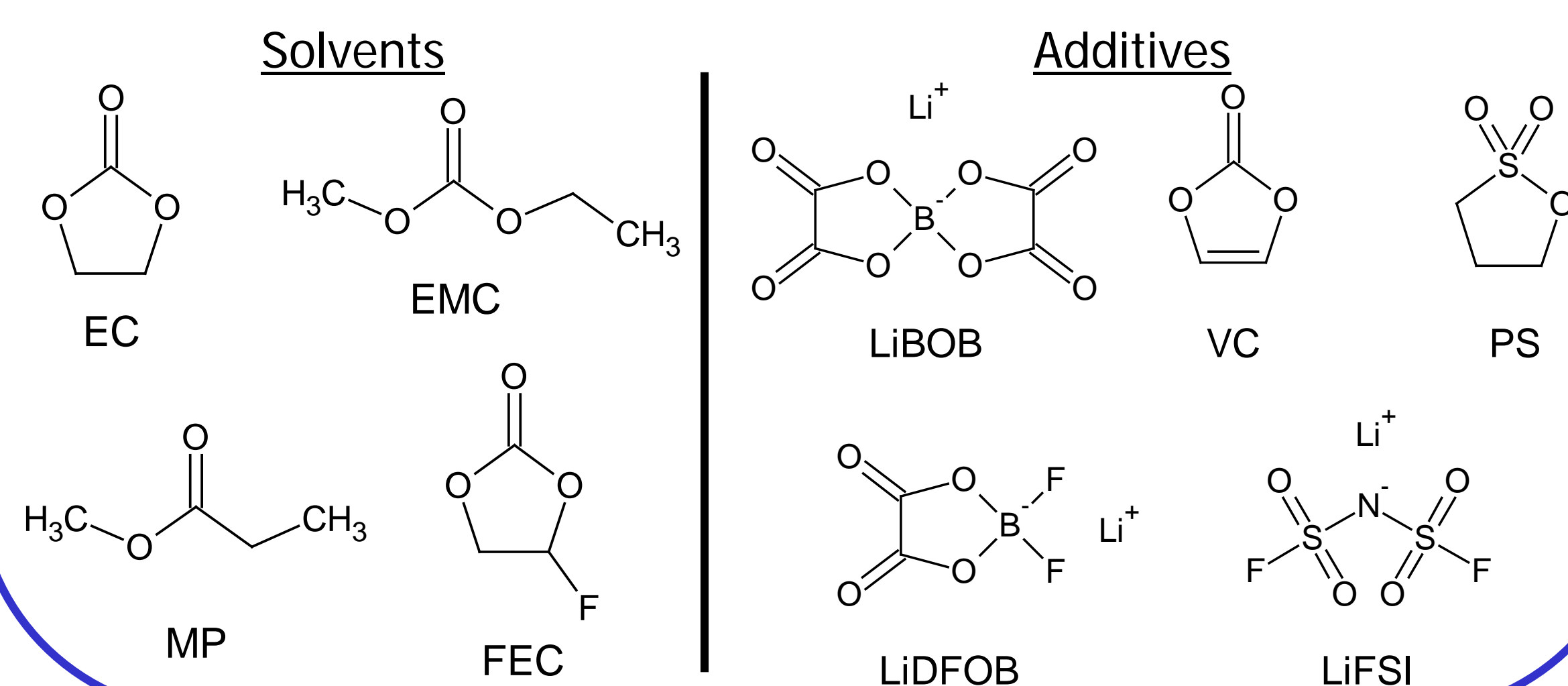
## What Causes Lithium Plating?

- During charging,  $\text{Li}^+$  ions migrate from cathode to anode
- They must pass through the protective SEI
- If the SEI becomes too resistive at low temp, lithium plating occurs
- The SEI is composed of breakdown products from the electrolyte
- Adjusting the composition of the electrolyte allows us to modify the SEI



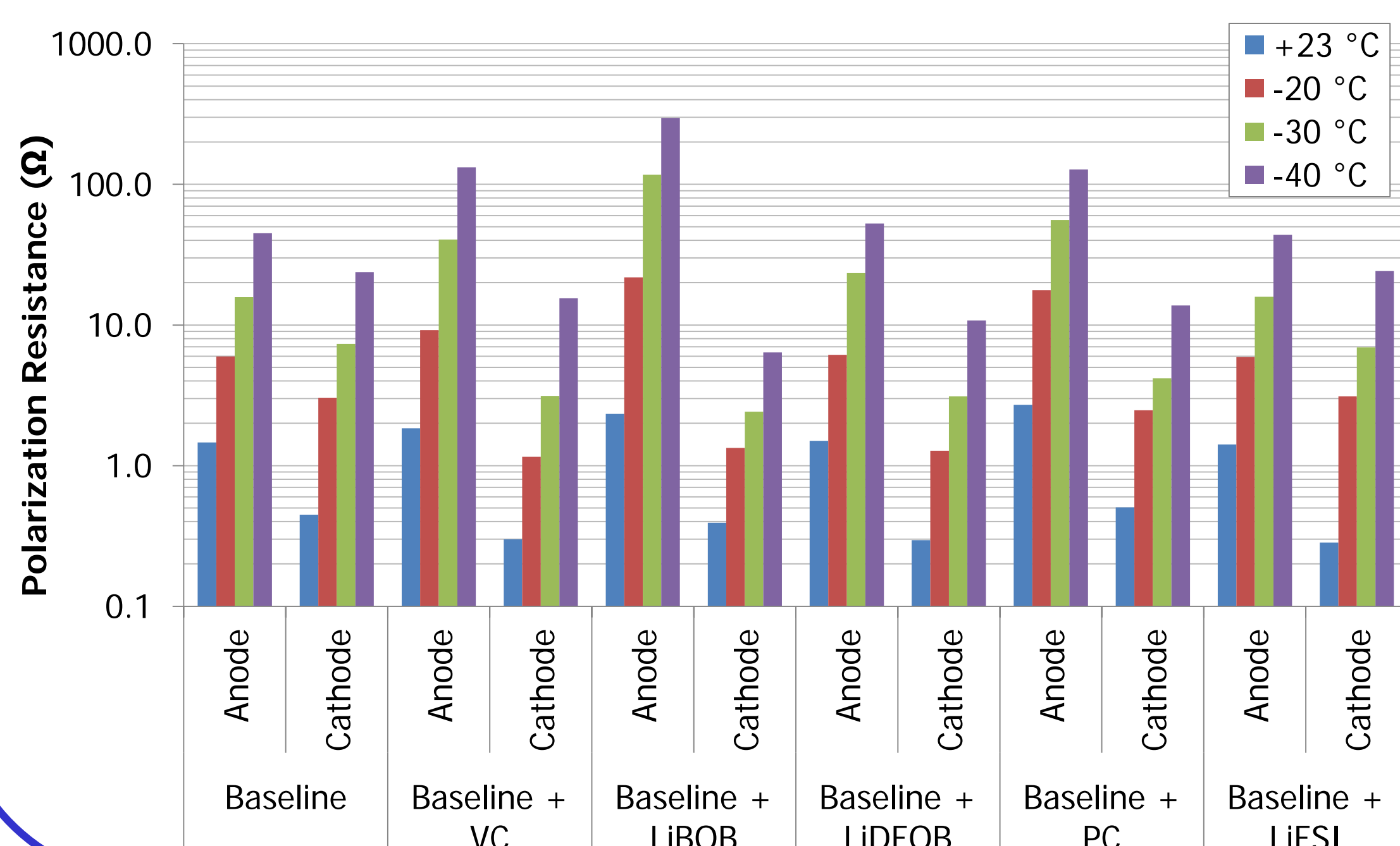
## Approach

- Use a previously developed EC:EMC:MP solvent blend optimized for low temperature operation
- Develop non-invasive techniques to detect lithium plating in-situ
  - Observe discharge following charge at low temperature
  - Cell voltage higher due to presence of metallic lithium
- Screen solvents and additives for beneficial effects during low temperature charging
- Compare lithium plating with SEI resistance measurements

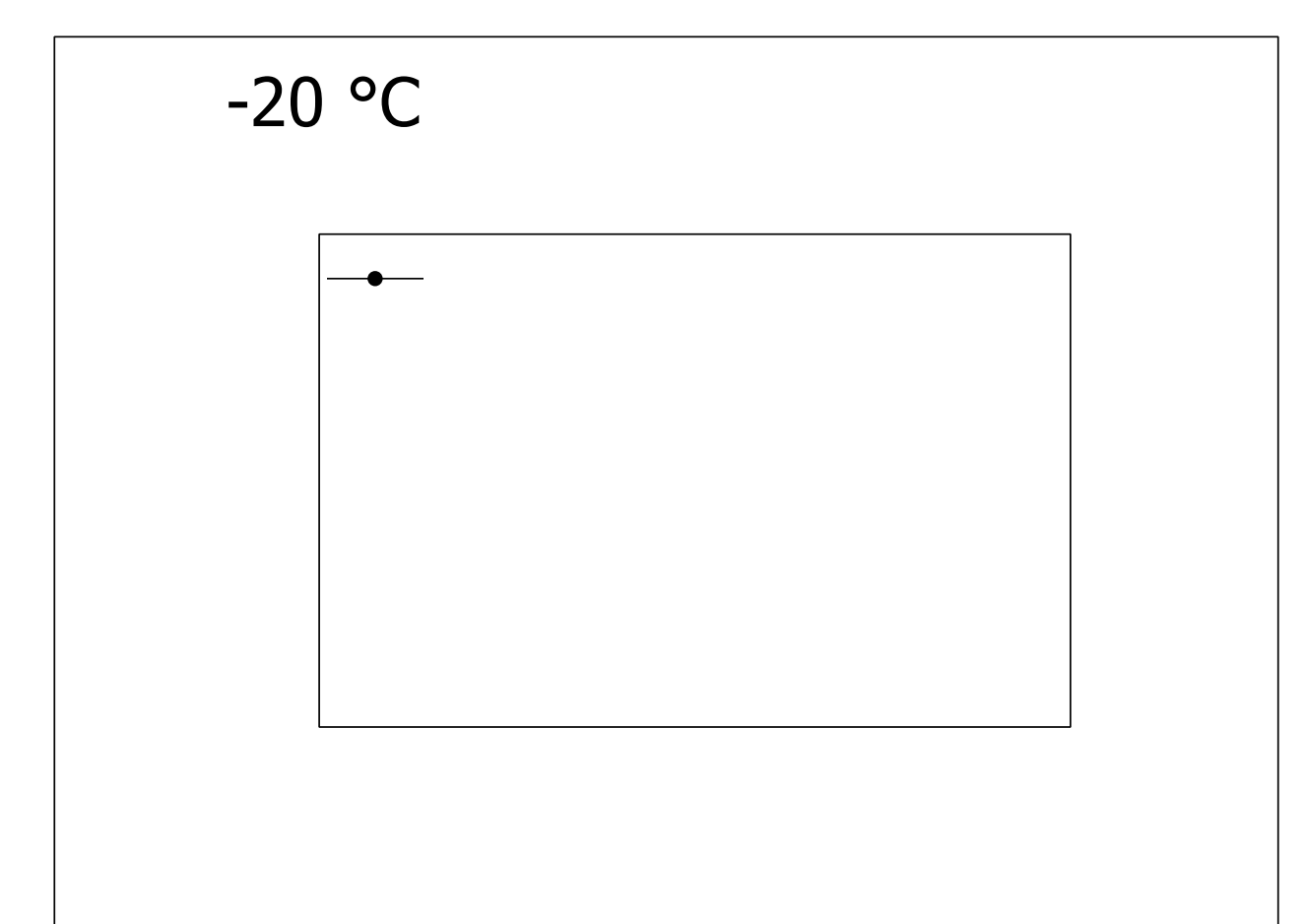
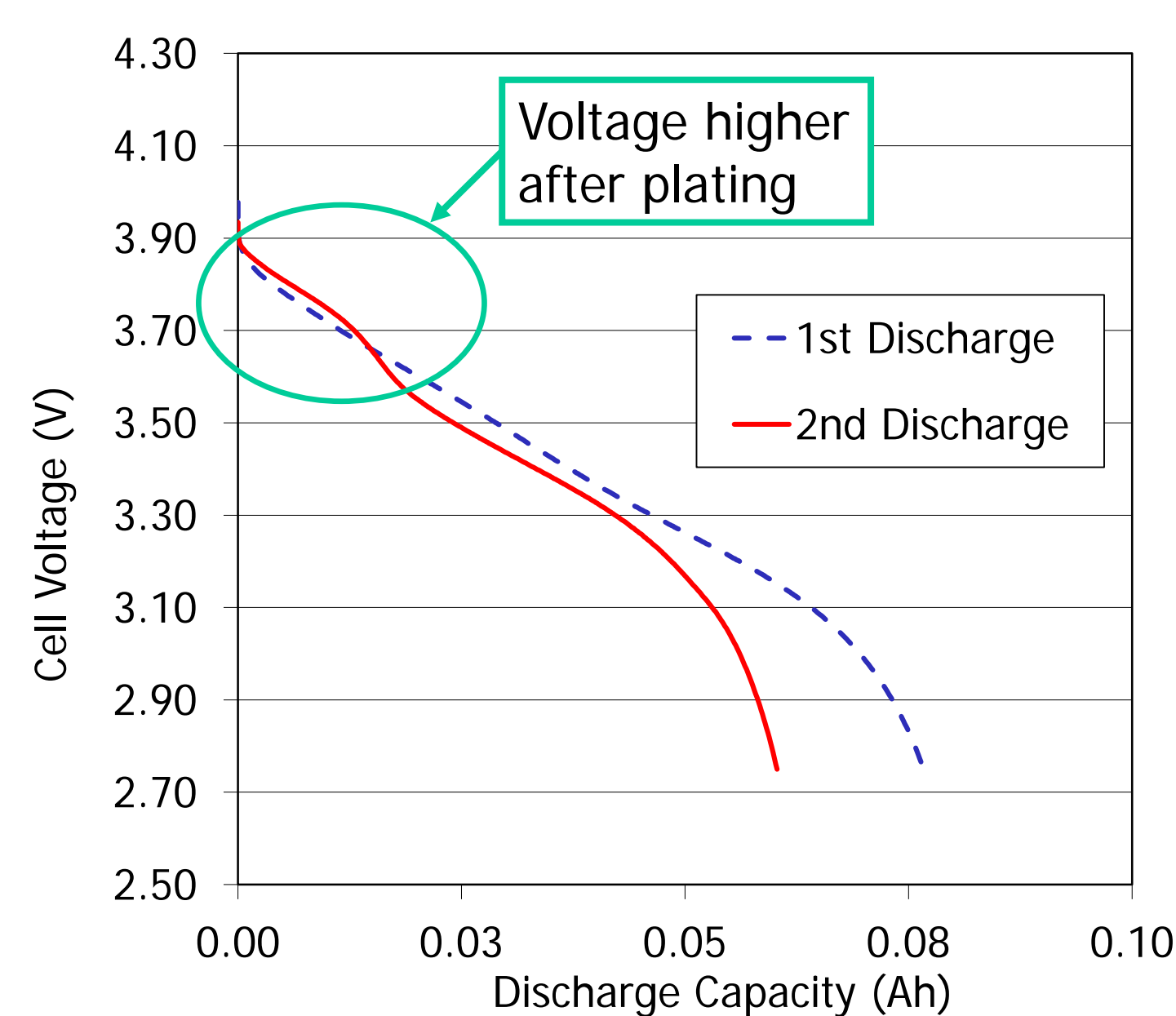


## SEI Resistance Measurements

- Apply small DC voltage to anode and cathode → resistance
- Measurement correlates to resistance of SEI



## High Voltage Plateau Reveals Lithium Plating



Take derivative

Differentiate voltage with respect to capacity to more precisely determine amount of plating

- Peak indicates presence of lithium metal
- x-axis value of peak maximum indicates amount of lithium plating
- Taller peak indicates abrupt change between lithium stripping and normal discharge

0 10 20 30 40 50 60 70  
Discharge Capacity (mAh)

## Results

- Additives have major effect on low temperature plating
- Semi-quantitative, non-destructive measurement is possible by taking derivative of discharge following low temp charge
- Most additives tested decrease resistance at cathode and increase resistance at anode
  - Increased plating at low temp
- LiFSI was the only additive tested that decreased lithium plating at low temperature**
  - Enables charging at 10 ° C lower compared to the baseline
- Balance between resistance on anode and cathode critical to avoiding plating at low temperature
- SEI resistance measurements generally correlate well with lithium plating data, however do not show improvement for LiFSI

# High Resolution Photoacoustic Spectroscopy of the Oxygen A-Band

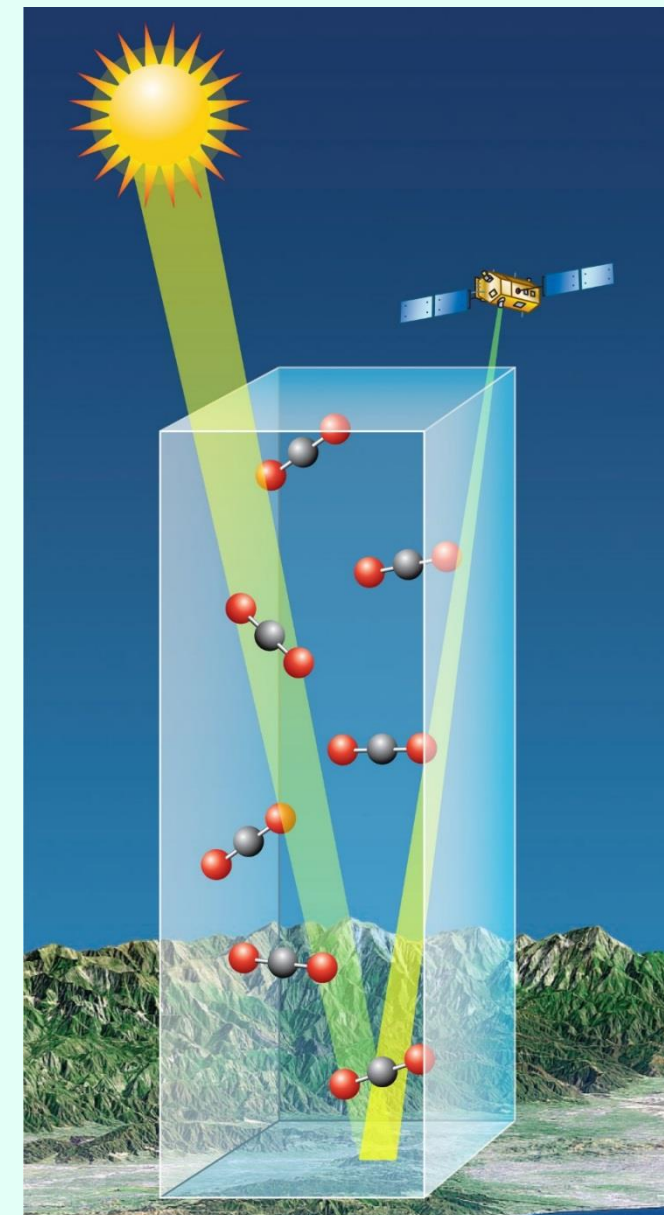
Matthew J. Cich (329H)

Elizabeth M. Lunny<sup>1</sup>, Gautam D. Stroschio<sup>1</sup>, Brian J. Drouin (329H), Mitchio Okumura<sup>1</sup>

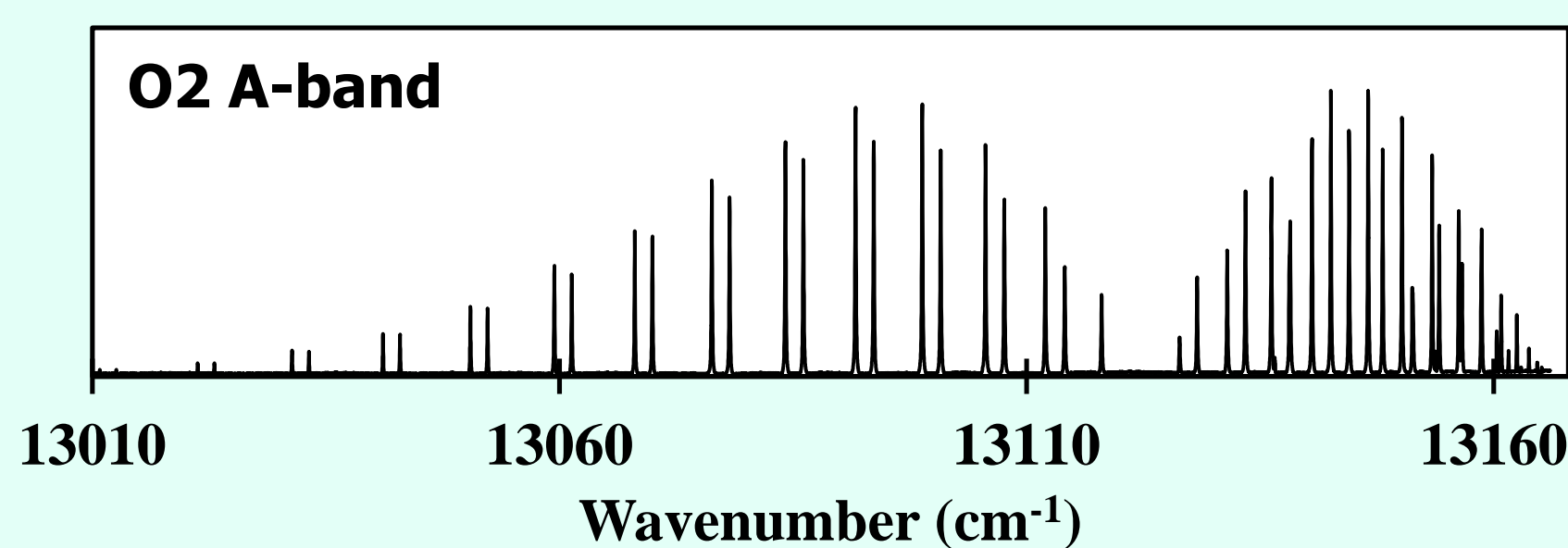
<sup>1</sup>Department of Chemistry and Chemical Engineering, California Institute of Technology, Pasadena, CA

## High resolution spectroscopy to support OCO-2

- O<sub>2</sub> is measured by OCO-2 to normalize airmass in the sunlight's path through the atmosphere
- CO<sub>2</sub> air fraction retrieval requires accurate spectroscopy (0.1%) for the O<sub>2</sub> A-band

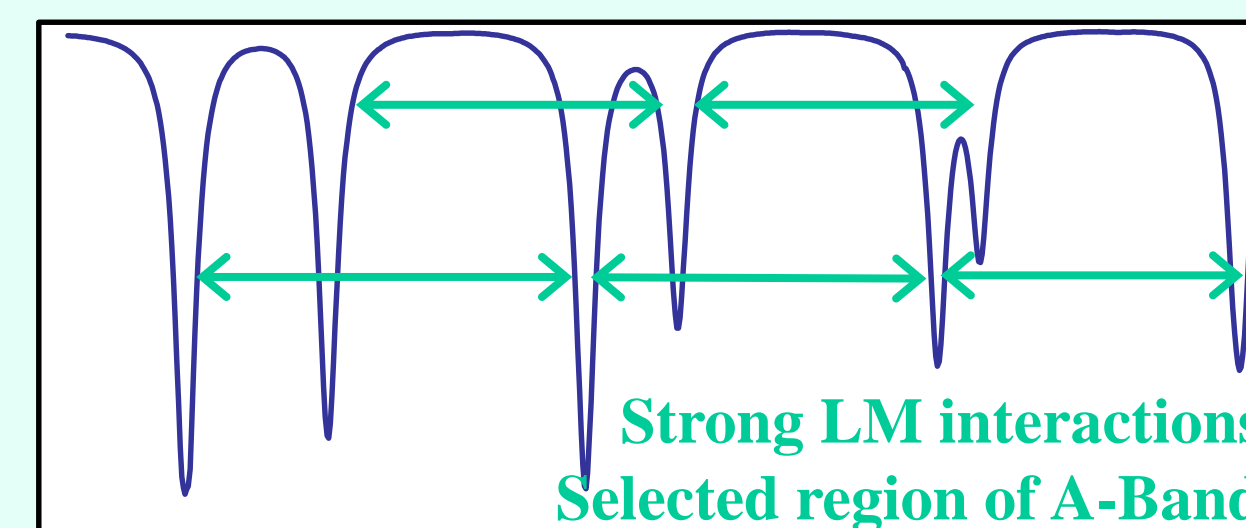


OCO-2 observes three bands: CO<sub>2</sub> (1.6 μm and 2.1 μm) and O<sub>2</sub> (0.8 μm)



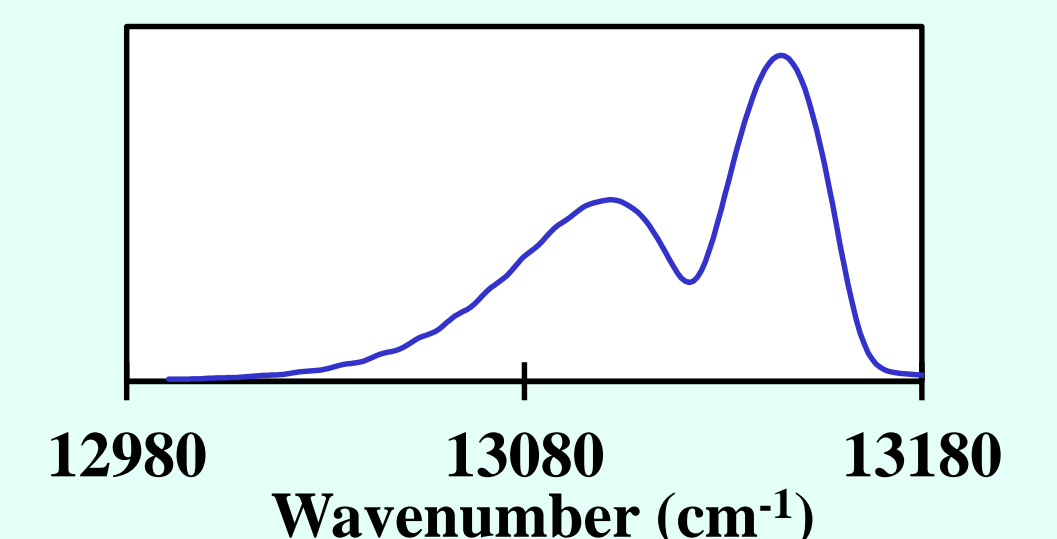
## Line mixing and collision induced absorption negatively affect satellite retrievals

### Line Mixing (LM)



When two nearby lines have interacting quantum levels, stronger lines will steal intensity from weaker lines, and both become asymmetric.

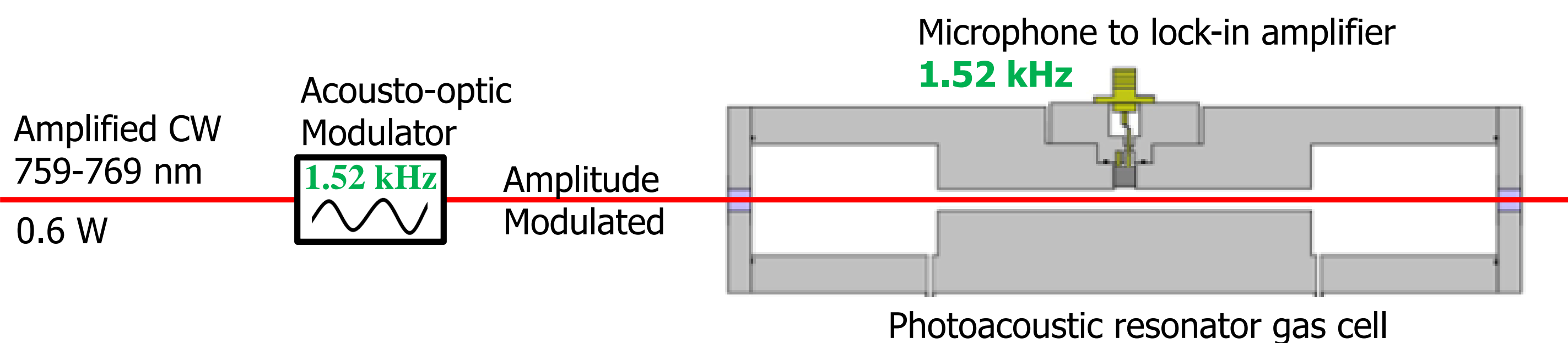
### Collision Induced Absorption (CIA)



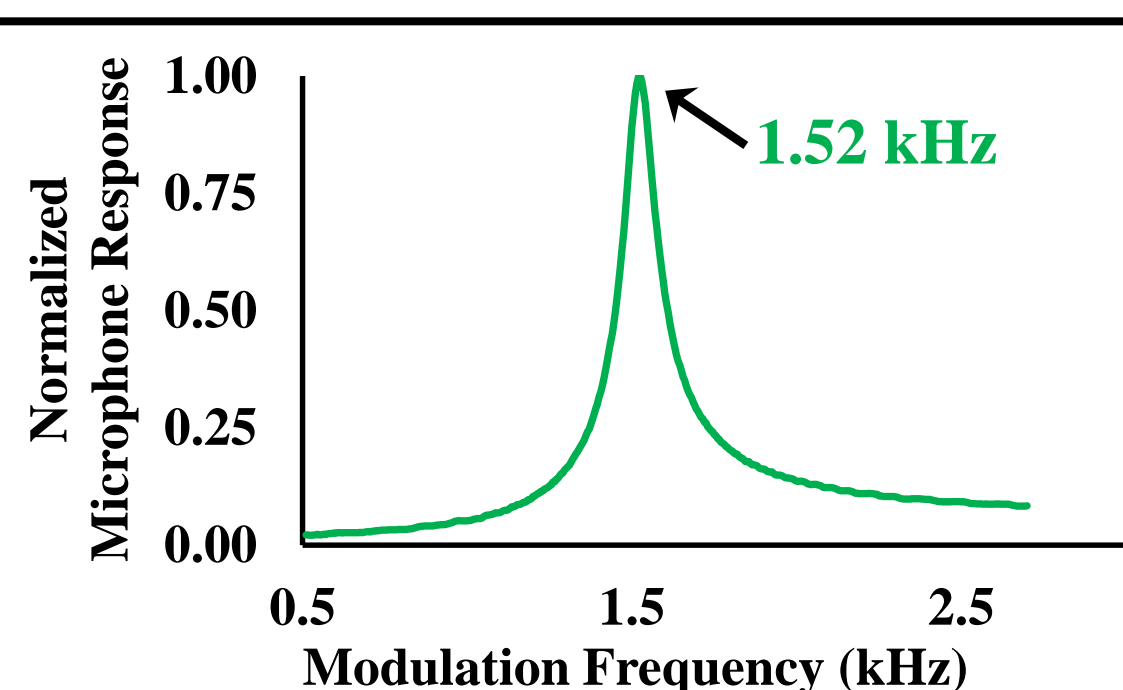
Weak 'continuum' absorption underneath the A-band caused by collision-allowed transitions.

**LM and CIA have >1% effect on satellite retrievals and must be better characterized using laboratory data.**

## Photoacoustic spectroscopy overview



**The photoacoustic effect: detecting gas absorption with a microphone**  
Modulated absorption → thermal expansion → pressure wave → sound at modulation frequency



The photoacoustic cell has a peak resonant frequency that depends on gas conditions.

For O<sub>2</sub>, a small quantity of quenching gas, e.g. CF<sub>3</sub>H, must be used to fully modulate absorption at this high frequency.

## Advantages of this spectrometer

### Zero Baseline

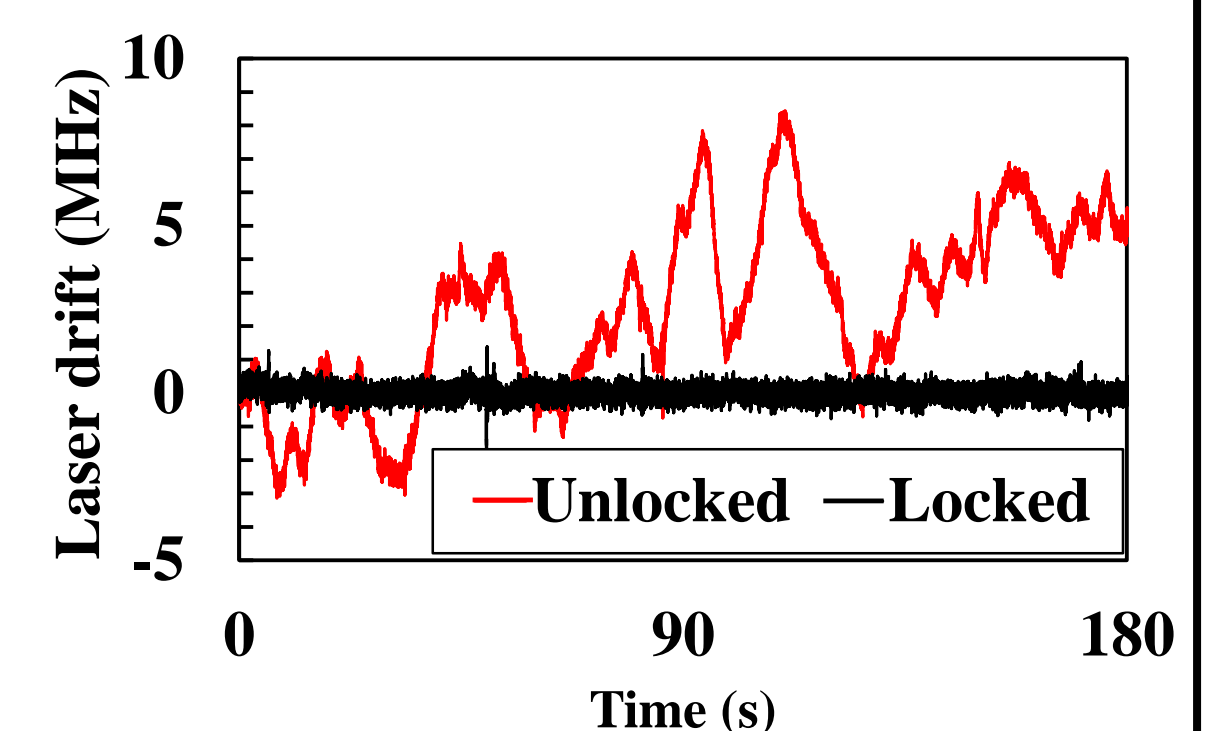
LM and CIA are subtle effects and can be lost in a spectrometer's baseline. This spectrometer has a flat baseline due to microphone response being wavelength independent.

### Large Dynamic Range

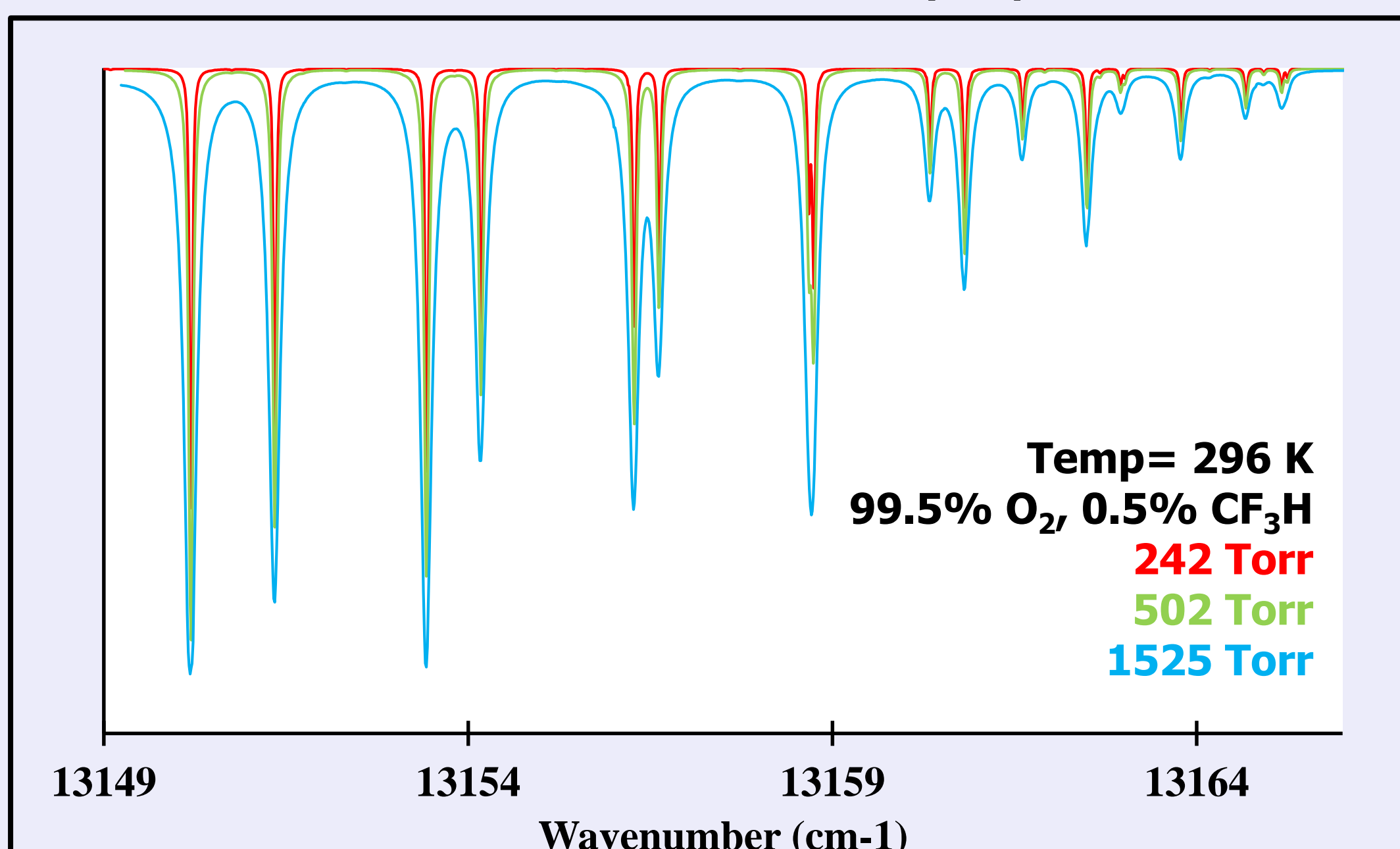
This spectrometer operates at a wide range of pressures from around 0.1 atm **up to >4 atm**, where LM and CIA are more easily characterized.

### High resolution, efficient, automated design

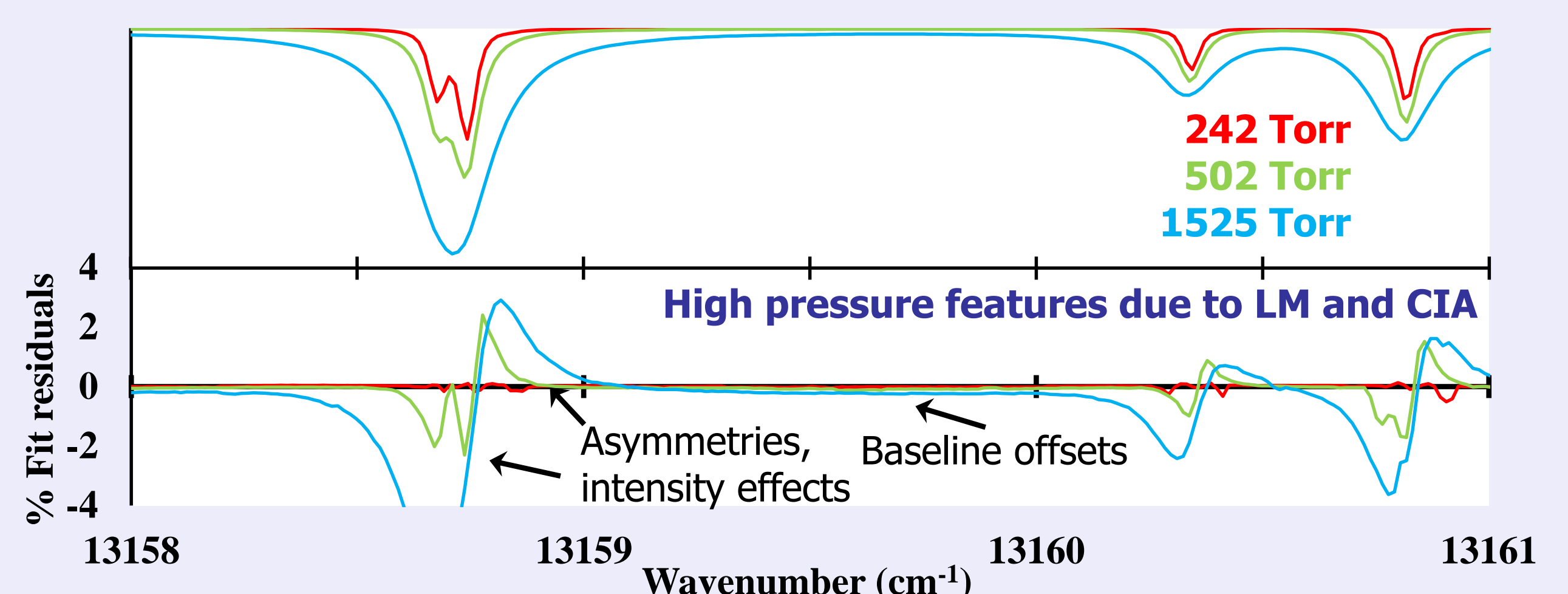
- **High resolution (FIGURE):** 2 MHz frequency uncertainty from laser lock to a high resolution wavemeter
- **Temperature control:** atmospherically relevant T's planned 220 K- 296 K
- **Fast spectrum acquisition:** Full A-Band scans in less than 1 day
- **'Autopilot':** Automatic scanning software identifies and corrects laser problems to allow continuous hands-free scanning



## Laboratory spectra contain observable line mixing and collision induced absorption



Photoacoustic spectrum of band head (r-branch). At high J values the band reverses direction creating additional overlap. This amplifies and complicates Line Mixing and CIA.



Fit 252 Torr spectrum (speed-dependent Voigt). Use these results to forward model high pressure spectra. These preliminary fit residuals demonstrate that this spectrometer's measurements are sensitive to LM and CIA.

**NEXT STEPS: Acquire full A-band spectra at pressures up to 4 atm and temperatures 220 K to 296 K to characterize LM and CIA**

# Levee monitoring using Interferometric Synthetic Aperture Radar of UAVSAR

Bekaert David (334G)

Cathleen Jones (334G), Brian Hawkins (334F), Karen An (UCLA)

## 1. Background and Hypothesis

### Monitoring of critical Levee infrastructure in California

- Sacramento delta provides water to 25 million residents, 2 million acres of farmland, and supports a unique ecosystem.
- >1,100 miles of levees protect reclaimed lands/agricultural industry
- Rapid subsidence (>5cm/yr) can affect levee integrity

### Can InSAR replace in-situ levee monitoring?

- Large swaths (up to 250 km) and high resolution (up to few m)
- **BUT:** InSAR is challenging in deltas and therefore not often applied:
  - ❑ Wet soils and vegetation results in rapid noise increase over time
  - ❑ Atmospheric noise mask small subtle displacement signals

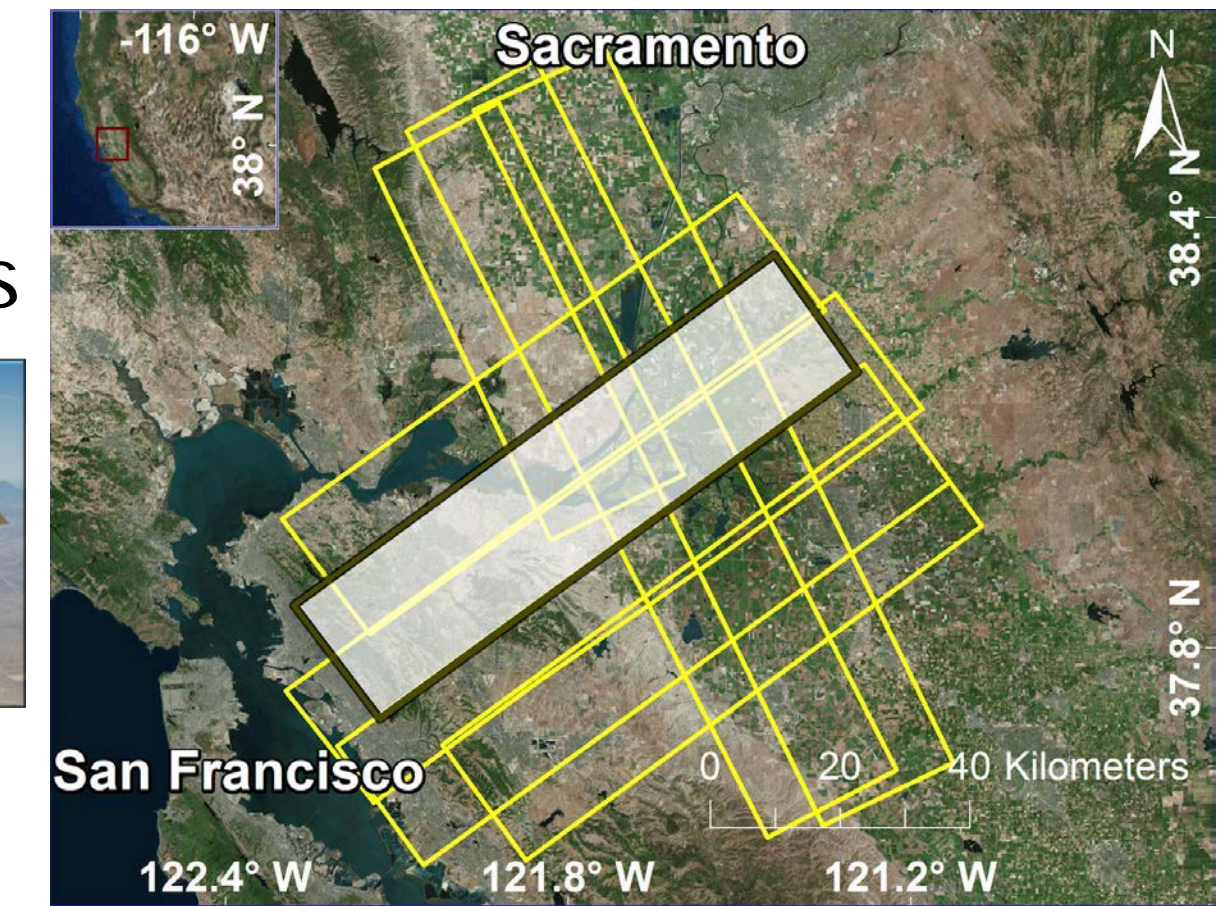
## 2. Applied approach

### Methodology:

- Include tropospheric correction from weather model data
- Apply state of the art time-series InSAR processing

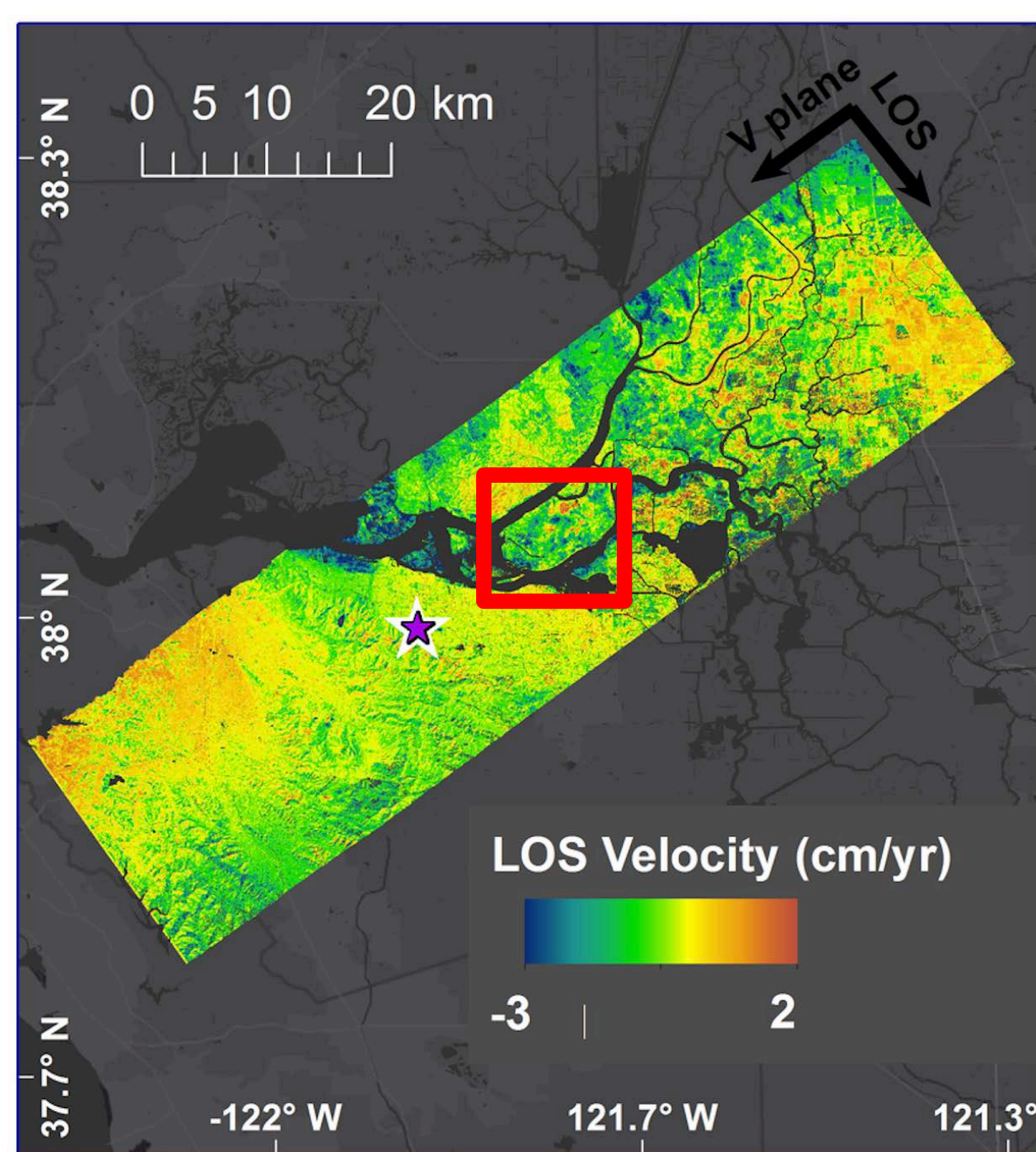
### Data:

- ❑ Space-borne SAR
- ❑ 9 UAVSAR lines (L-band)
- 56 acquisitions (400GB/line)

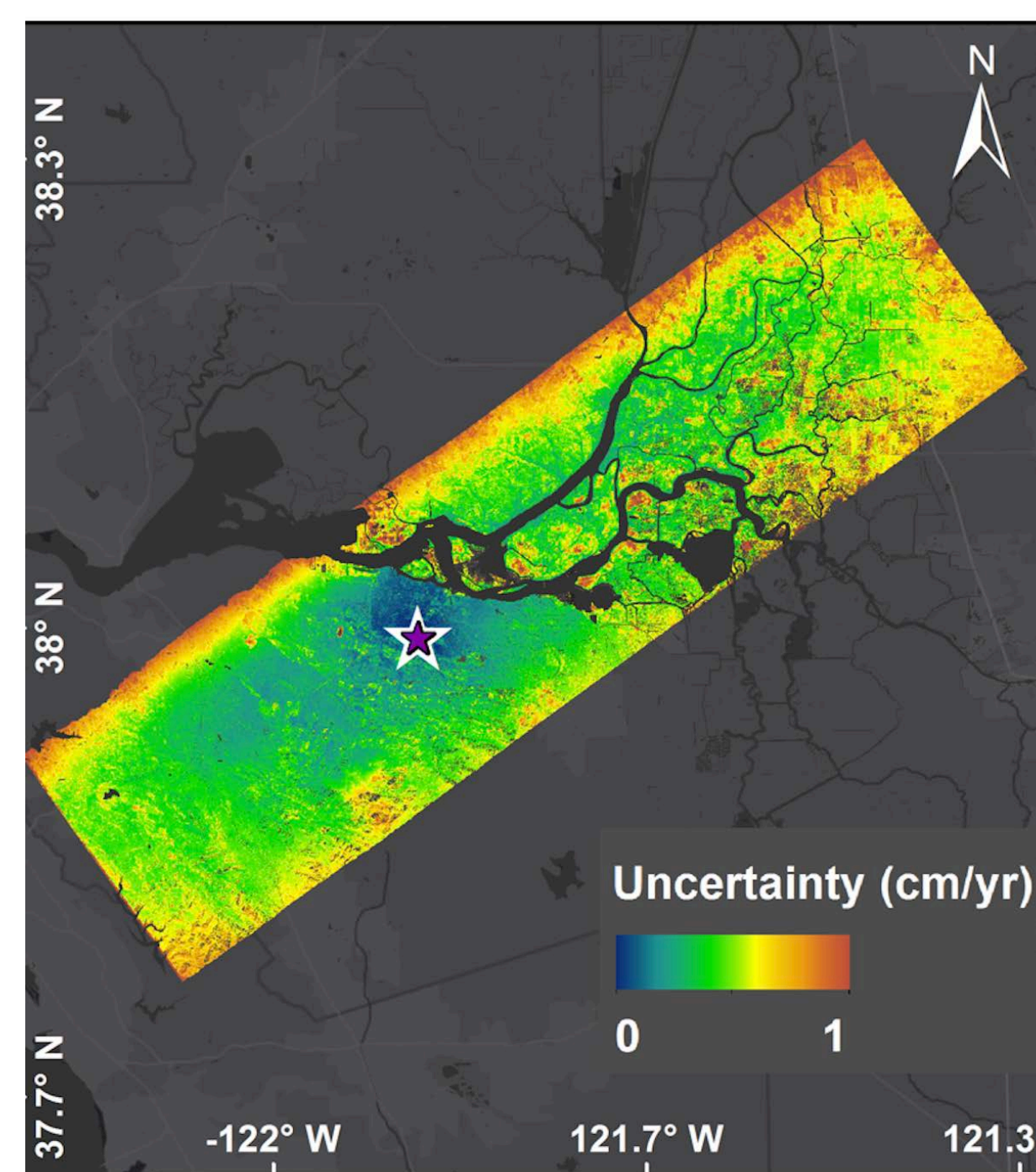


## 3. UAVSAR Time-series analysis (2009-2016)

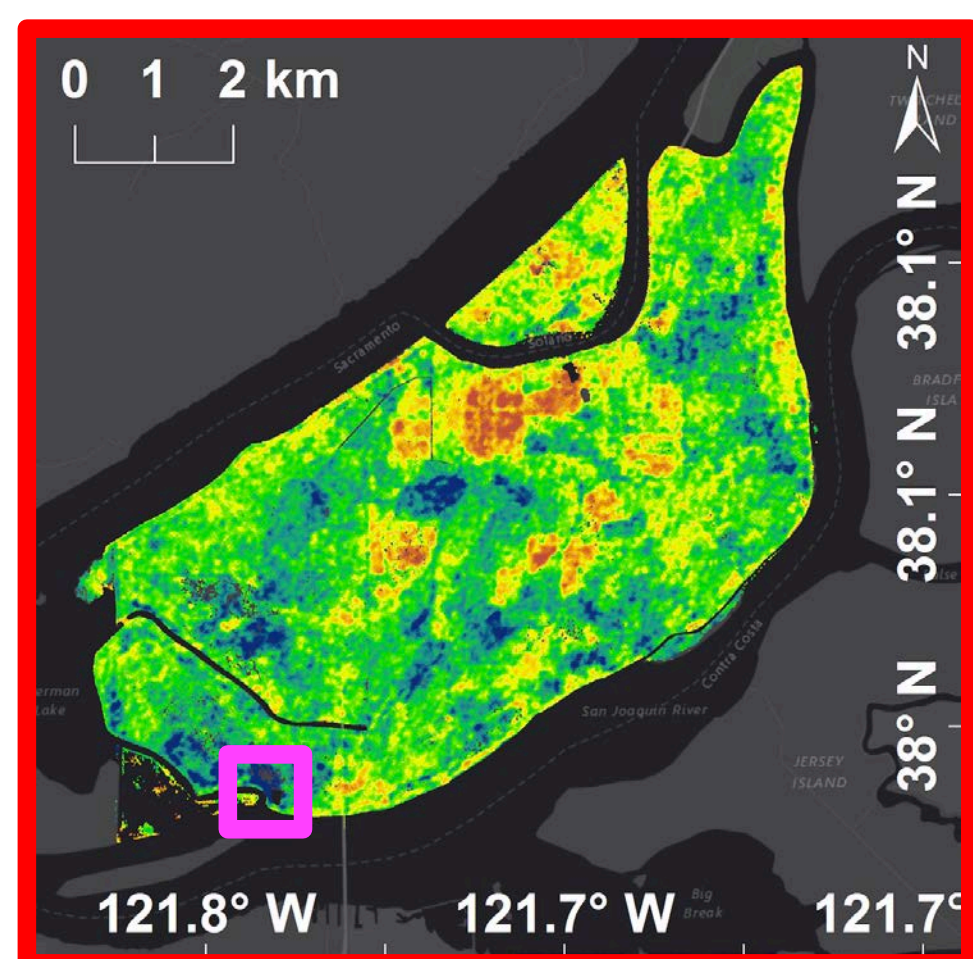
### Estimated line-of-sight velocity



### Uncertainties



### Zoom on Sherman Island



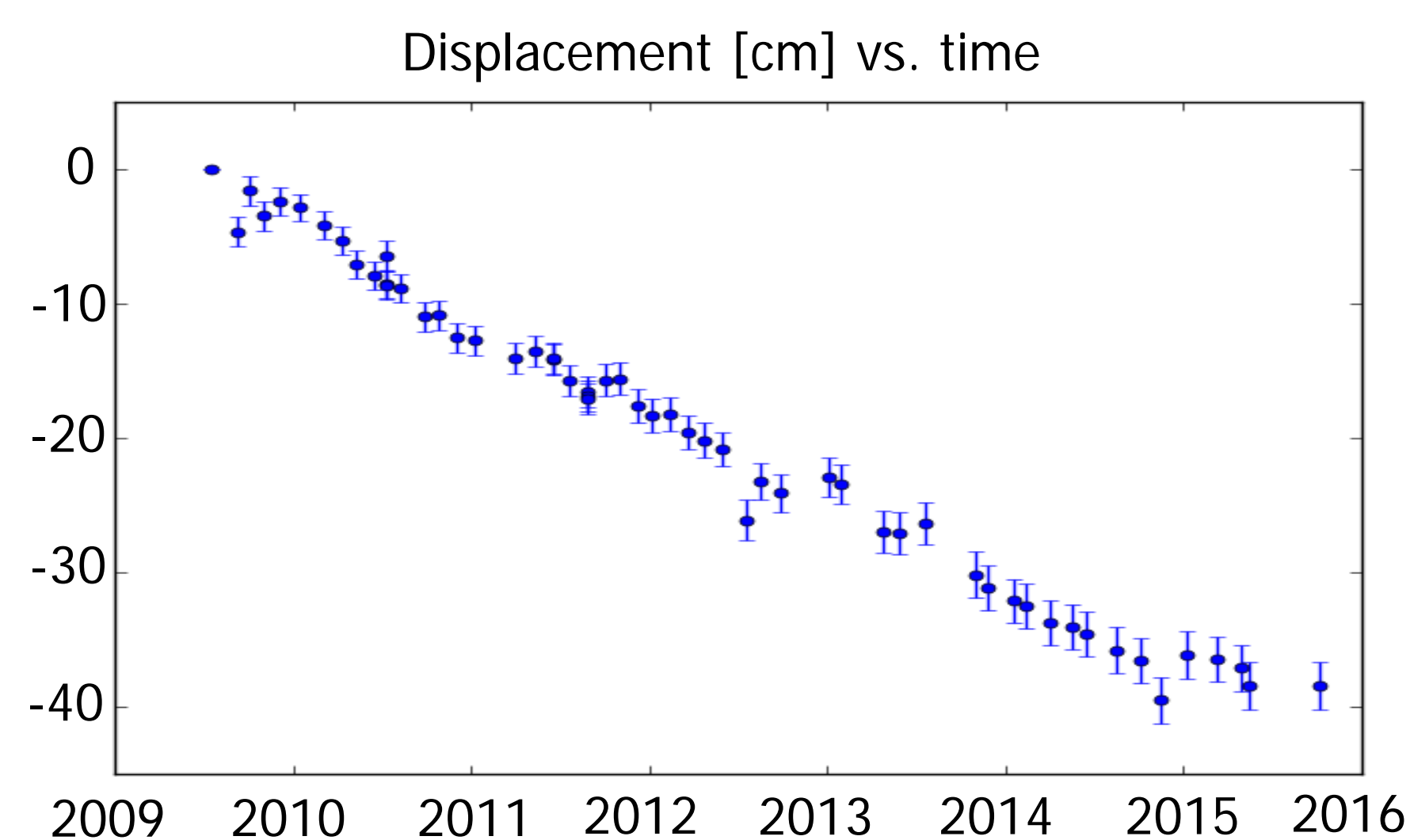
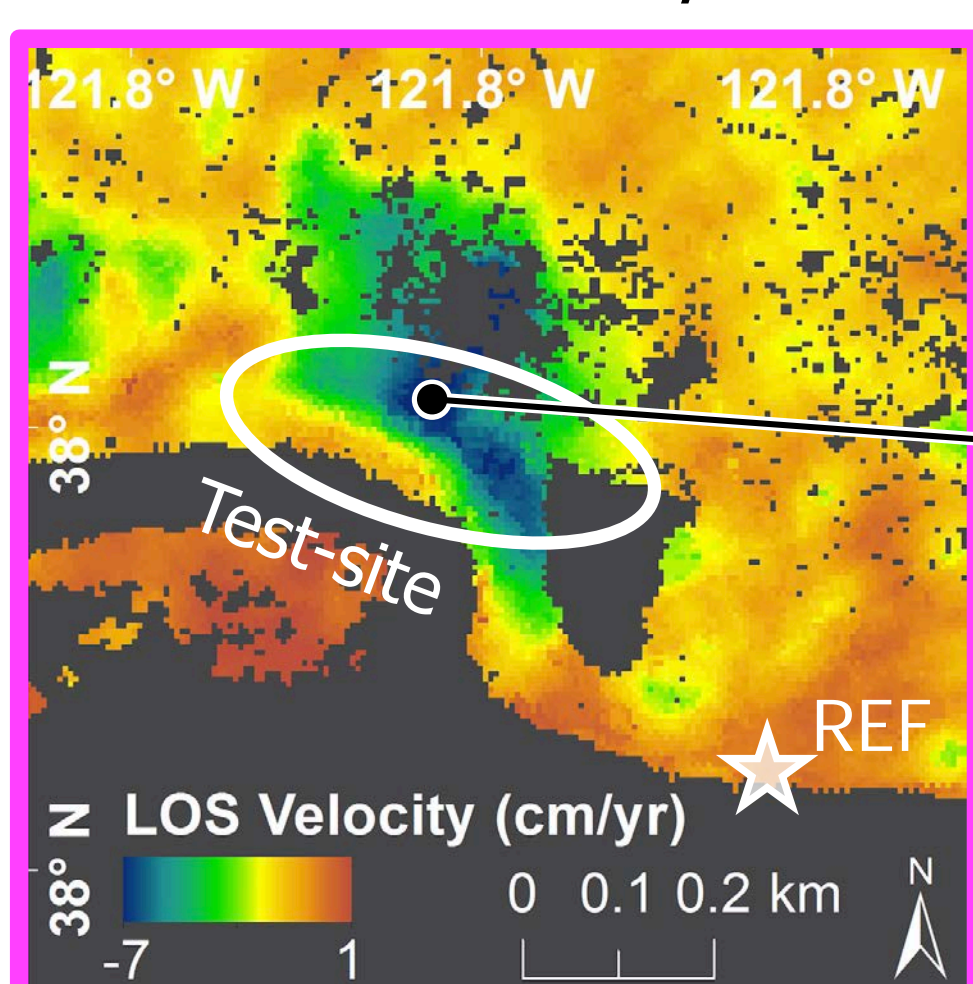
### Observations

- UAVSAR is suitable for subsidence mapping
- Localized subsidence on levees
- 40 cm of subsidence over 6 years at test-site
- Residual tropospheric noise
- Small uncertainties after time-series analysis

### Current work in progress:

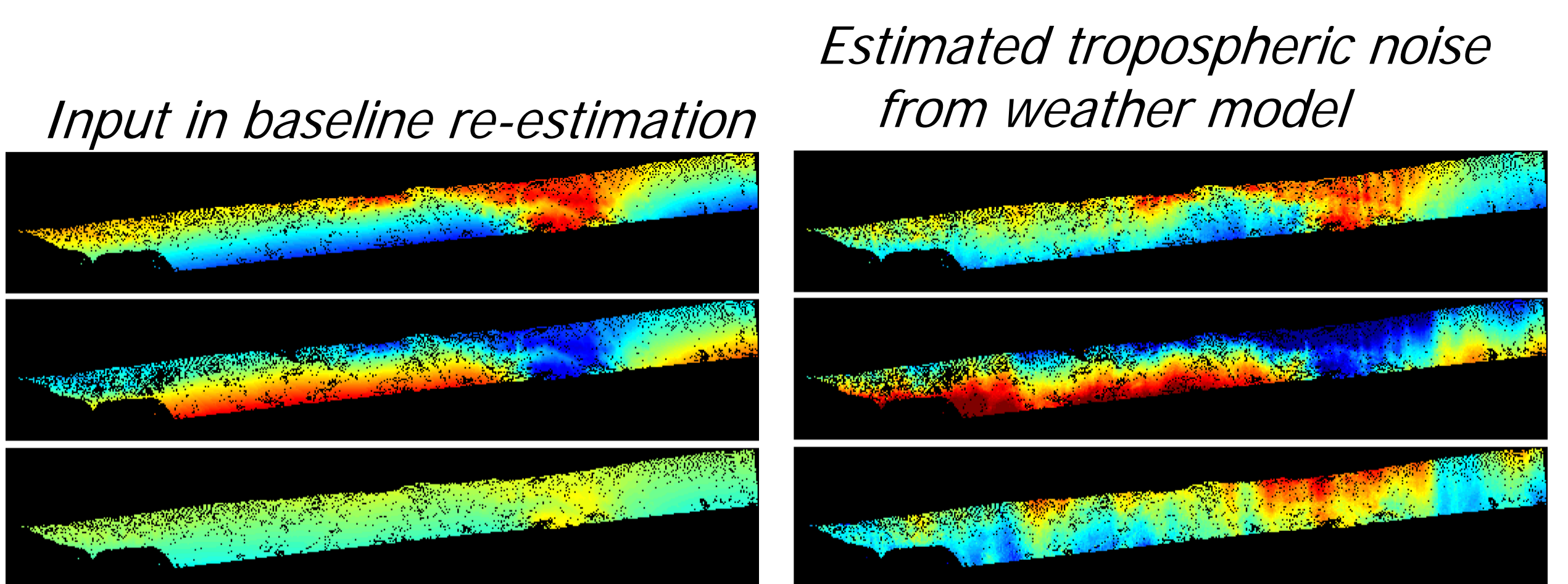
- Process remaining flight lines
- Perform tropospheric noise corrections
- Generation of large-scale subsidence map
- Integration with GPS

### Test-site levee slope/toe



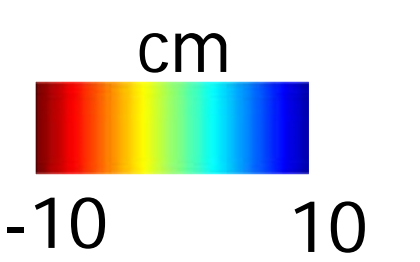
## 4. UAVSAR atmospheric noise

UAVSAR interferograms as inputted into baseline re-estimation are contaminated by tropospheric InSAR noise affecting potentially >75% of all released products



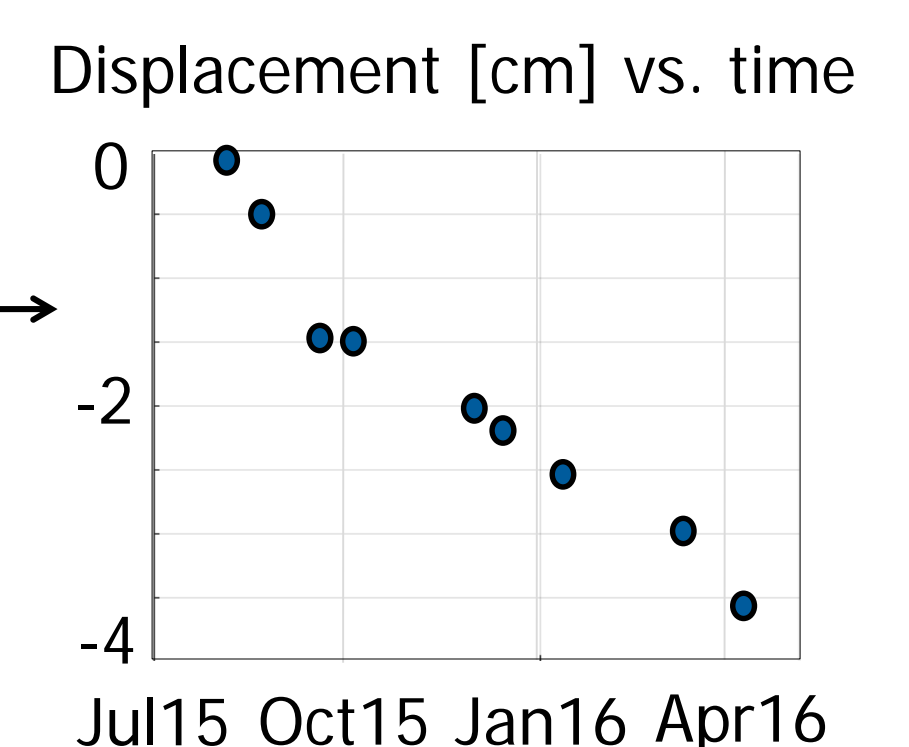
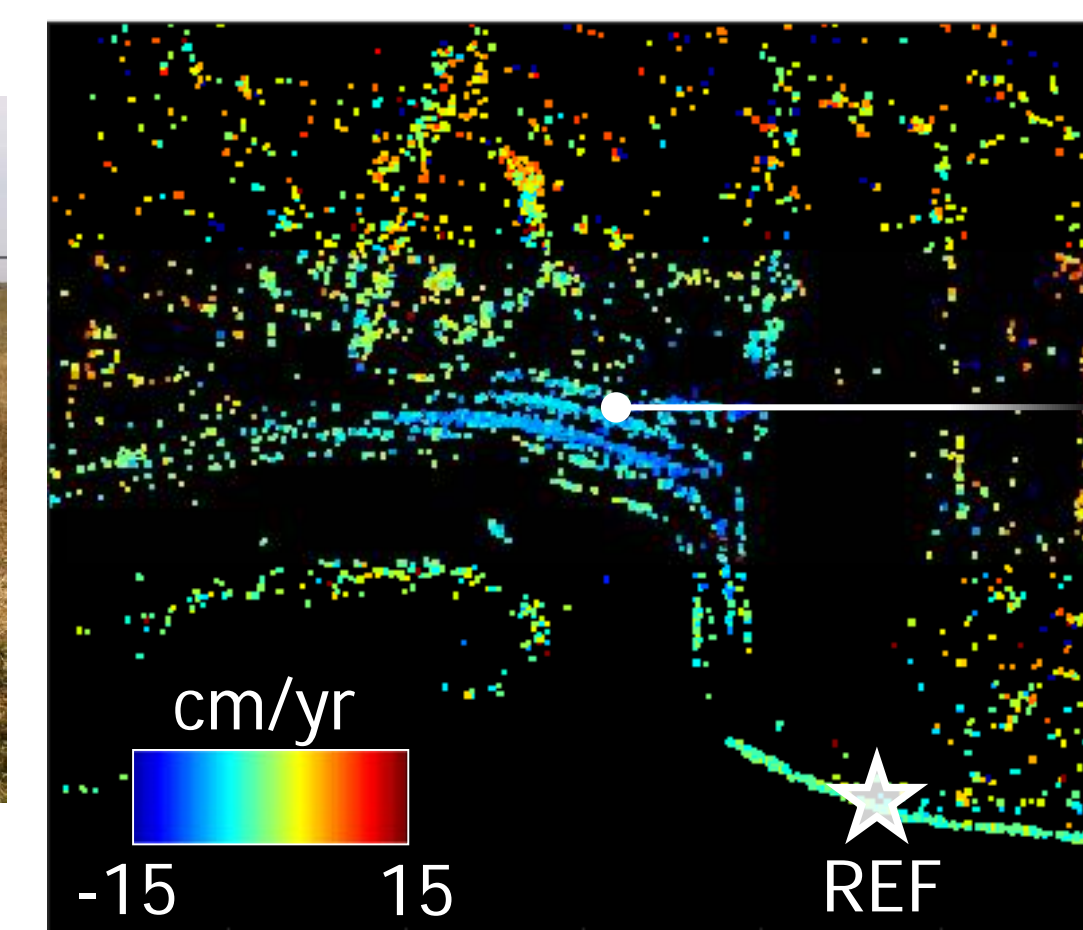
### Current work in progress:

- Statistical analysis of tropospheric noise contamination on baseline re-estimation
- Remove estimate of tropospheric noise prior to baseline re-estimation processing



## 5. L-band Space-borne SAR

### Sliding of Levee slope at test-site from ALOS 2 (L-band)



## 6. Conclusions and NASA Relevance

- ❑ L-band UAVSAR as testbed for NISAR (NASA-ISRO SAR) is well suited for monitoring levee integrity.
- ❑ Tropospheric noise leaks into the NISAR and UAVSAR data and needs to be accounted for.
- ❑ CA Department of Water Resources plans using results for decision making support and investigates in a UAVSAR for operational use.

# Hydrologic remote sensing using GPS signals recorded by TechDemoSat-1 and the SMAP radar receiver

Clara C. Chew (335-G)

Stephen Lowe (335-F), Stephan Esterhuizen (335-F), Shadi Oveisgharan (334-H), and Anthony J. Mannucci (335-G)

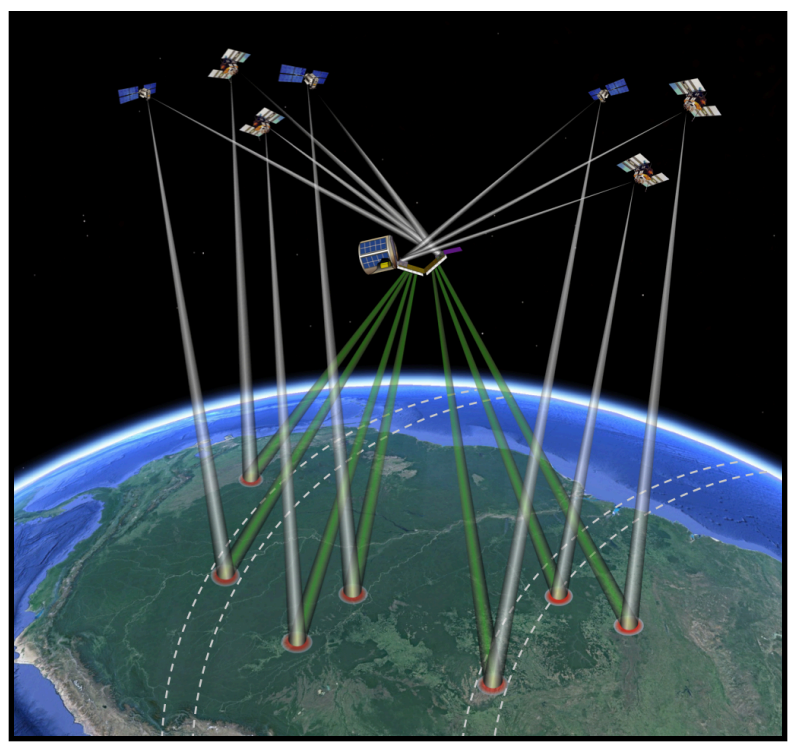
## What are GPS reflections?

- An inexpensive source of L-band bistatic radar.
- Reflections are altered by changes in the moisture content or roughness of the surface.
- Spatial resolution of spaceborne reflections: 0.3 km (smooth surface) or 25 km (rough surface).
- Currently, two spaceborne sensors: TechDemoSat-1 (TDS-1), SMAP radar receiver

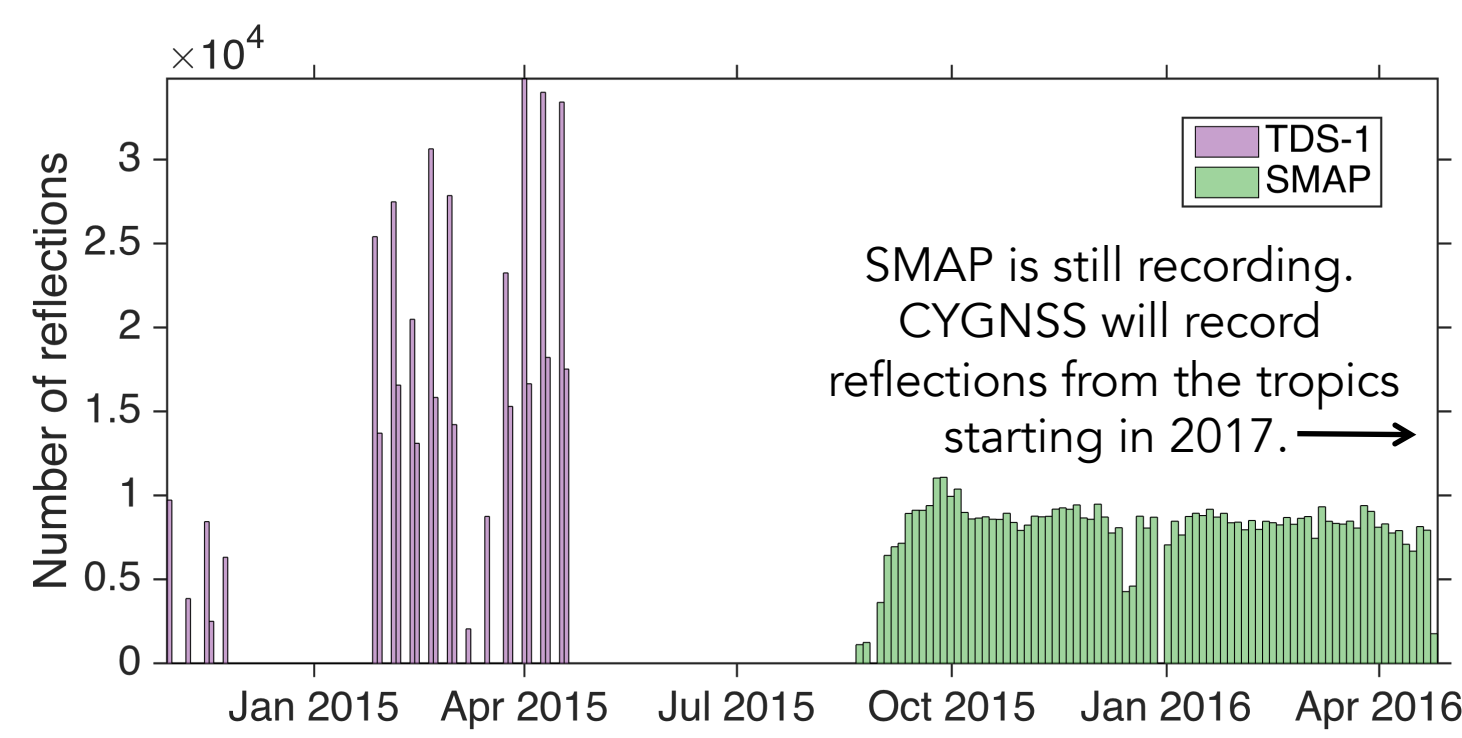
It has been shown that potential applications of reflections include:

- Soil moisture estimation
- Flood inundation mapping
- Sea ice monitoring

This work focuses on whether or not spaceborne GPS reflections could provide soil moisture data.



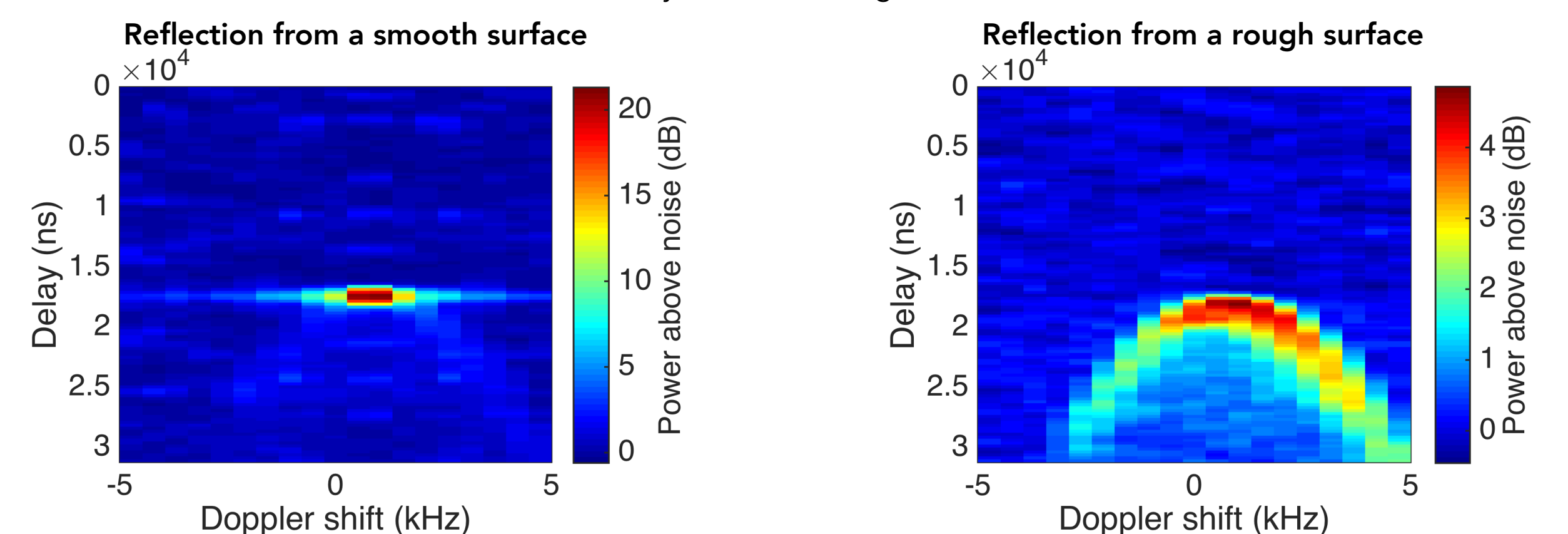
GPS or GNSS satellites transmit signals, some of which reflect off the Earth's surface. A GPS or GNSS receiver in orbit with a down-looking antenna can record these reflections.



Above are the number of GPS reflections recorded by either TDS-1 or the SMAP radar receiver. A constellation of small satellites called CYGNSS will be launched at the end of this year, which will also record reflections over the tropics.

## Data Processing

Delay-Doppler maps (DDMs) are two-dimensional cross correlations of the received signal and a known replica signal. Two examples of DDMs are shown below, which are characteristically different depending on whether or not the reflecting surface is very smooth or rough.



The DDM above was recorded by TDS-1 over a flood plain.

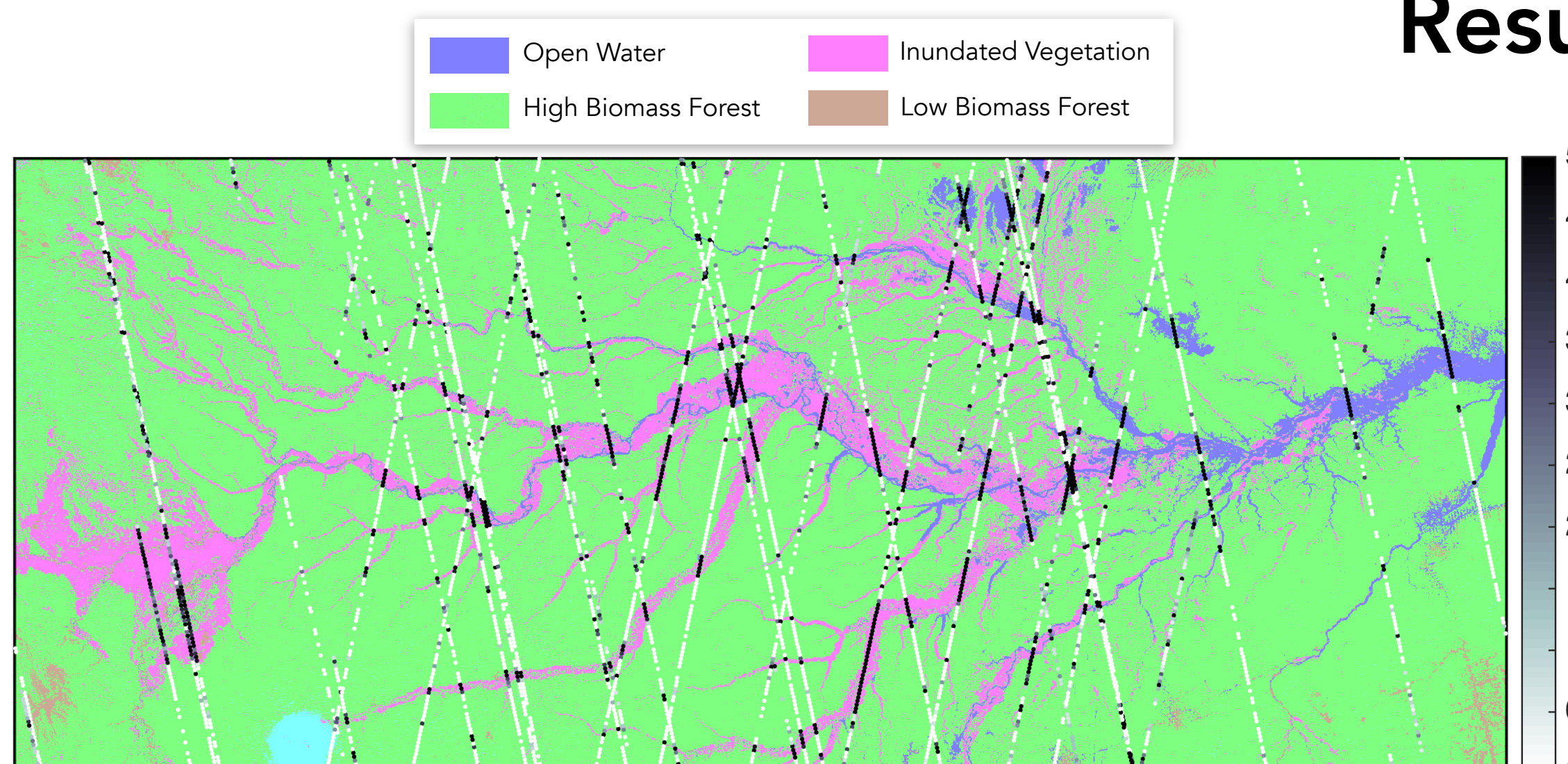
The DDM above was recorded by TDS-1 over the ocean.

$$P_{eff} = 10 \log \left( \frac{P}{N} \right) - 10 \log G_r + 20 \log (R_t + R_r) + 20 \log (\cos \theta)$$

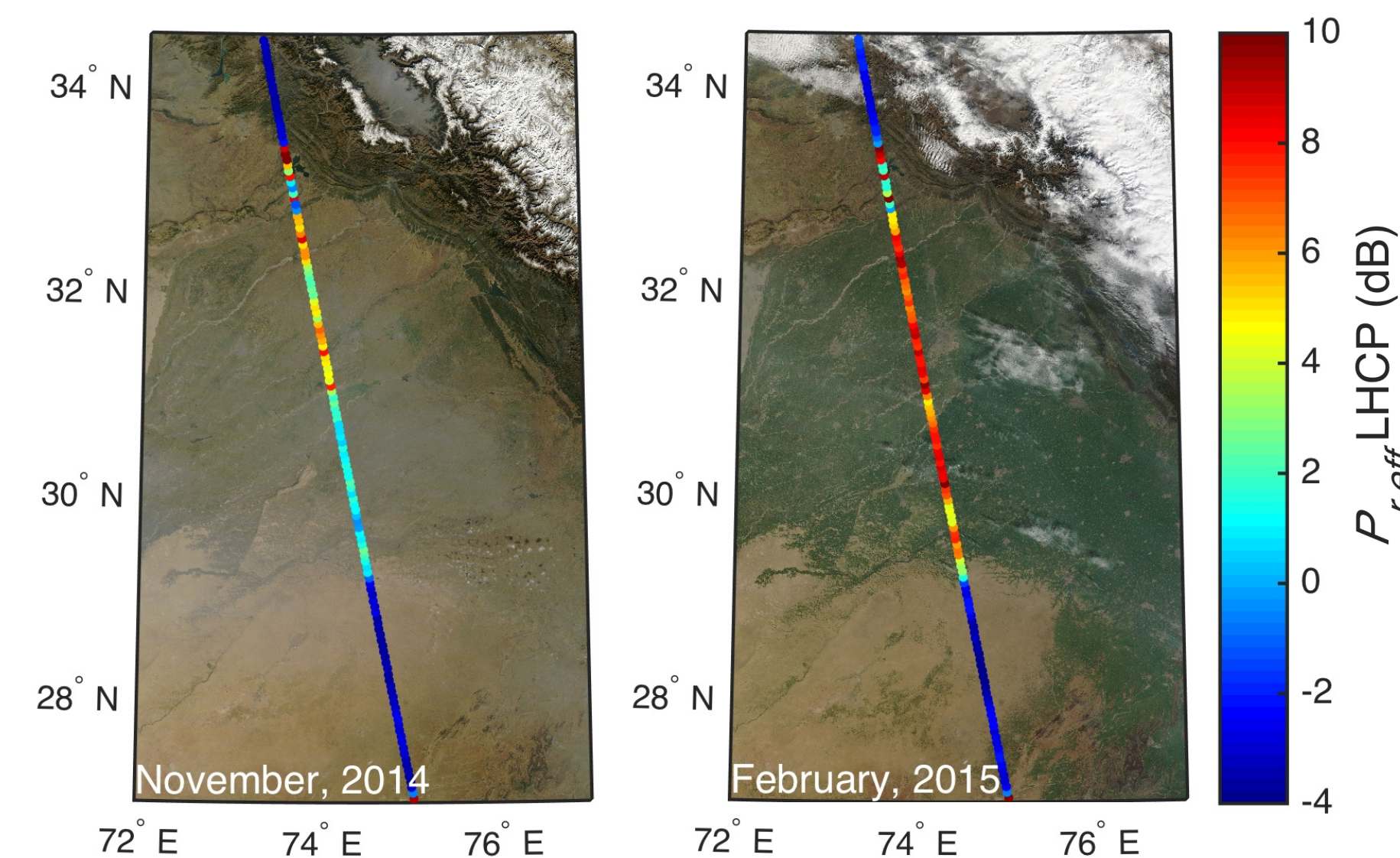
The equation above is used to estimate the reflected power ( $P_{eff}$ ) at a particular polarization. The peak correlative power ( $P$ ) of each DDM is normalized by the noise floor ( $N$ ). Corrections are made for the gain of the receiving antenna ( $G_r$ ), range ( $R_t, R_r$ ) and incidence angle ( $\theta$ ).

Here, we compare  $P_{eff}$  to the SMAP and SMOS radiometer products, in addition to soil moisture data provided by the SCAN network.

## Results from TDS-1



Above is a land cover map of the Amazon that was derived using SMAP radar backscatter data as well as Landsat imagery. Superimposed on top are tracks from TDS-1. Points are colored with respect to the median reflected power over land. There is a significant increase in reflected power over areas with flooded vegetation.



On the left are reflections recorded by TDS-1 over the Punjab region of India and Pakistan from November, 2014 (left) and from February, 2015 (right). Points are colored with respect to the median reflected power over land. The underlying image is the MODIS corrected reflectance.

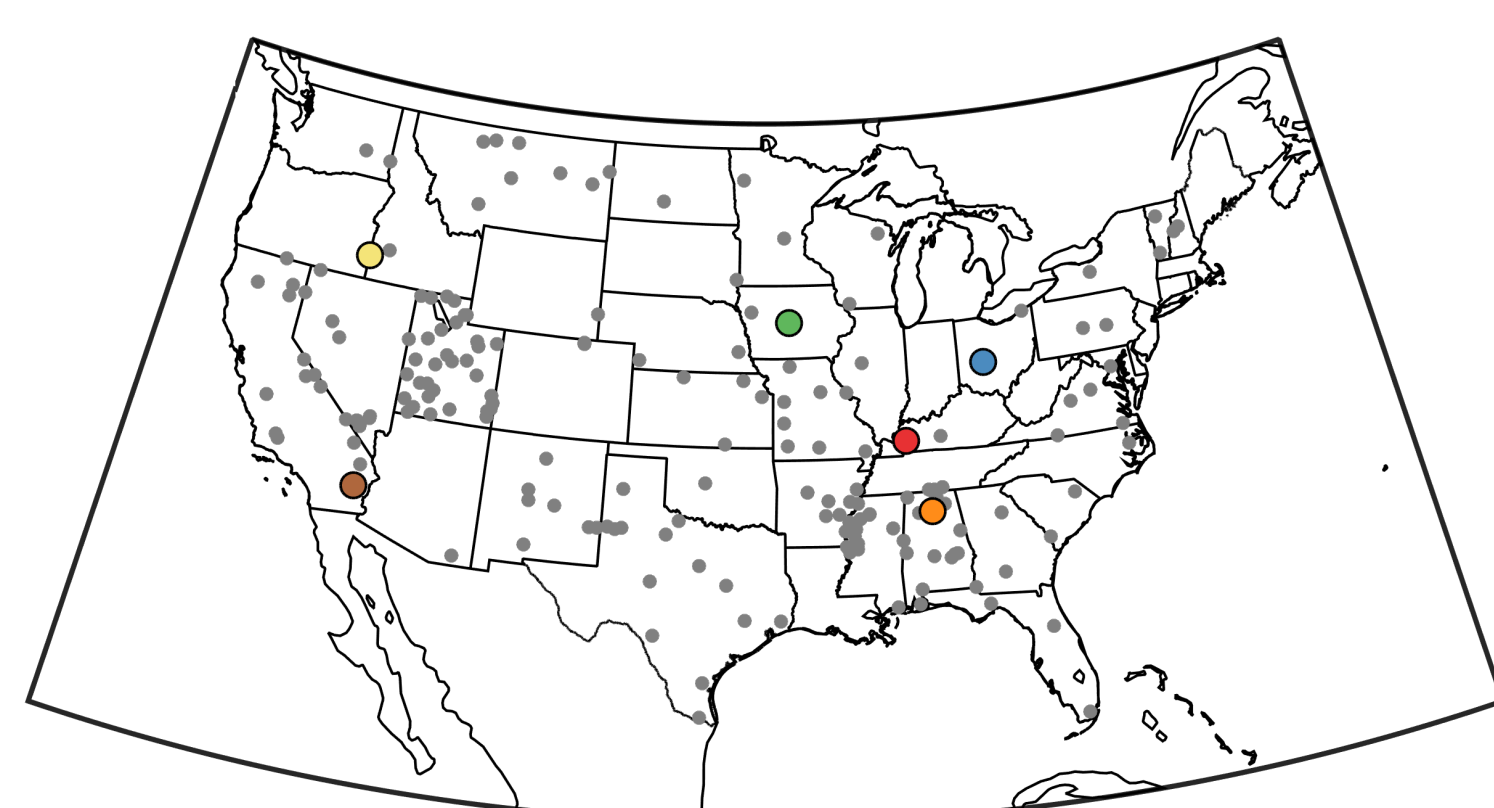
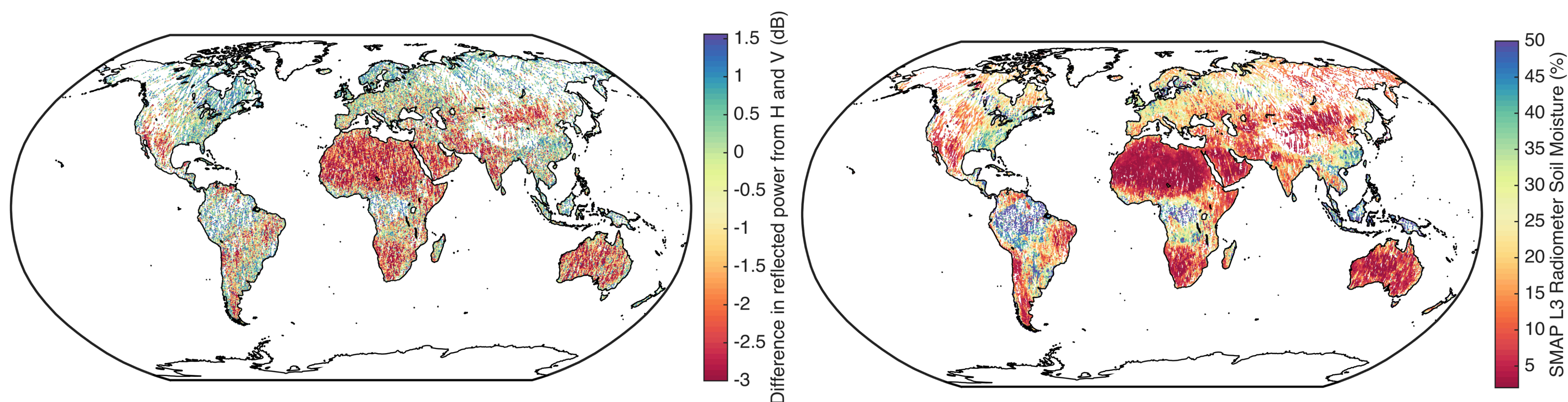
Vegetation has been shown to decrease reflected power, so the increase in power may be due to the  $\sim 0.2 \text{ cm}^3 \text{ cm}^{-3}$  increase in soil moisture for the region, as estimated from the SMOS satellite.

## Results from the SMAP radar receiver

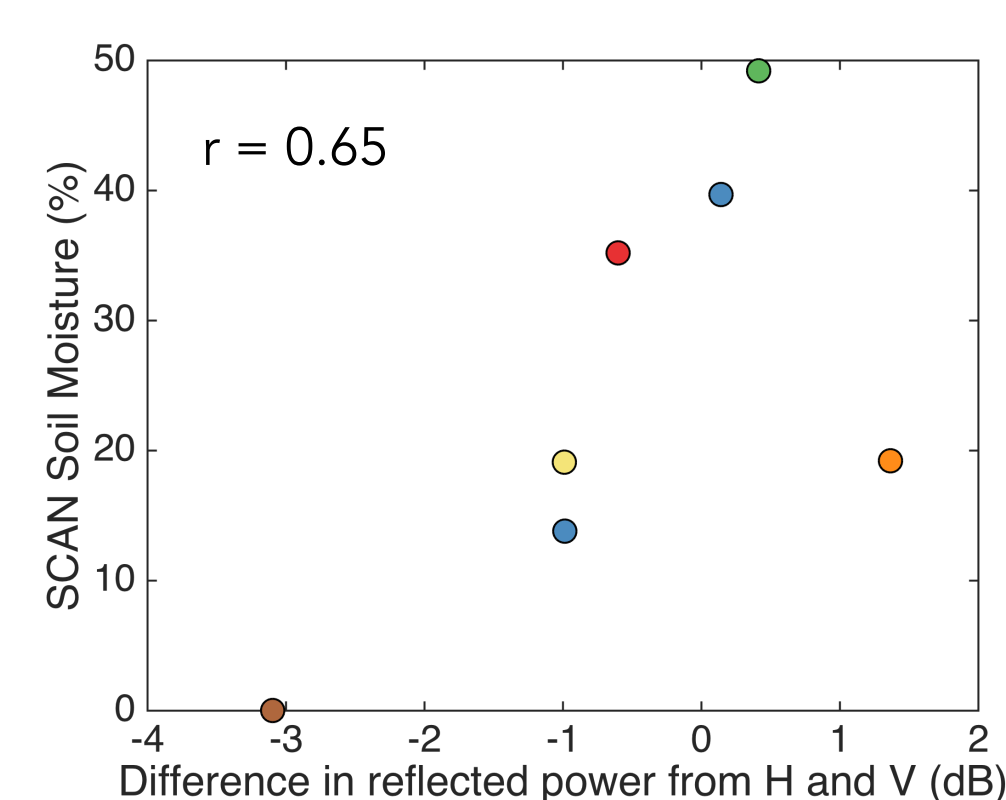
On the right are the high-quality GPS reflections recorded by SMAP over land, which also coincide with the SMAP L3 radiometer soil moisture product. Here is shown the difference in reflected power recorded by the H and V channels (polarization ratio).

Also shown are SMAP L3 radiometer soil moisture product estimates that were collocated/coincided with a high-quality GPS reflection also recorded by SMAP.

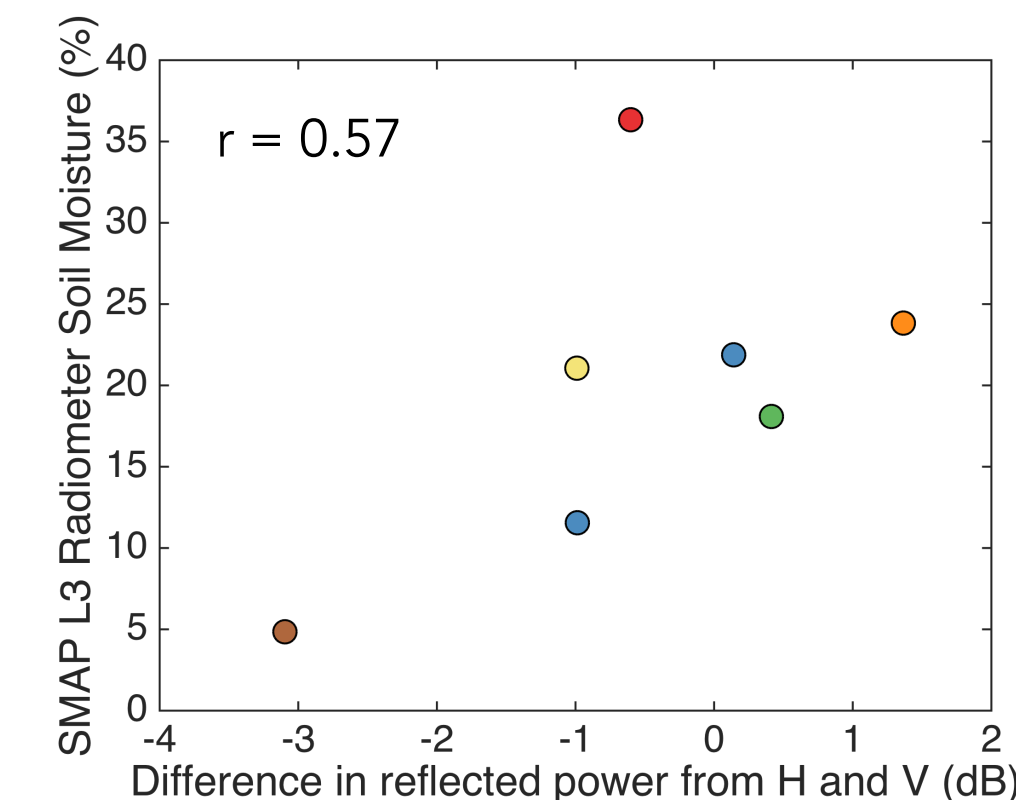
The correlation coefficient between the two maps is 0.52.



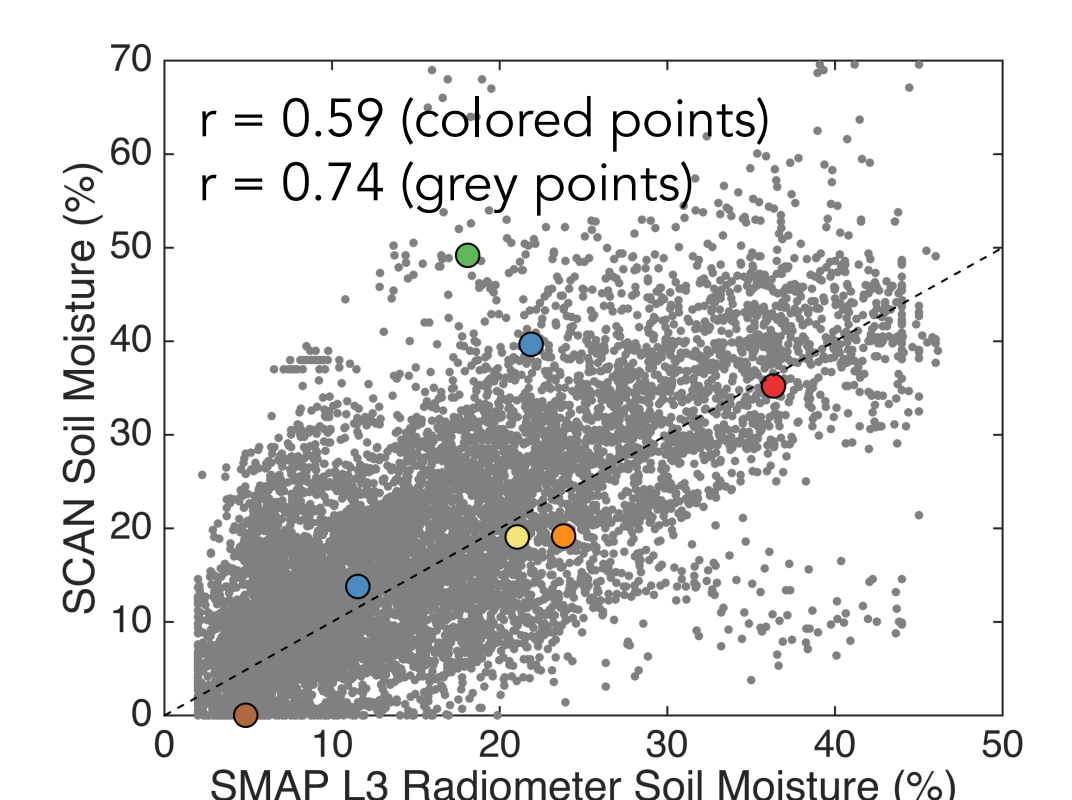
Grey points are locations of SCAN soil moisture stations. Colored points are SCAN soil moisture stations <3 km from a GPS reflection recorded by SMAP. This subset of stations was used in the plots to the right.



The polarization ratio of GPS signals recorded by SMAP show an encouraging relationship with soil moisture, though many more observations are needed.



This subset of data shows a similar relationship as the above map—the polarization ratio of reflected GPS signals is correlated with the SMAP L3 radiometer soil moisture product.



The correlation between SMAP soil moisture and the entire SCAN network is better than the correlation between SMAP soil moisture and the subset of SCAN stations. The same could be true for the GPS reflections, if more data are collected.

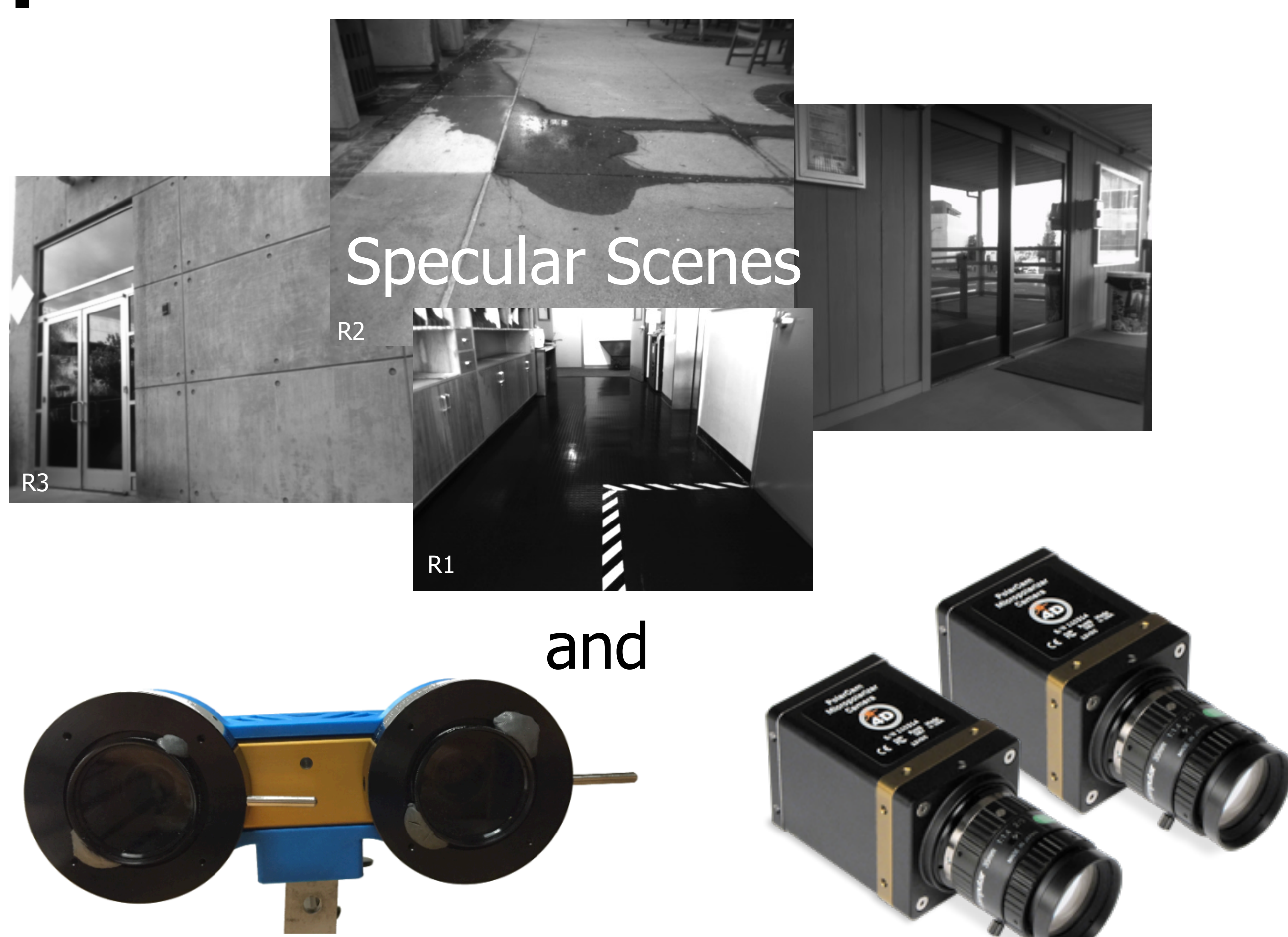
# Stereo vision in Non-Lambertian 3D environments

Author: Kai Berger (347)  
Larry H. Matthies (347)

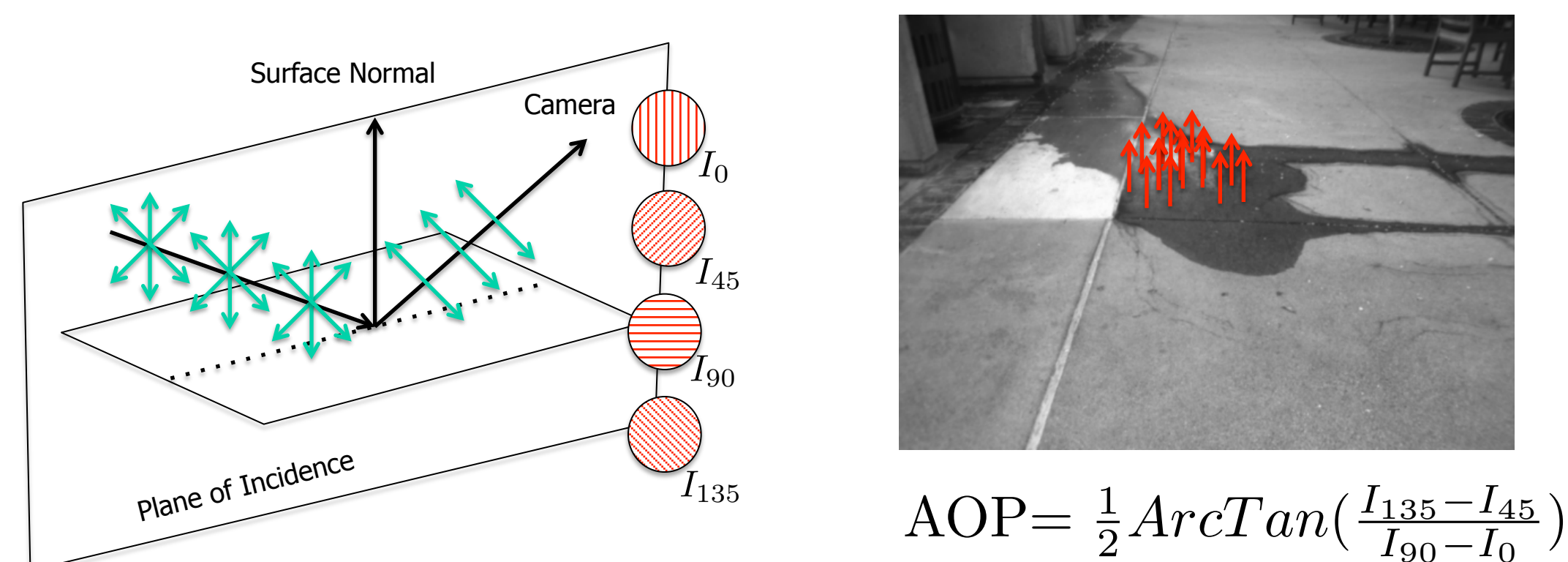
Benefit: Robotics Navigation, Environment Awareness  
Scientific Foundation: Polarization Stereo

Impact: Robust recovery of scene geometry including specular surfaces

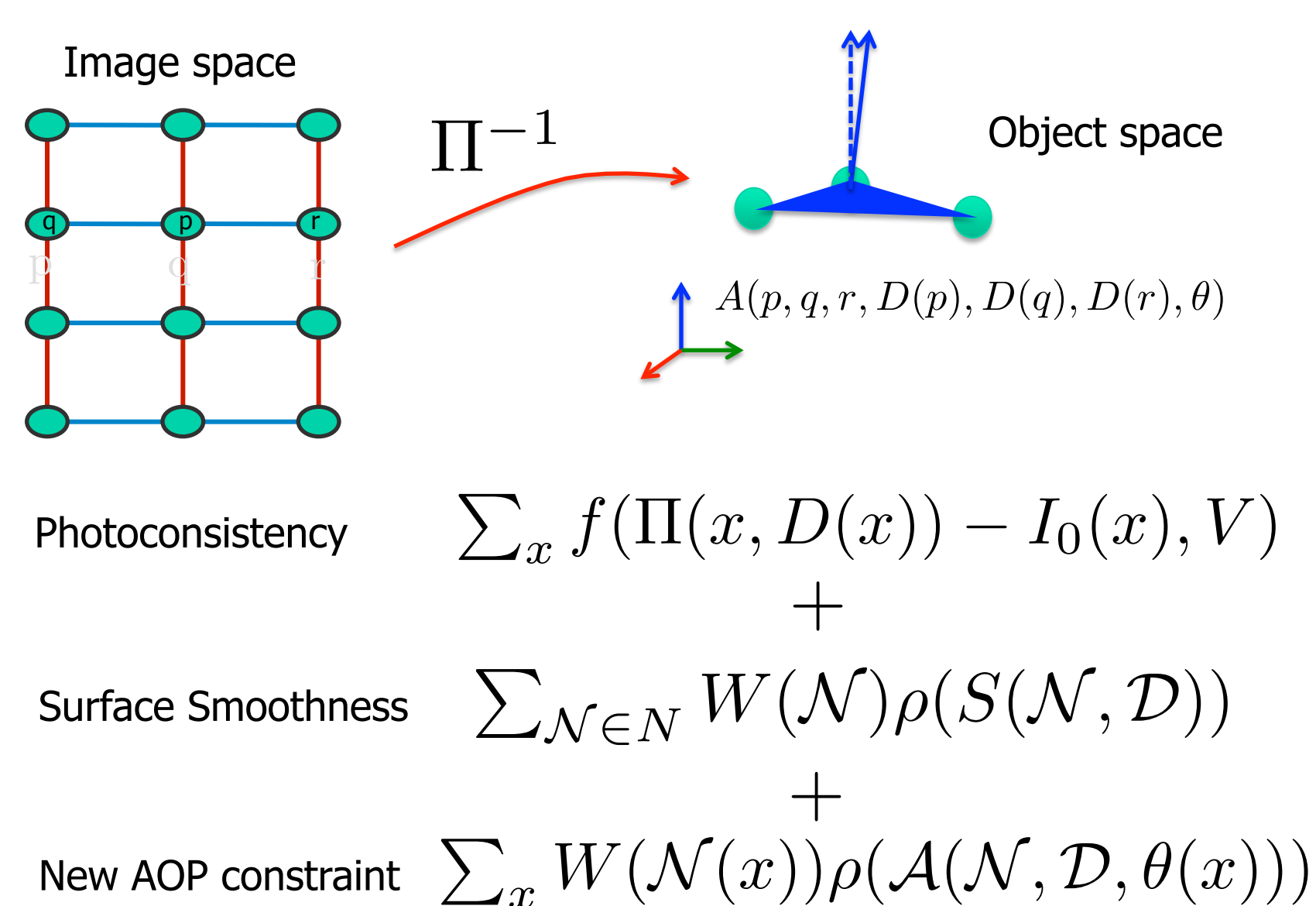
## Approach



### 1) Compute Angle of Polarization (AOP)

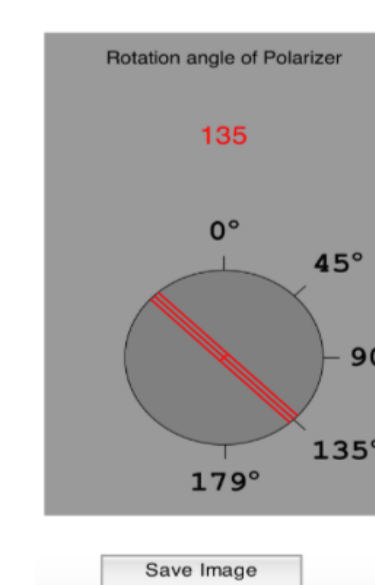
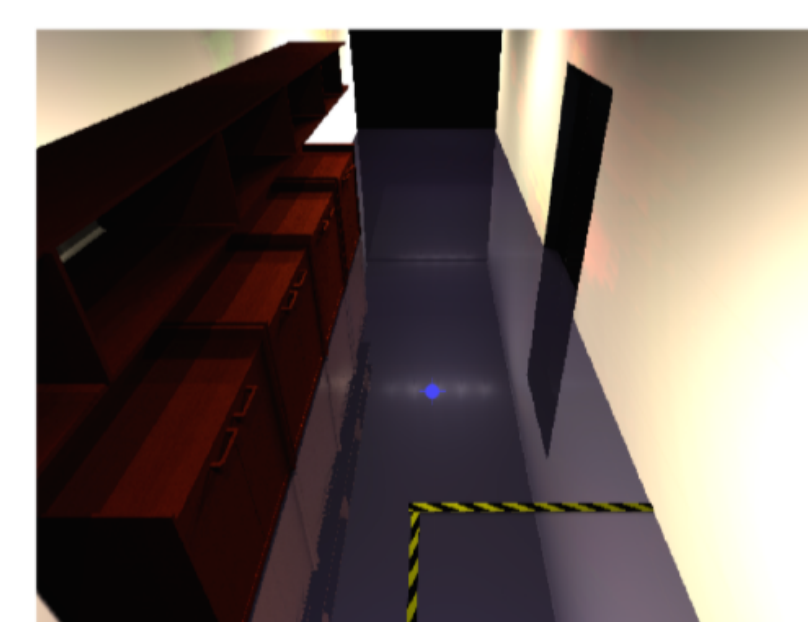


### 2) Solve Graph-Cut with AOP-constraint



## Results

Provide Ground Truth to test the algorithm on

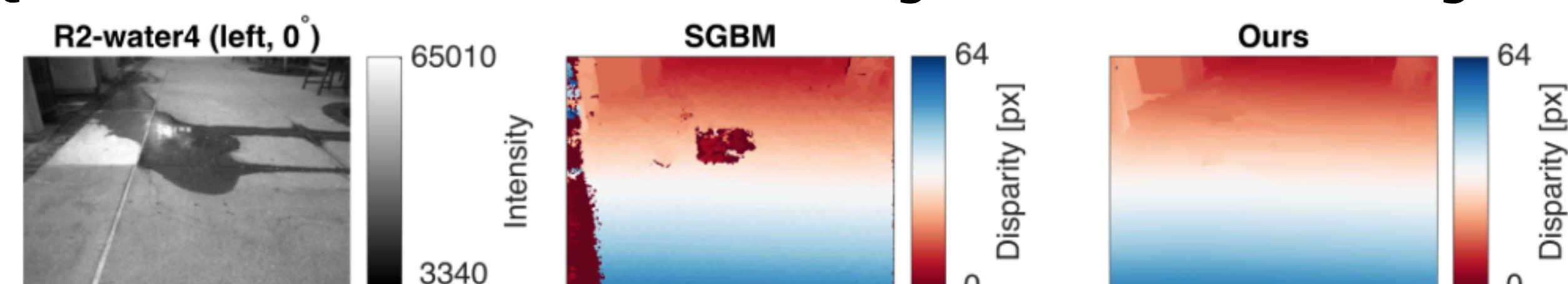


Generate virtual scenes V1, V2, V3 with polarization ray tracer

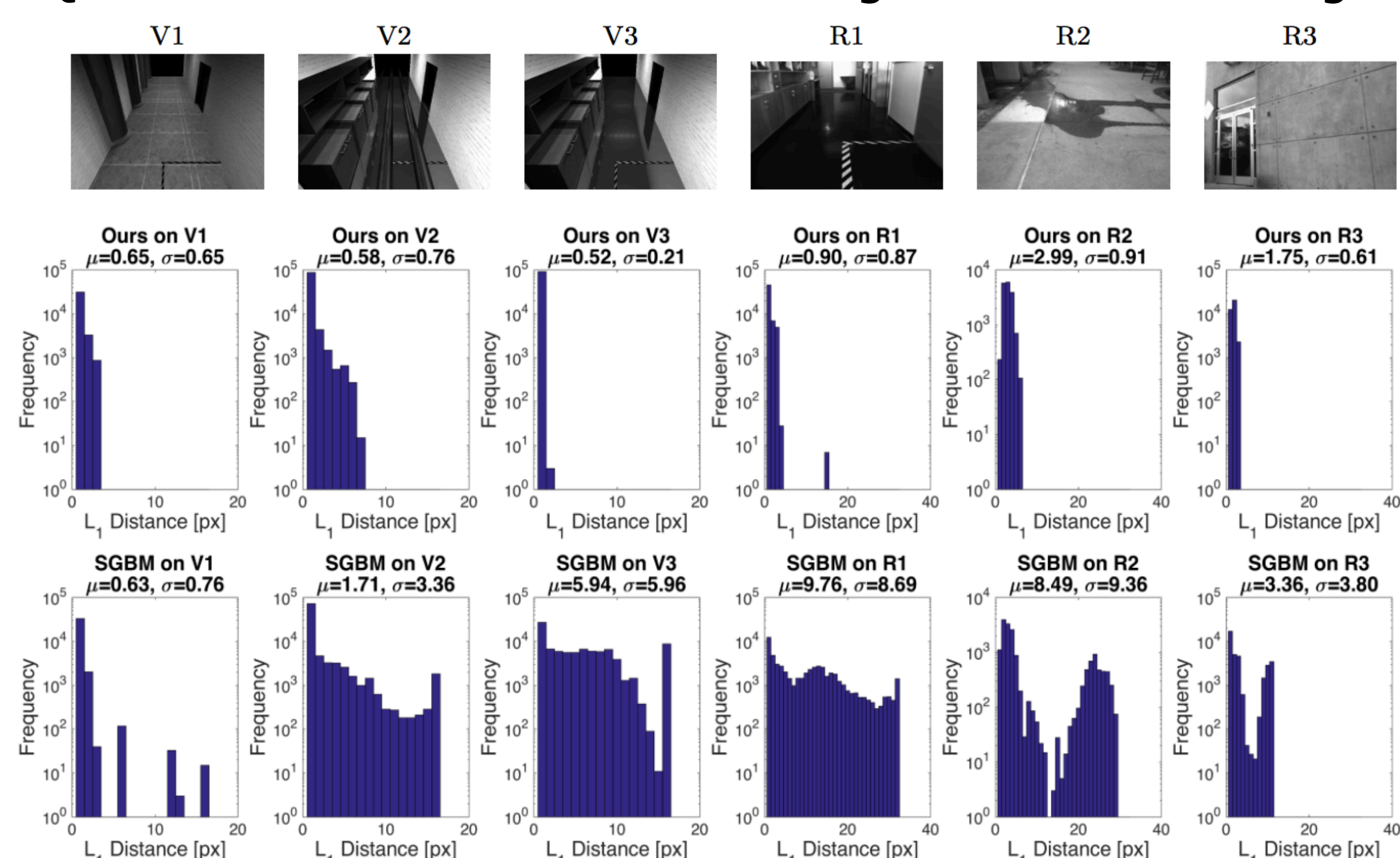
1) Simulate polarized light transport. Store polarization states for each pixel.

2) Display, apply virtual linear polarizer

Qualitative Results: Ours vs. Semi-global block matching



Quantitative Results: Ours vs. Semi-global block matching



These semilogarithmic histograms bin the number of pixels in the result depth map that have a certain L1-distance to the ground truth depth. The more pixels with zero or low L1-distance, the better the result.

## Our Path Forward



- Test on glass and transparencies
- Parallelize on GPU
- Explore near-unpolarized surface reflections

# Development of the Spacecraft Atmosphere Monitor

Author: Steven Schowalter (382D)

B. Bae (382D), W. Rellergert (382D), S. Jackson (389D), M. Homer (3463), J. Urrutia (357B), D. Nikolić (382D), J. Simcic (382D), R. Kidd (382D), E. Neidholdt (382D), S. Madzunkov (382D), M. Darrach (382D)

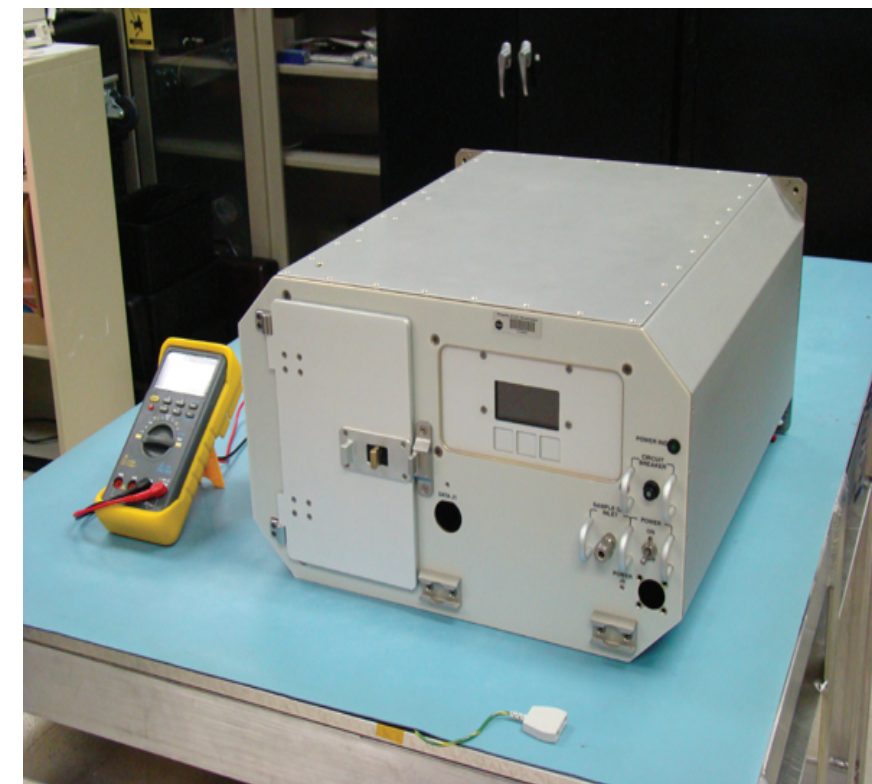
## Motivation

The ISS is in the need of a new instrument to monitor the levels of both **major constituents** ( $N_2$ ,  $O_2$ ,  $CO_2$ ,  $H_2O$ , etc.) and **trace volatile organic compounds** (VOCs) in the onboard atmosphere.

This device is crucial in continuing to **make longterm spaceflight safe and productive** and will be used as a science demonstration for potential future use for flight missions to Mars on the **Orion spacecraft**.



The SAM is a miniature gas chromatograph/mass spectrometer (GCMS). The SAM is a **smaller, more powerful, less power-consuming** analyzer than the previous instrument: the Vehicle Cabin Atmosphere Monitor (VCAM), which performed **trace gas analysis (TGA)** of certain VOCs. The SAM adds the ability to perform **major constituent analysis (MCA)**, as well.



## Instrument Design

The main functional components of the SAM:

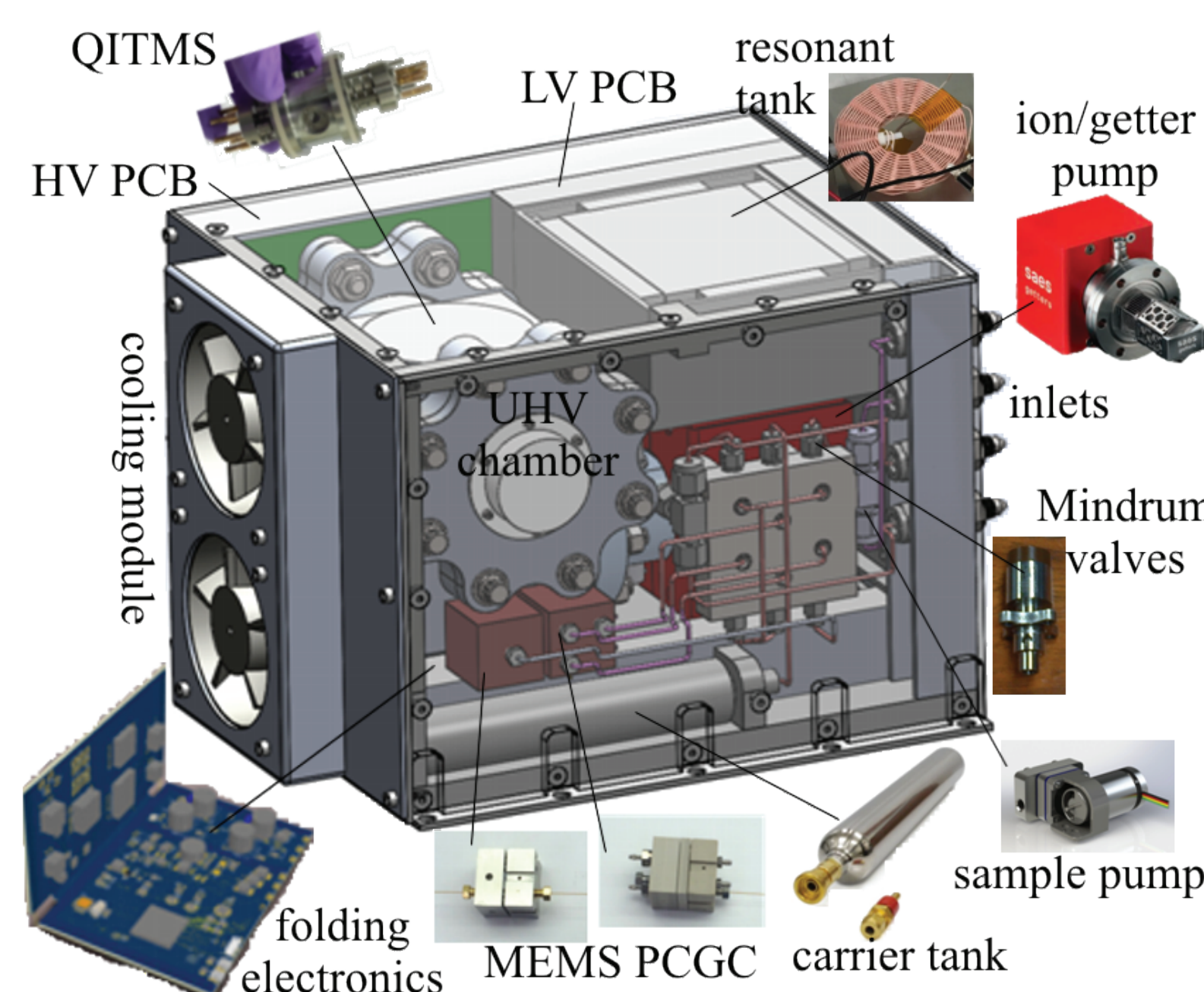
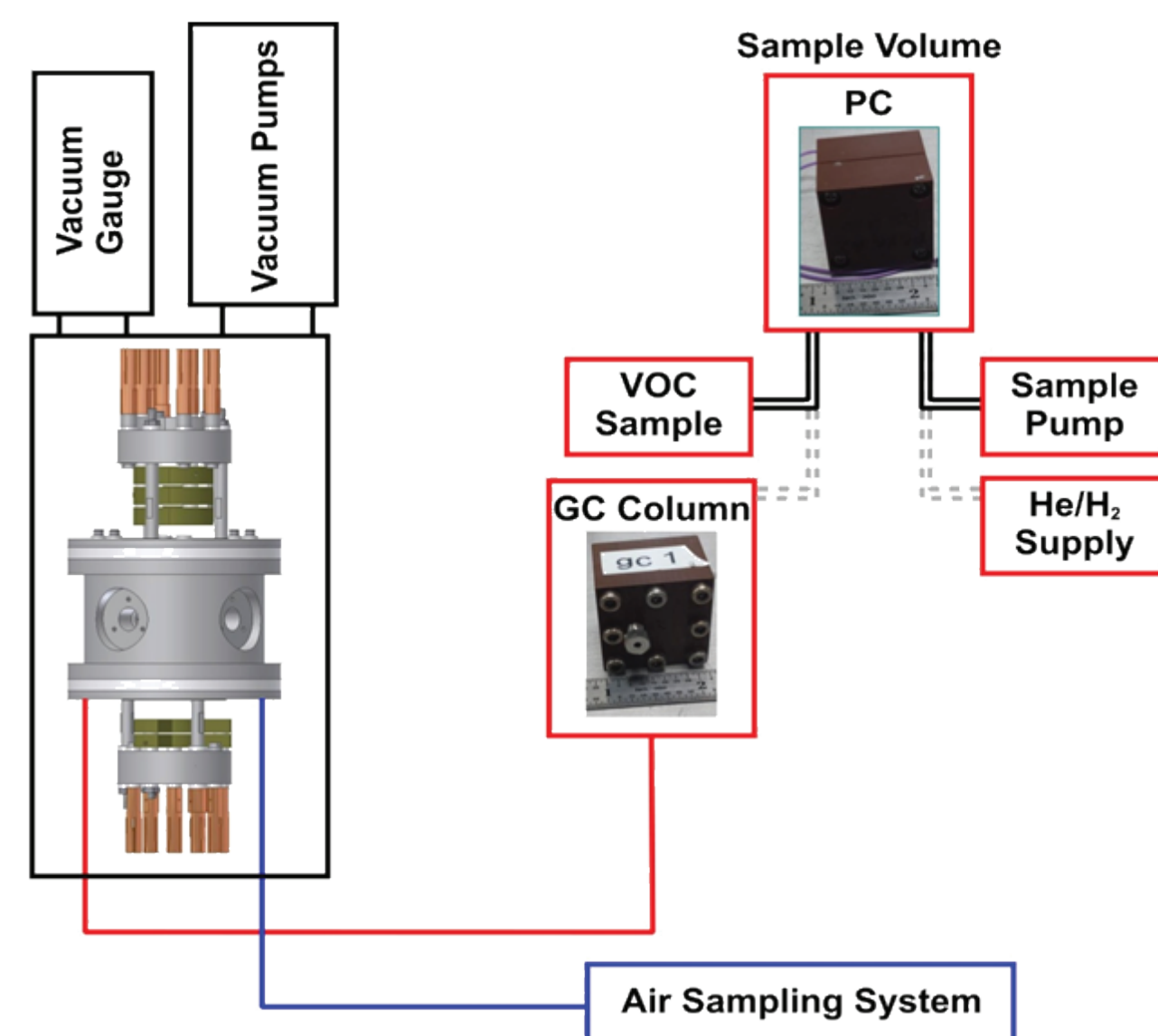
- **MEMS GC system**
  - MEMS microvalves (MVs)
  - Sample Preconcentrator (PC)
  - GC microcolumn (MC)
- **Miniaturized Quadrupole Ion Trap MS (QITMS)**
  - Wireless trap, electronics controlled by FPGA
  - Housed in 3D-printed Ti UHV chamber
  - Miniature ion/getter pump

### MCA operation:

1. Spacecraft air flows directly into QITMS via constricted plumbing.
2. Air is ionized and its composition is analyzed/recorded.

### TGA operation:

1. Spacecraft air flows into GC unit and is preconcentrated (sampling)
2. MV opens and allows  $H_2$  carrier gas to enter the heated sample volume
3. Sample and carrier enters the MC where GC occurs
4. Separated VOCs enter QITMS
5. VOCs are ionized and compositions are analyzed/recorded



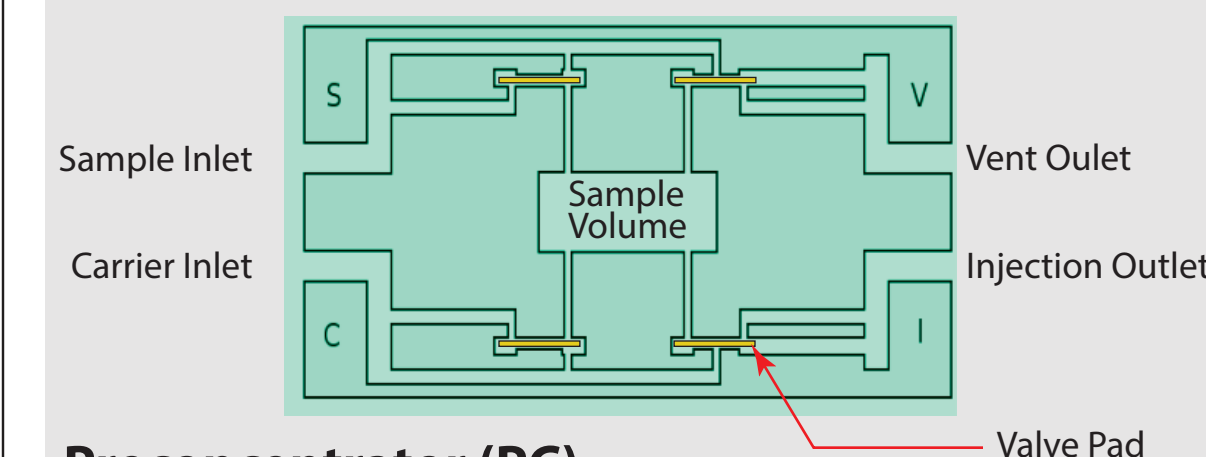
### SAM Specifications (vs VCAM)

Quantity	SAM	VCAM
Mass (kg)	9.5	37.9
Dimensions (in)	9.5x8.75x7.5	10.8x18.1x20.4
Volume (L)	10	64.4
Average Power (W)	45	120
Start Up Time (min)	<2	150
MCA Time	2 s	3-5 hours
TGA Time	10 min	40 min
Carrier Gas (cc/min)	0.1 ( $H_2$ )	1.2 (He)
Valve Power (W)	<1	12
PC Gain	400	100
GC Injector	MEMS MV	Large valves
GC Column	MC (2 m)	Column (10 m)
Elution Time (min)	<10	20
QIT Size (mm)	10	10
Vacuum Pump (L/s)	6 (ion/getter)	70 (turbo)
Thermal Control	convection/conduction	convection

## MEMS-PCGC

### Microvalve (MV)

- Four electrostatic valves: **Sample Inlet (S)**, **Vent outlet (V)**, **Carrier inlet (C)**, and **Injection outlet (I)**.
- Polyimide membrane with embedded Ti/Au/Ti valve pads
- "Zipper" valve design to reduce closing stress
- Housed in two highly-, and two regular-doped **Si wafers**.
- Bonded using benzocyclobutene (BCB) epoxy
- Anti-stiction coating and Pressure balancing

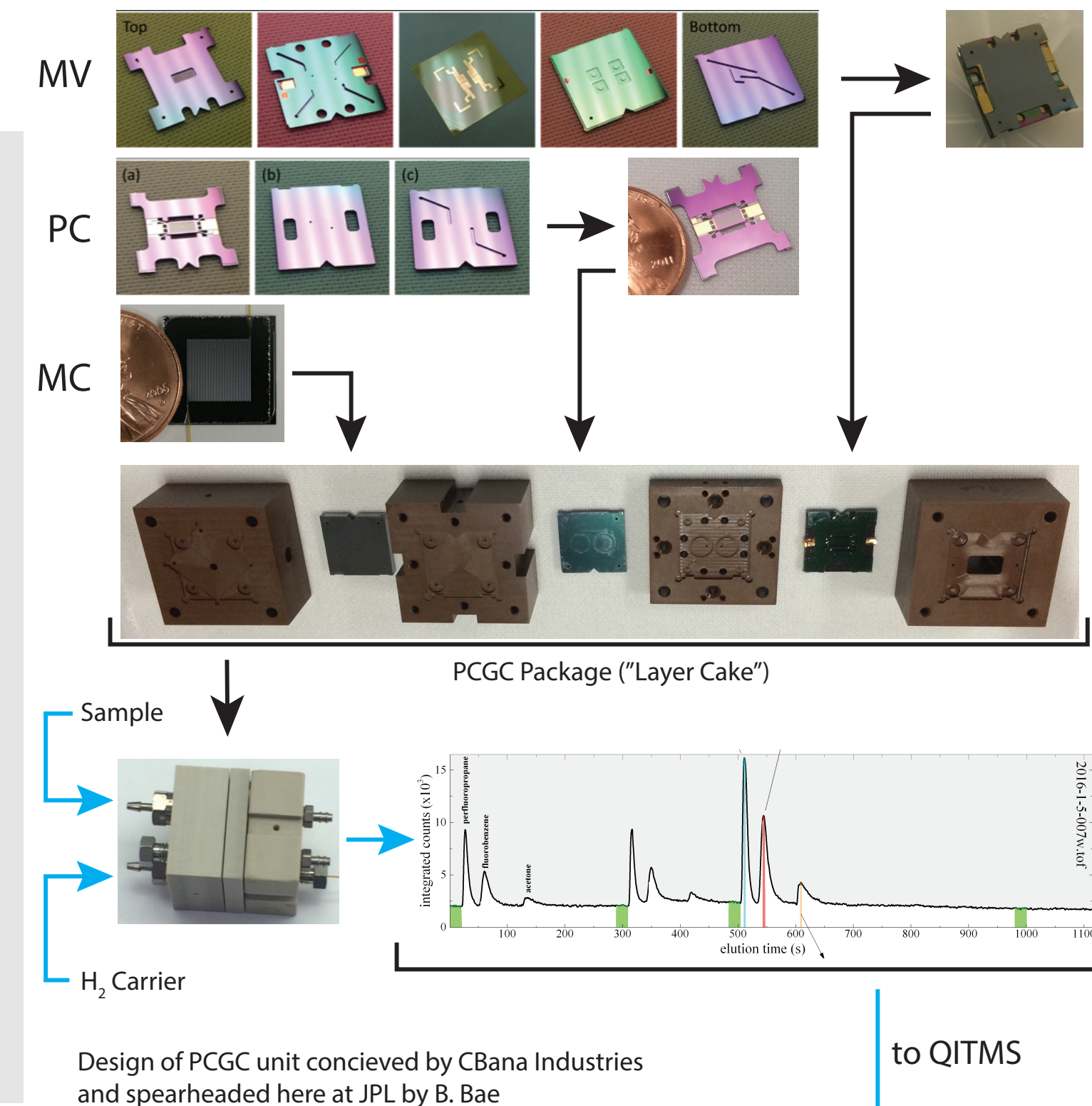


### Preconcentrator (PC)

- PC volume (1.5  $\mu$ L)
- Filled with Carboxen 1000 (~200  $\mu$ m particles, 1 nm pores)
- Equipped with silicon heater for PC Gain (up to 250  $^{\circ}$ C in < 1 s)
- Housed in two ~500  $\mu$ m Si wafers (regular and Si-on-insulator)

### GC Microcolumn (MC)

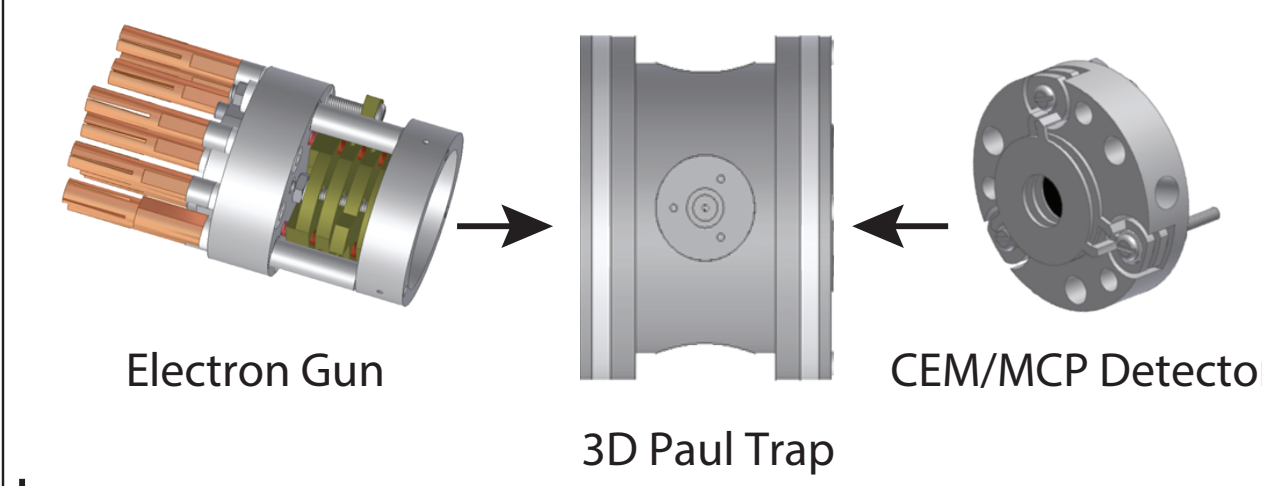
- 2 m x 86  $\mu$ m serpentine column
- OV-5 stationary phase (5% diphenyl/95% dimethylpolysiloxane)
- Housed in two ~500  $\mu$ m regular-doped Si wafers



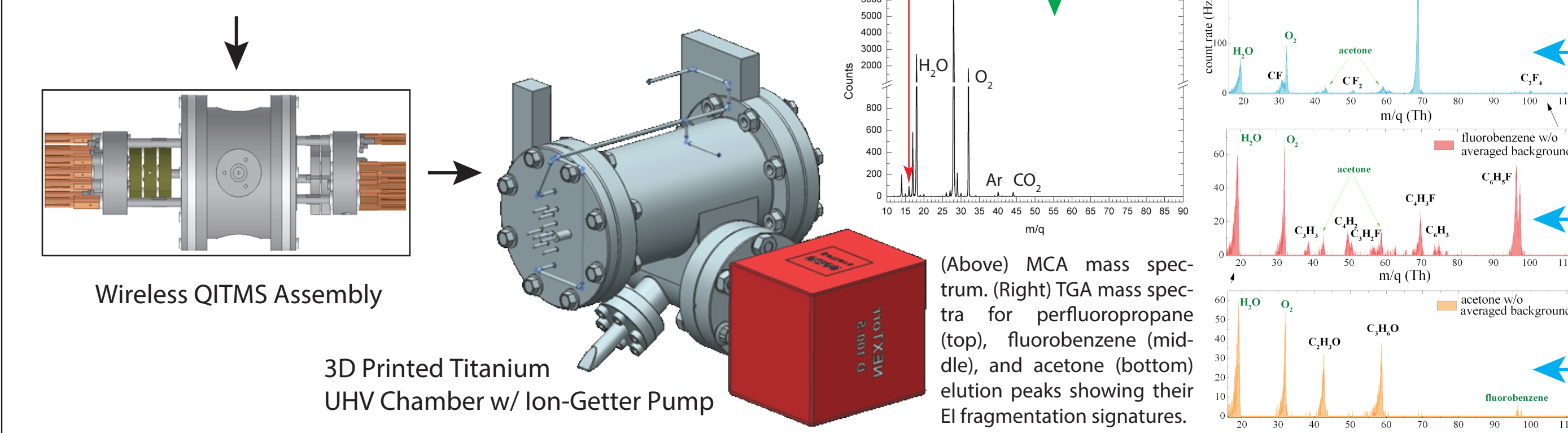
Design of PCGC unit conceived by CBana Industries and spearheaded here at JPL by B. Bae

to QITMS

## Quadrupole Ion Trap MS (QITMS)



1. Entering air molecules are ionized (EI) by an axial electron gun and trapped
2. The applied trapping rf amplitude is ramped, ejecting ions of increasing mass (Q-Scanning)
3. Ejected ions are detected by an axial CEM/MCP
4. Mass spectra are analyzed and VOC concentrations and air compositions are recorded



(Above) MCA mass spectrum. (Right) TGA mass spectra for perfluoropropane (top), fluorobenzene (middle), and acetone (bottom) elution peaks showing their EI fragmentation signatures.

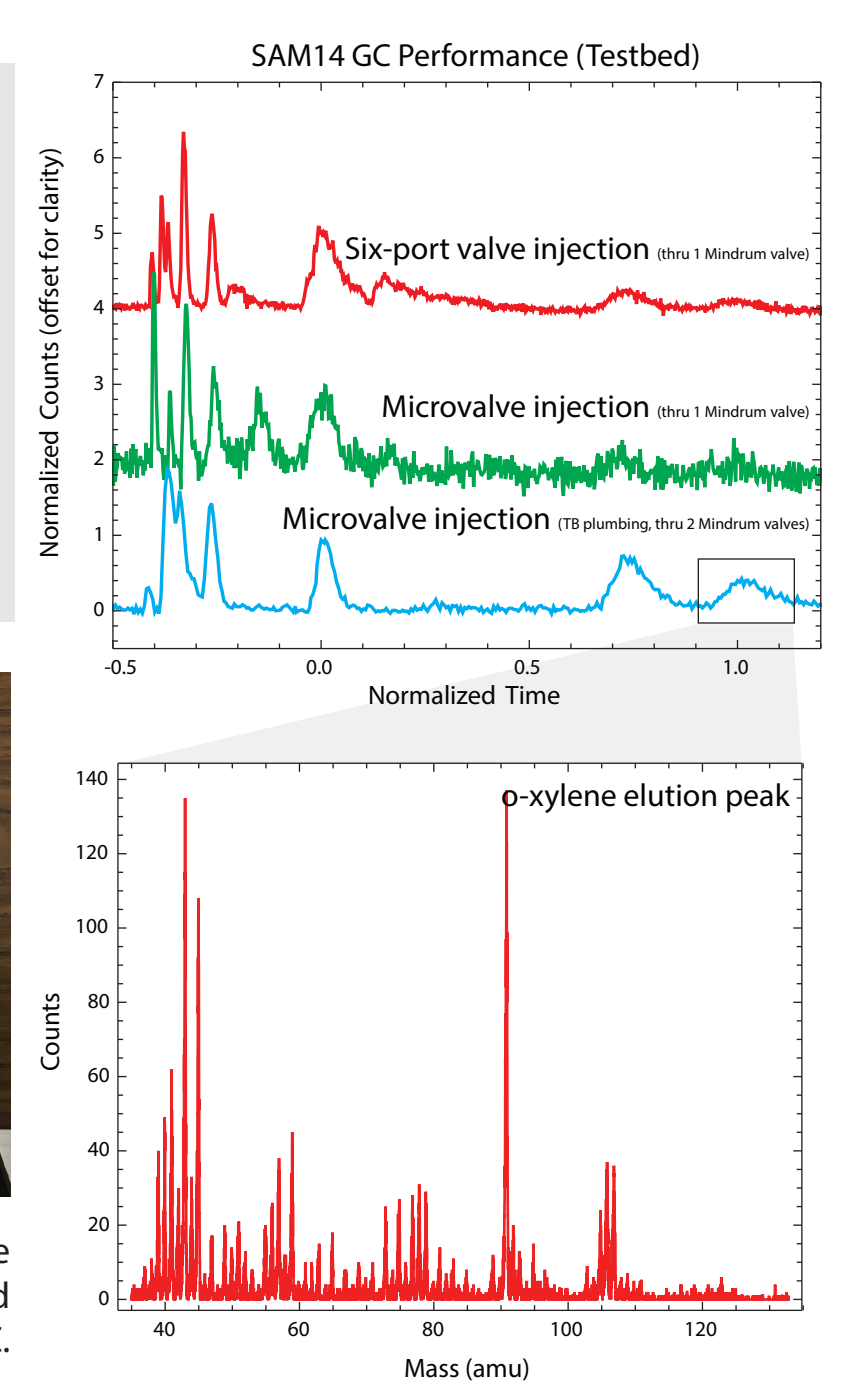
## Testbed Performance

### SAM Development Stages:

1. **Prototype:** Fabricate and test individual GC elements with non-flight QITMS. (Done!)
2. **Testbed:** Implement and test packaged GC unit with nonflight QITMS. (Underway!)
3. **Engineering Model:** Interface GC unit with flight QITMS.
4. **Flight Model:** Implement flight control electronics.

### Testbed Checklist:

- Fabricate MC, PC and MV
- Build GC control electronics
- Develop GC control software
- Construct the GC unit
- Test GC through MV/PC/MC using the GC unit interfaced with nonflight QITMS



## SAM Electronics

### SAM Operations

- Timing control for duty cycles
  - Open/close valves
  - Toggle heaters, pumps, fans
- Generate rf, HV, pulses for QITMS
- Sensor input/analysis
- MS signal input/analysis

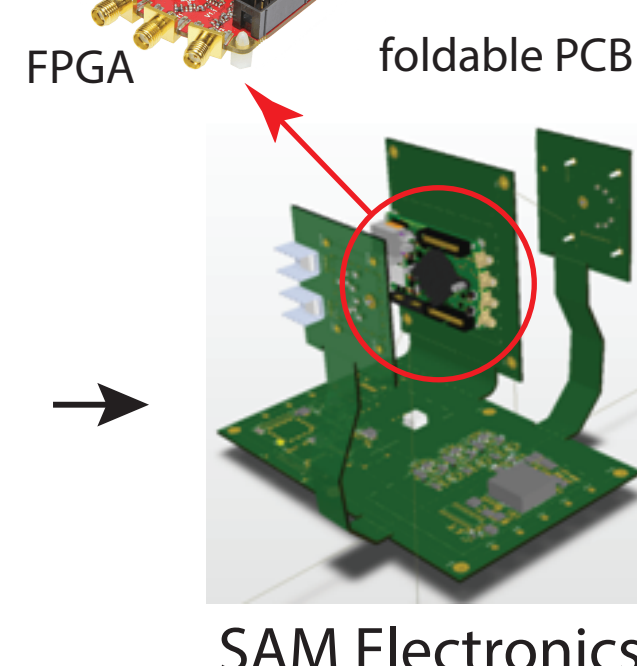
→ FPGA

### QITMS Electronics

- ~1 MHz, 1 kV ion trapping radiofrequency (rf)
  - Rf generated by FPGA
  - Amplified by resonant circuit
- Various pulsed DC signals for ion trapping
- Various pulsed DC signals for ion optics
- High current for EI filament (ion production)
- Electronics for ion signal detection
  - HV for CEM
  - CEM signal counting/discrimination
- Internal signal handling analysis
- All this with low noise!

### Testbed Electronics for GC Unit

- Simple Valve Heater Control Electronics (VHCE) for low-level tests
- Timing controlled by Numato Labs microcontroller
- QT GUI for software control
- Multiple ADCs for temperature, pressure sensing



## Future Steps and Prospects

### Testbed Stage:

- Fabricate and implement bonded PC/MV/GC GC unit
- Finalize GC control electronics
- Test the Testbed

### Onwards to the Engineering/Flight Model:

- Interface GC unit with flight QITMS and chamber
- Finalize optimal MEMS GC design/composition
- Finalize and implement flight electronics
- Package the SAM
- Test and test and test and test...

Prepare for Orion spacecraft?

### Other Flight Missions?

Can we adapt and use this PCGC/QITMS device to look for evidence of life in our solar system?

# A 2 THz Schottky Solid-State Heterodyne Receiver for Atmospheric Studies

**J. TREUTTEL, E. SCHLECHT, J. SILES, C. LEE, R. LIN, D. GONZALEZ and I. MEHDI (389A)**

Both the interstellar medium and planetary atmospheres are incredibly rich in molecular species with spectral rotational and vibrational signatures that lie in the 1-10 THz frequency range. The atomic oxygen (OI) emission at 2.06 THz (145.525  $\mu\text{m}$ ) is one of the two brightest emission lines in the terrestrial thermosphere and has been observed from balloon, sounding rocket and orbital platforms. Schottky diode front-end receivers have been demonstrated up to 2.5 THz with a CO<sub>2</sub>-pumped methanol gas laser local oscillator (LO) source [1]. However, recent developments in Schottky multiplier sources show that sufficient power can be obtained at 1 THz to drive a 2 THz sub-harmonic mixer. This makes possible the development of a 2-THz all solid state front-end heterodyne receiver that can be deployed on CubeSat or similar miniature platforms. We will describe the 2THz receiver front-end key parameters and give a global overview of the system in order to understand the different sub-system interactions and their implications on the 2THz receiver performance and its dimensional compactness. We will present the status of the laboratory demonstrator and address novel solutions including a novel bias-able sub-harmonic 2THz mixer under fabrication at MDL.

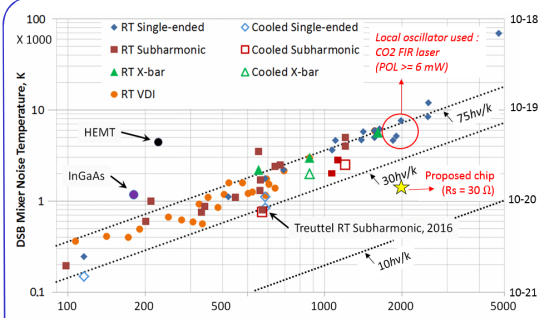


Fig. 1: State of the art Schottky Mixers [Courtesy : JPL, VDI, LERMA-LPN, Chalmers, ...]:

### Receiver requirements :

- High spectral resolution receiver (typical  $v/\Delta v \sim 106$ )
- Room temperature (could be passively cooled down to  $\sim 150\text{K}$ )
- Low-power (current goal  $< 40\text{W}$ , ultimate goal  $< 10\text{W}$ )
- Compact and Low mass (goal  $10 \times 10 \times 10\text{ cm}^3$ )

### Possible target missions:

- DYNAMIC (Dynamical Atmosphere Ionosphere Coupling), 2014 Roadmap as a Solar Terrestrial Probes (STP) mission.
- Concepts responding to the Decadal Survey DRIVE (Diversify, Realize, Integrate, Venture, and Educate) initiative.

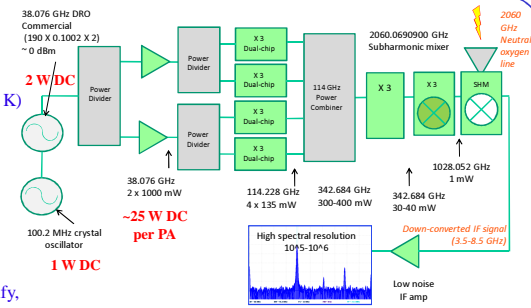


Fig. 2: Proposed 2 THz all-Schottky heterodyne Receiver scheme working at room temperature

### Receiver key parameters: Low parasitics (R-L-C) / LO power availability (mW)

#### Solution 1 : A novel antiparallele bias able 2THz Sub-harmonic mixer configuration

- combines both on chip capacitor and a planar transmission line to differentiate the RF, LO and IF port directly at the diode cell level
- Low loss transmission lines suspended by gold beam leads on both sides of the chip : designed to minimize the loss while providing effective impedance matching.
- A photolithographic backside process (MDL JPL) is used in order to reduce the substrate parasitic loss at diode cell level, and below the transmission lines so that the membrane thickness does not affect the mixer performance.
- The dimensions are defined to ensure that the RF and LO signals are propagated with the quasi-TEM mode of the central channel line on two different channel sections with respectively 140, 160 dB/m loss at RF frequency, and 550 to 800 dB/m loss at the LO frequencies.
- The methodology uses a combination of nonlinear multi-harmonic circuit simulations (Agilent ADS) and 3-D electro-magnetic simulations (Ansoft HFSS)
- A serie resistance of  $30\ \Omega$  will be achieved for a epilayer structure dedicated for mixing application.

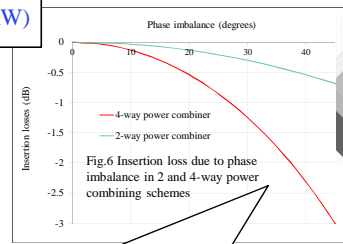


Fig. 6: Insertion loss due to phase imbalance in 2 and 4-way power combining schemes

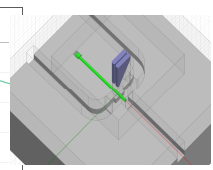


Fig. 7: K-band Magic tee used to reduce the total phase imbalance

#### Solution 2 : A 4-way Power combined 110 GHz Source

- The local oscillator (LO) source consists of a fixed-frequency DRO at 38 GHz which output is split and amplified in two separate amplifiers, each giving over a watt of power at Ka-band. These are then fed into a cascade of three triplers at 114GHz, 350 GHz and 1 THz in order to generate the LO signal required to pump the sub-harmonic mixer. The first 114 GHz stage and second 350 GHz triplers feature dual-chip triplers based on [2]. Despite their high-power handling and efficiency, their performances reaches an optimum at a designed input power. Therefore we use power combining techniques to raise up the power above 30 mW at 350 GHz. The most suitable option consists in combining four separate branches, each consisting of a dual chip 110 GHz to obtain around 300 mW to drive the 350 GHz tripler stage.
- A tradeoff between insertion losses introduced by the coaxial interfaces after the amplifiers and the losses from the phase imbalance is considered. (see Fig. 6).
  - Ka-band magic tee combiners minimize a total phase imbalance below 22 degrees, so that the corresponding insertion losses remain below 0.5 dB (see Fig. 7).
  - A phase shifter is added to the schematic shown in Fig 2. and is used to compensate the amplifier phase mismatch.

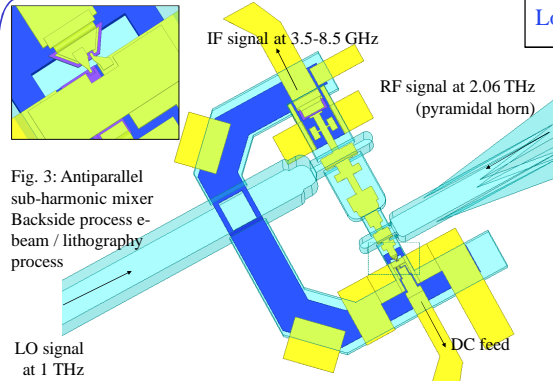


Fig. 3: Antiparallele sub-harmonic mixer Backside process e-beam / lithography process

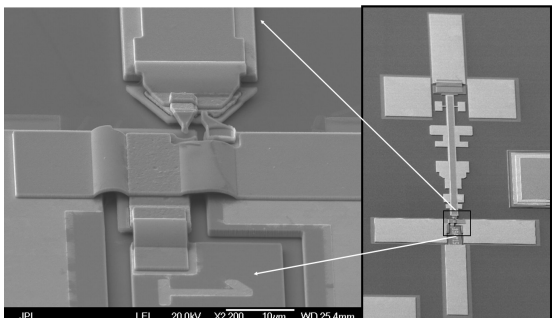
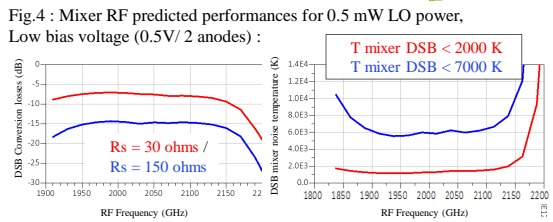


Fig. 5 : Fabricated mixer at MDL- JPL

The current fabricated mixer features a multiplier-based epilayer thickness, with an expected serie resistance  $R_s = 150\ \text{ohms}$ .

Recent developments in Schottky multiplier sources show that sufficient power can be obtained at 1 THz to drive a 2 THz sub-harmonic Schottky mixer. This makes possible the development of a very compact 2-THz all solid state front-end heterodyne receiver that can be deployed on miniature platforms. We present the development of a novel 2.06 THz bias-able sub-harmonic mixer circuit proposed to reduce the LO power requirements down to a LO power level of 0.5 mW with predicted DSB mixer noise temperature between 2000 K and 6,000 K respectively for an ideal optimal and non-optimal Schottky contact wafer layer structure. The predicted output power of the LO chain is between 1 and 3 mW at 1.03 THz, depending strongly on the power available from the combined 343 GHz pump chains. At the time of this writing the antiparallele pair mixer configuration is being fabricated at the Micro-Device Laboratory JPL, and the 350 GHz LO driver chain under assembly.

# THz Heterodyne Array Development for Suborbital Missions

Principal Investigator: Jenna Kloosterman (389A)

Jonathan Kawamura (389A), Jose Siles (389A), Alejandro Peralta (389A), Robert Lin (389A), Fahouzi Boussaha (Observatoire de Paris), Bruce Bumble (389I), Choonsup Lee (389A), Imran Medhi (389A)

## Introduction

### Key Science Goal:

Understanding the lifecycle of clouds of gas and dust in the Interstellar Medium (ISM)

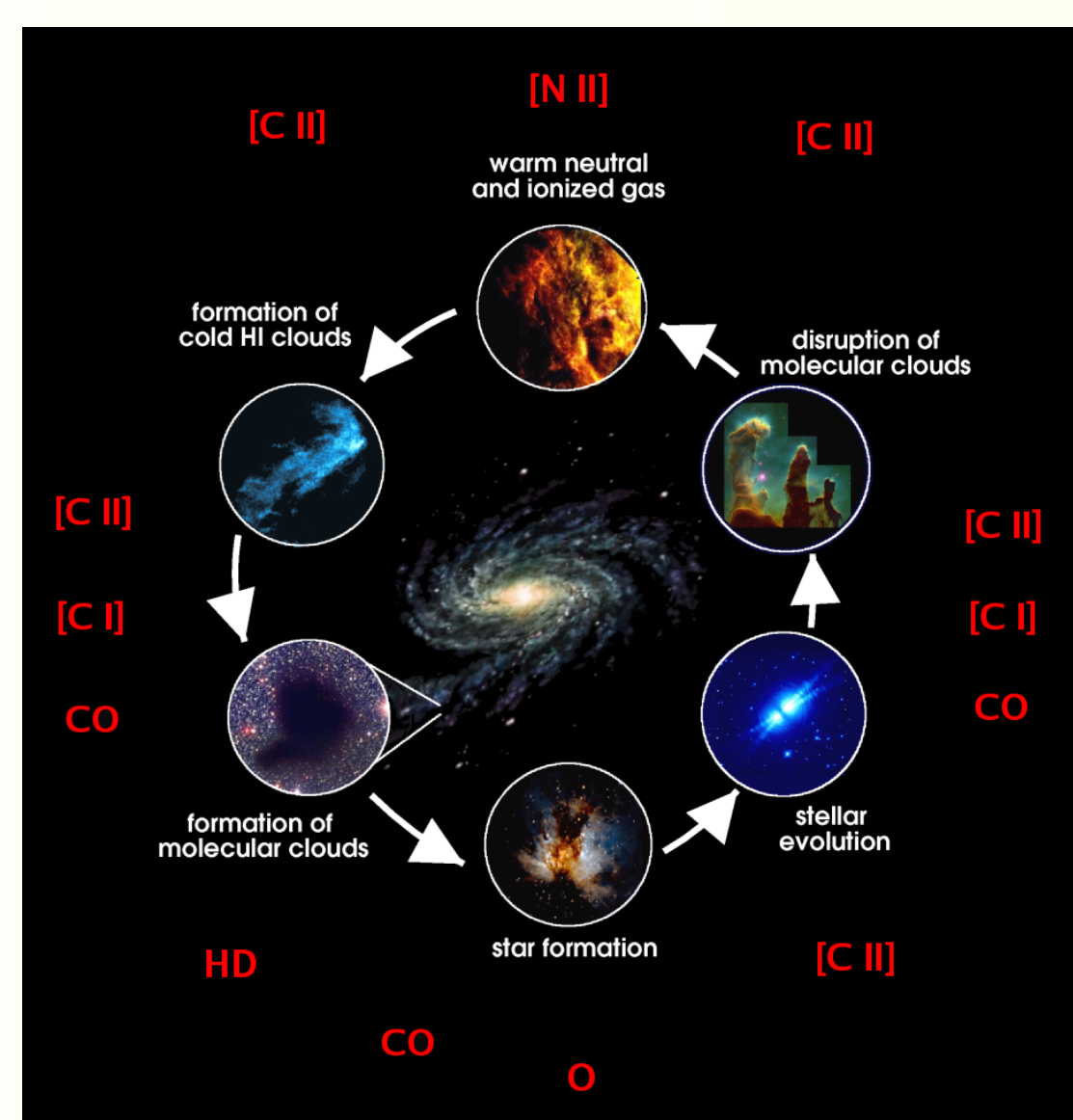


Image credit: Craig Kulesa and Chris Walker

### Heterodyne receivers

- Maintain wave coherence
- Provide high spectral resolution ( $v/\Delta v \geq 10^7$ )
- Provide high sensitivity

### THz (defined as 0.3-3 THz) heterodyne receivers require the development of:

- Local Oscillator (LO) sources
- Mixers

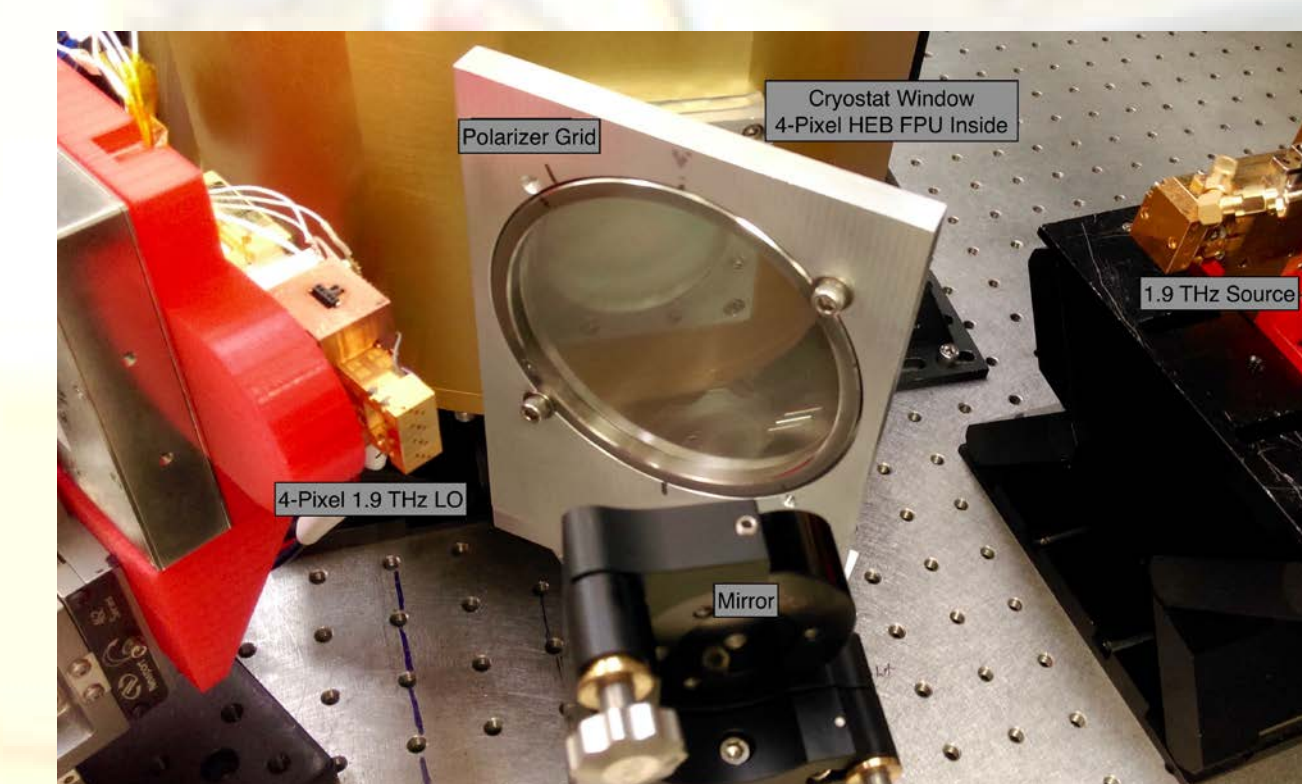
### THz heterodyne arrays are needed to:

- Detect atomic and molecular tracers of the lifecycle of the ISM including CO, N<sup>+</sup>, C<sup>+</sup>, and O
- Increase mapping efficiency
- Provide high resolution spectra to understand large-scale kinematics

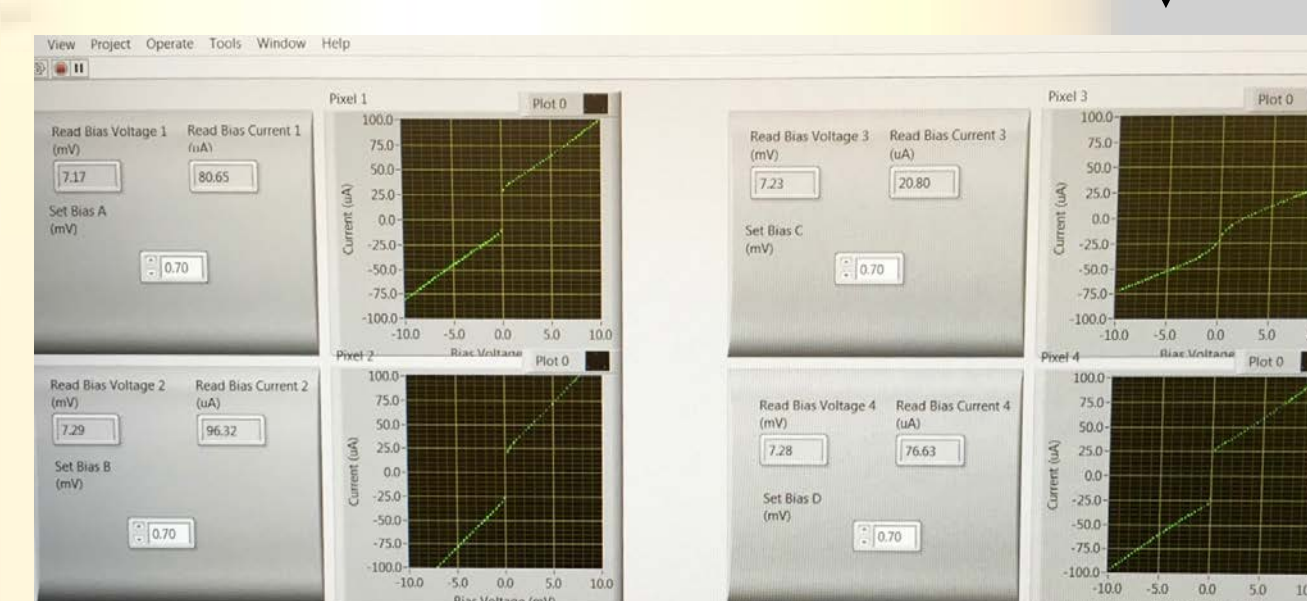
Water absorption in Earth's atmosphere requires that most astronomical observations above ~1 THz be taken from orbital or suborbital platforms including airplanes, balloons, and spacecraft.

## Results

LO signal is quasi-optically coupled through a polarizer grid and re-imaging optics to the focal plane unit (FPU) inside the cryostat. The focal plane consists of 4 waveguide-coupled superconducting hot electron bolometer (HEB) mixers. The resulting intermediate frequency (IF) is amplified via low noise amplifiers (LNAs), also housed inside the cryostat. The IF is then amplified again at room temperature, filtered, and down-converted to baseband. Spectra have been obtained using IBOB spectrometers.



Measurement setup for 4-pixel heterodyne array receiver verification at 1.9 THz.

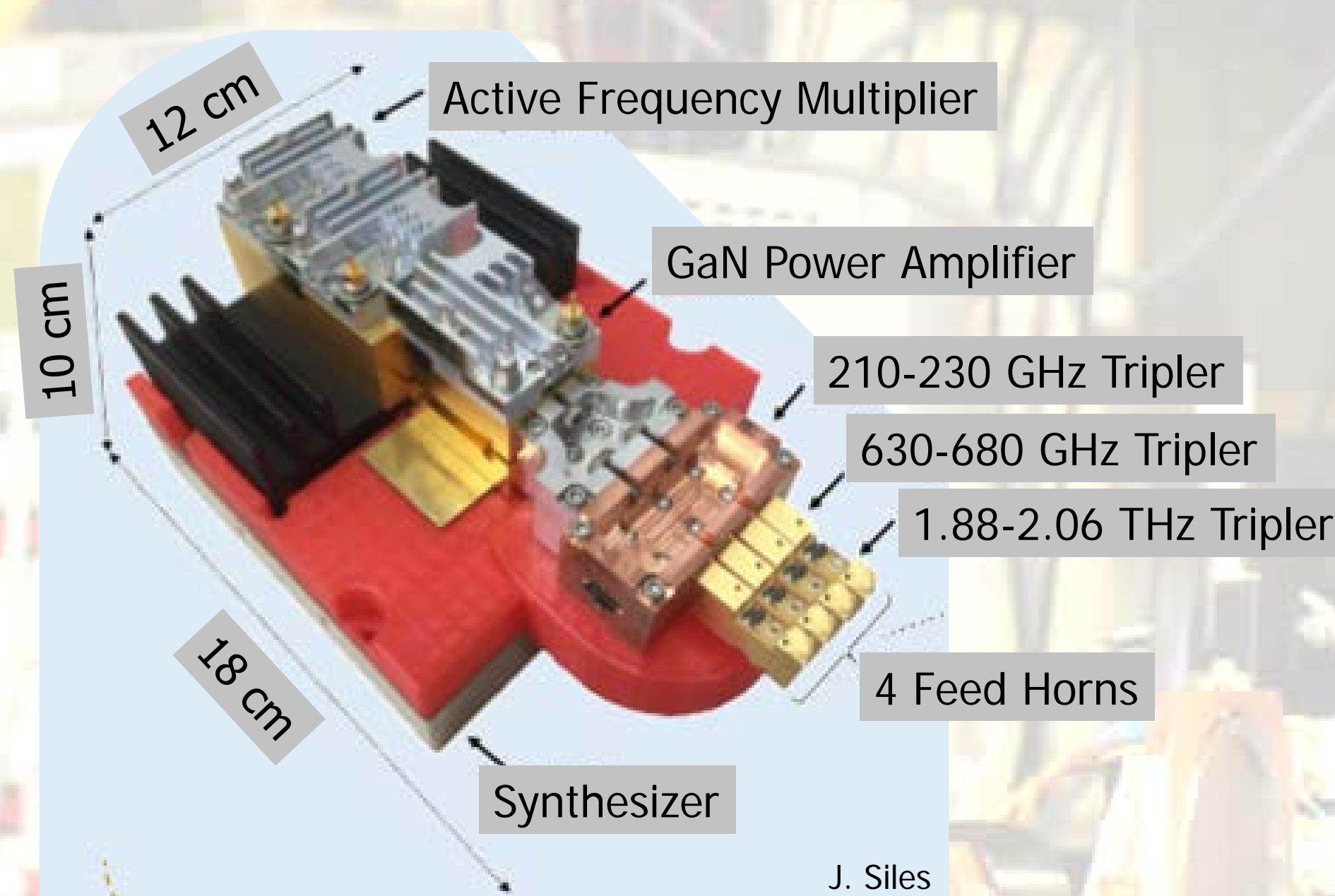


IV curves for 4 HEB mixers showing simultaneous pumping from the 4-Pixel LO (ie good coupling).

## Local Oscillator: 4-Pixel Multiplier Chain

Frequency multiplier chains are based on the harmonics output by GaAs Schottky diodes. The frequency multiplication process is as follows:

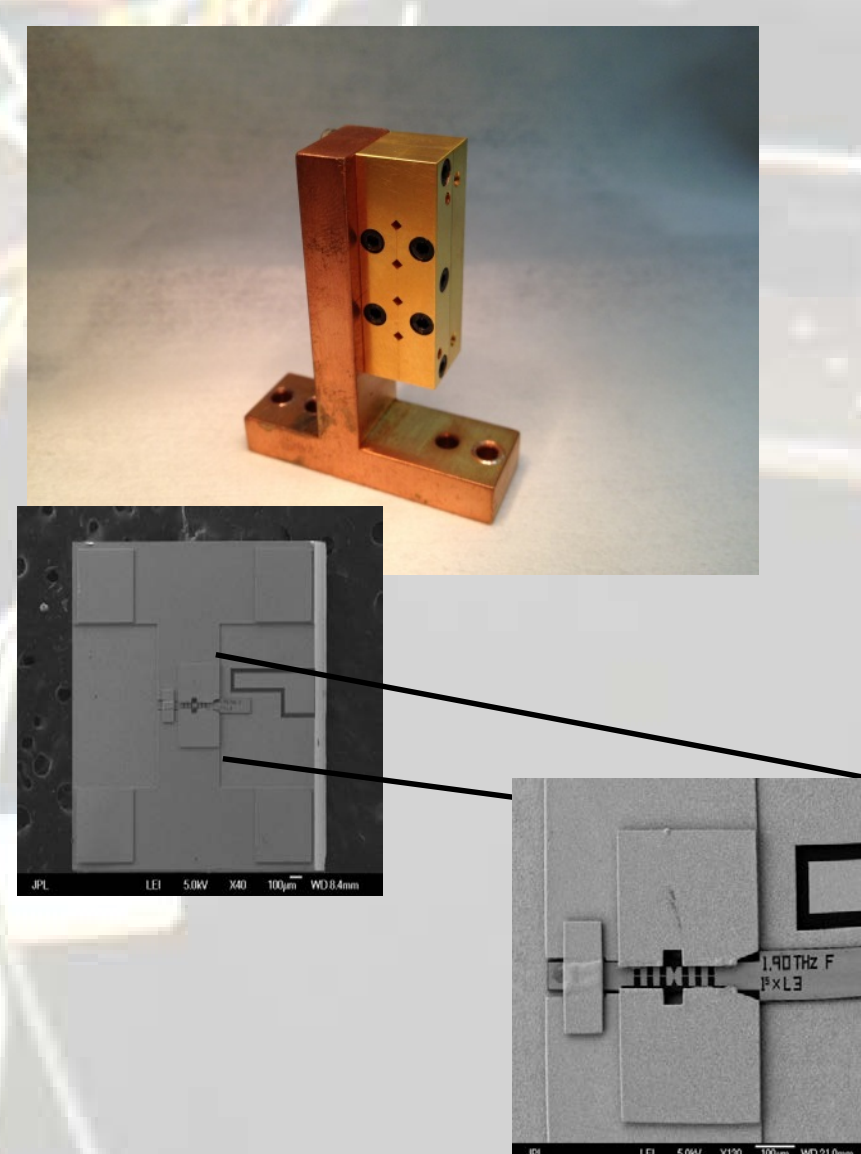
- Synthesizer ~8-10 GHz
- AMC active frequency multiplier (x8)
- GaN Power Amplifier
- 210-230 Tripler Diode
- 630-680 Tripler Diode
- 1.88-206 Tripler Diode



Each pixel puts out 10+  $\mu$ W of power at from 1.88 – 2.06 THz, which is more than sufficient to pump the HEB mixers. The power seen by the mixers can be optimized through the bias of the pixels and angle of the polarization grid.

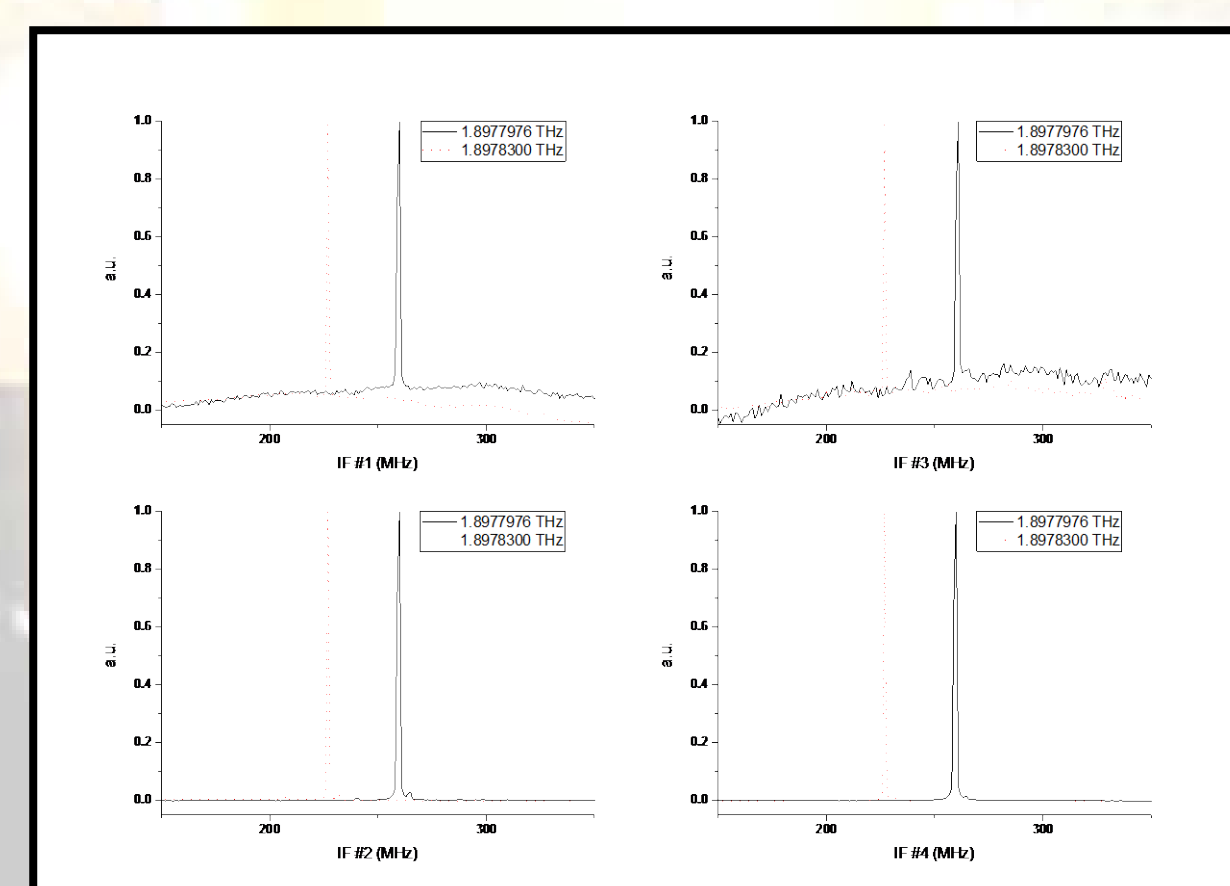
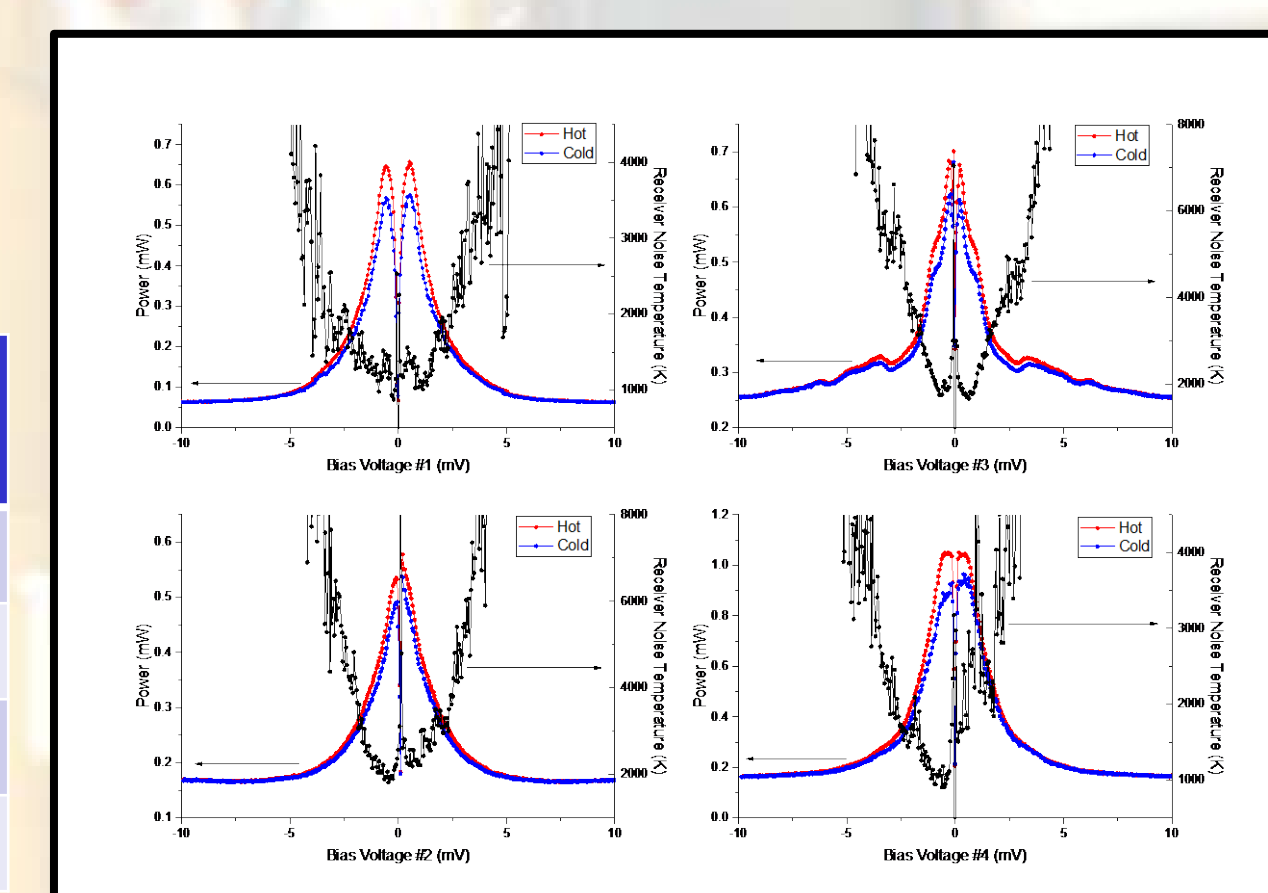
## Mixers: Hot Electron Bolometer (HEB)

- Superconducting mixers require  $T_b < \sim 10$  K
- Application of electrical bias and optical pumping from an LO source maintains a temperature distribution of "hot" electrons producing a resistive state at the center of the bridge
- Incoming signals modulate temperature causing a modulation in resistance.
- 4-pixel mixer block prototype fabricated with high precision Kern Machine
- Diagonal feedhorns have 5 mm spacing
- Full height waveguide designed for the C<sup>+</sup> line at 1.9 THz



Y-factors, the ratio of a room temperature blackbody to a 77 K blackbody, are measured to determine receiver sensitivity.

Pixel	$\Omega_{RT}$ ( $\Omega$ )	$\Omega_{100K}$ ( $\Omega$ )	$I_c$ ( $\mu$ A)	$T_{RX, DSB}$ (K)
1	109	126	130	900
2	82	93	165	1800
3	130	179	30	1700
4	105	120	185	900



A tone at 1.8977976 THz (see 1.9 THz source in top right picture) was quasi-optically injected via the polarizer grid and observed at baseband by all 4 pixels simultaneously. The tone moved through the band pass when it was adjusted in frequency. A second frequency is shown at 1.8978300 THz, which is ~32 MHz from the initial tone.

## Conclusions

We have demonstrated an end-to-end test of a 4x1-pixel heterodyne array receiver at 1.9 THz. The receiver:

- Has high sensitivity - ~900 K DSB noise temperature for the best pixels
- Design is scalable to other frequencies such as 1.46 THz for N<sup>+</sup>
- These new designs can be extended into larger arrays by stacking the 4x1 LO and mixer block modules
- Ready for flight in either balloon or airplane based observing platform



# Spectrometer and Radar Development from 90 to 600 GHz

Tristan Ossama El Bouayadi, Ken B. Cooper (389A)

Submillimeter-Wave Advanced Technologies Group (SWAT)

## Overview

### Science background

Comets are icy primitive objects that were formed at large distances from the sun. This property is the key element behind the preservation of their physical and chemical characteristics representing the early stages of the formation of our solar system. Consequently, the improvement of our knowledge about the comets is one step towards understanding the origins of habitable environments and especially life on Earth.

### A brief history of cometary exploration / Motivations

From ICE (launched in 1978) to Rosetta and its Philae lander (launched in 2004 and landed on 67P/Churyumov-Gerasimenko in 2014), cometary space missions have come a long way in their approach for **gathering information about the physical and chemical activity of comets**. While a potential future mission such as CSSR (Comet Surface Sample Return) places a sample return on top of its priorities, we believe that an observation instrument will complement our knowledge about comets by providing information on the interesting (and yet mysterious) dynamics of ice and gas cometary jets. For instance, following the legacy of previous instruments like HIFI and MIRO, this instrument would help evaluate the abundance of some chemical species on comets (such as water and its isotopes) and appreciate their similarities with planet Earth.

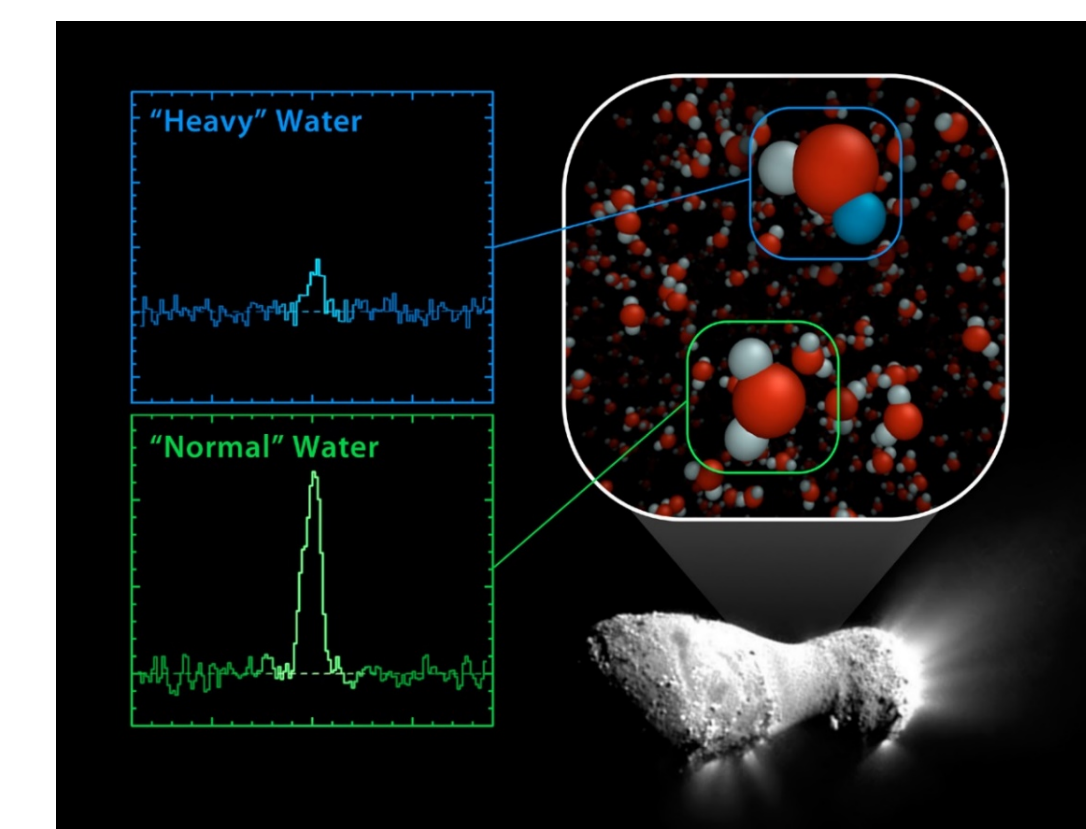


Fig.1) Astronomers have discovered that comet Hartley 2 possesses a ratio of 'heavy water' to light, or normal, water that matches what's found in Earth's oceans (NASA's Herschel Space Observatory), [1].

## GAISR project

GAISR stands for **Gas And Ice Spectrometer Radar**. This project aims to develop a fully integrated system, capable of performing **radiometric, spectroscopic and Doppler**-type measurements during approach and fly-by operations of a cometary exploration vehicle. GAISR would be the first fully integrated particle and gas remote sensing instrument combining a millimeter-wave radar and two spectrometers operating respectively around 95, 270 and 560 GHz. In this NPP Postdoctoral assignment, our goal is to support the characterization of IF, RF and quasi-optical subsystems from a Systems' Engineering perspective as well as to propose new solutions for their improvement.

### Submm-Wave, RF and intermediate frequency (IF) hardware

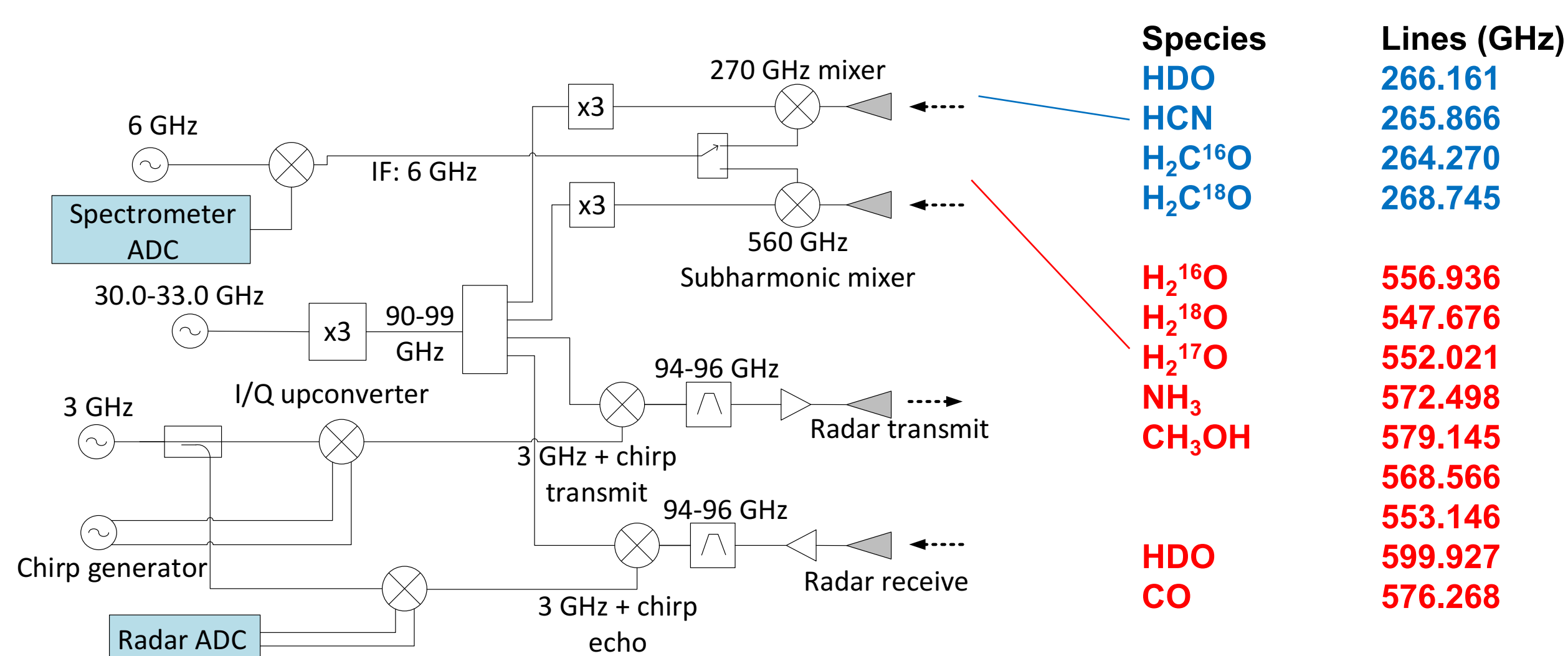


Fig.2) Block diagram of GAISR's back- and front-end subsystems. The frequency plan allows for the radar and spectrometer to share a single Ka-band synthesizer and IF processor. Courtesy of Ken B. Cooper [2].

The core submillimeter-wave components of the heterodyne receiver are the mixers and the local oscillator (LO) W-band source. GAISR capitalizes on state-of-the-art frequency multipliers and mixers using Schottky diode technology developed by MDL and SWAT teams. These efforts are supported by expertise in antenna design, analog and digital electronics as well as digital signal processing. The instrument targets 13 emission lines (4 for the 270 GHz channel and 9 for the 560 GHz channel respectively) and is tuned thanks to a CMOS synthesizer delivering a Ka band signal from a 50 MHz reference.

### Submm-wave heterodyne receivers test

Noise temperature measurements are performed using an in-house calibrated instrument. The Y factor technique consists of measuring the receiver's noise temperature (and received noise power) when an external noise source is ON and OFF (hot and cold). This can be achieved by using two similar absorbers at room (290 K) and cryogenic temperatures respectively (77 K for liquid nitrogen).

$$Y = \frac{N_{ON}}{N_{OFF}} \quad (eq. 1) \quad T_{mix} = \frac{T_{source}^{ON} - Y T_{source}^{OFF}}{Y - 1} \quad (eq. 2)$$

## Conclusion

Cometary exploration is nowadays considered not only a major part of space exploration but also a key element of Earth science. GAISR project supports these efforts by offering a compact, high-performance and comprehensive remote sensing instrument that provides valuable information about the physical dynamics and chemical composition of comets. This only can be achieved by using jointly high-TRL JPL technologies as well as innovative approaches to improve the RF back-end, mm/submm-wave front-end and quasi-optical components.

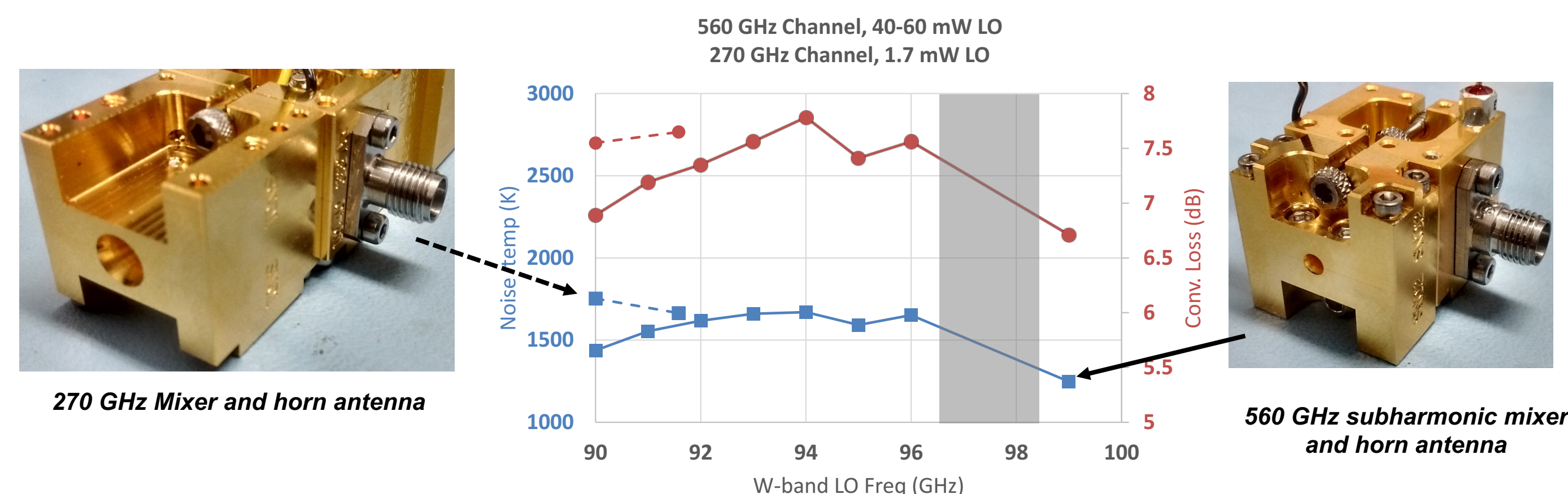
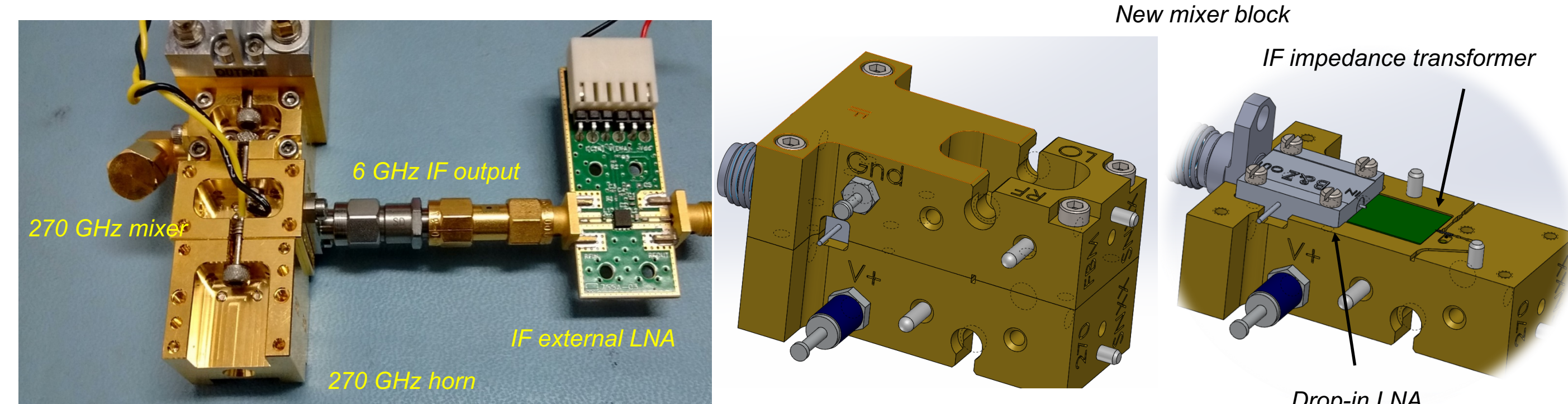


Fig.3) Measured noise temperature and conversion loss of the 270 GHz (dashed line) and 560 GHz (solid line) mixers with no external IF amplification.

### Mixer/LNA Integration

A reverse link budget is performed using the mixers' measured noise temperature and the Analog-to-Digital Converter specifications. This step allows us to determine the requirements of the IF low-noise amplifier in terms of gain and noise figure. The receiver's sensitivity can be improved by using a better LNA and by reducing the mixer's conversion loss according to equation 3. The interconnect losses can be reduced by co-integrating the LNA in the same block as the mixer as shown in Fig.4) (b).

$$T_{rec} \approx T_{mix} + \frac{T_{LNA} - 1}{G_{mix}} \quad (eq. 3)$$



	Mixer noise temp.	Mixer CL	LNA NF	LNA Noise temp.	Receiver noise temp.
Initial	2500 K	8 dB	1.5 dB	120 K	3290 K
Expected	2500 K	5 dB	0.6 dB	43 K	2643 K

Fig.4) Present 270 GHz receiver setup with external commercial LNA (a) and new integration concepting a drop-in LNA (b)

### Ongoing development of calibration targets

A common way of calibrating a submm-wave radiometer consists of using two reference loads at well known or monitored temperatures (hot and cold). For GAISR the cold load calibration is performed by pointing at the cold sky (2.7 K) while the hot calibration uses a high-performance conical load at room temperature. On the 2<sup>nd</sup> year of the NPP assignment, the efforts will be focused on the design of a low-mass and compact calibration target. The initial study involves at first a quantitative evaluation of the different sources of calibration error (standing waves, temperature gradient,...).

### References

- [1] <http://www.jpl.nasa.gov/spaceimages>  
[2] Ken B. Cooper *et al.*, "A Combination Millimeter-Wave Doppler Radar and THz Spectrometer for Planetary Science", EuMW/EuRad, London 2016 (accepted for publication)

# HIGH-EFFICIENCY UV SUPERCONDUCTING NANOWIRE SINGLE PHOTON DETECTORS

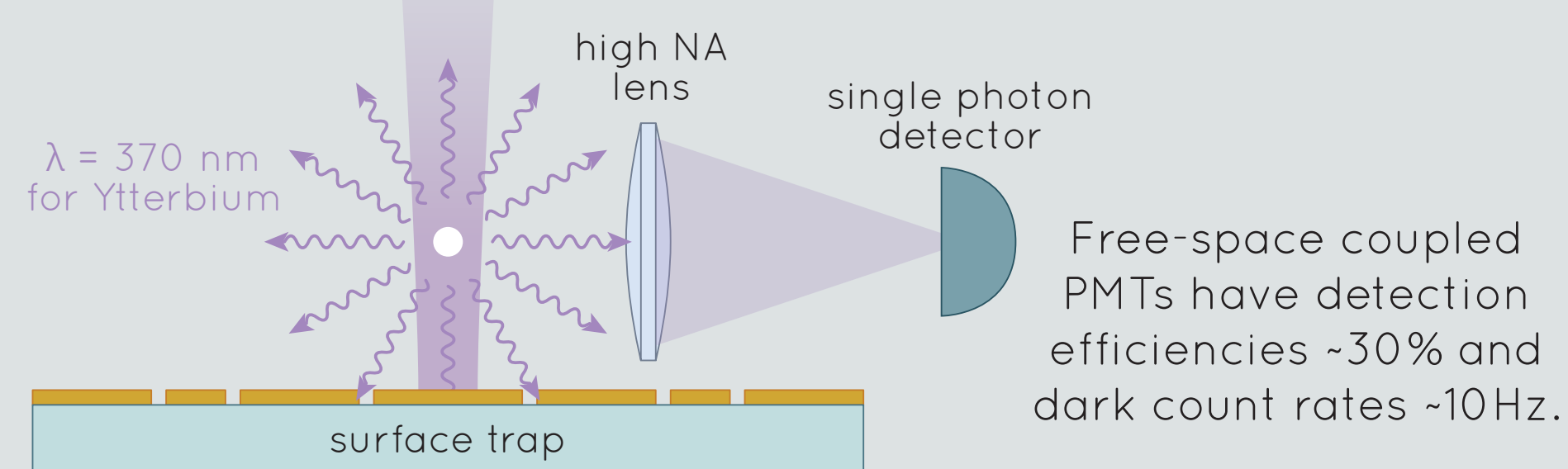
E. E. Wollman (389I), A. D. Beyer (389I), R. M. Briggs (389K), F. Marsili (389I), M. D. Shaw (389I)  
Jet Propulsion Laboratory, California Institute of Technology

V. B. Verma, R. P. Mirin, S. W. Nam  
National Institute of Standards & Technology



## OBJECTIVES

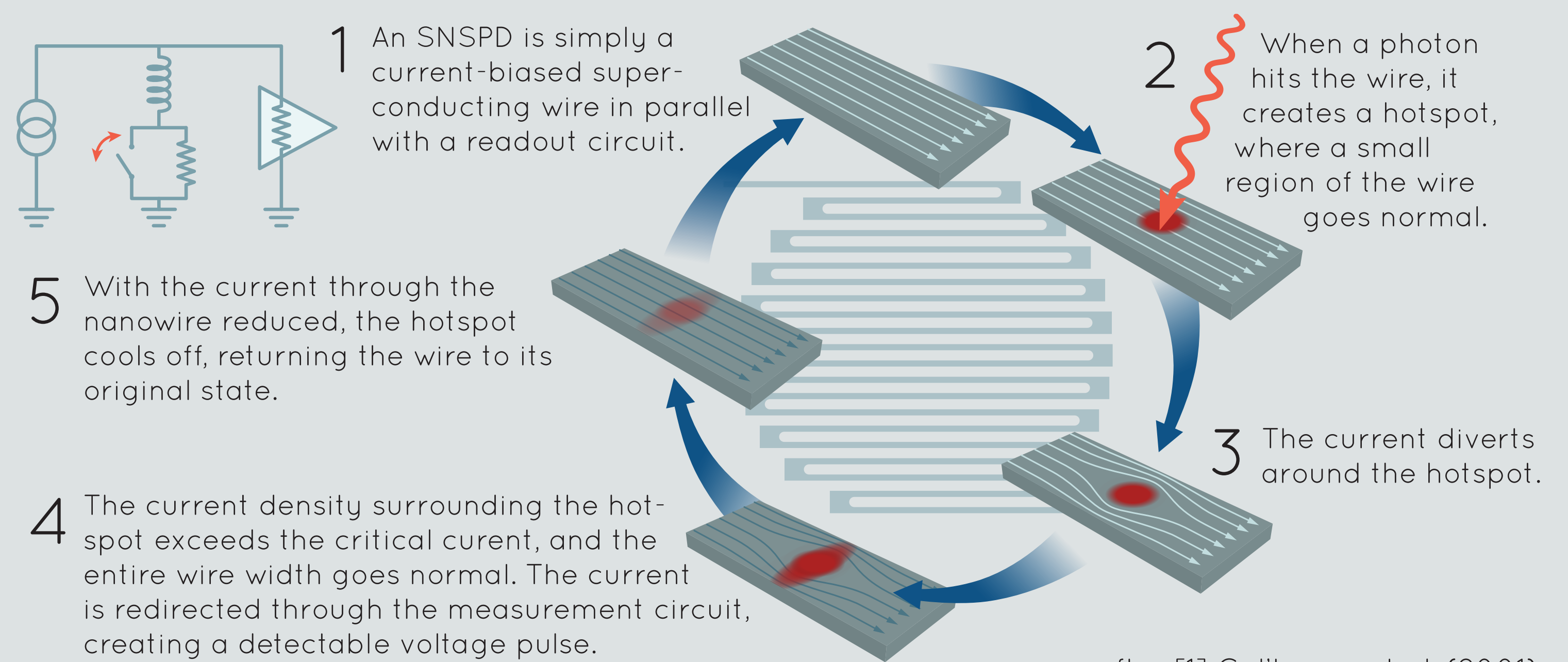
Trapped ion qubits have long coherence times and high fidelities. However, qubit readout via state-dependent fluorescence is slow due to inefficiencies in photon detection. We want to improve measurement time by an order of magnitude by replacing inefficient photomultiplier tubes (PMTs) with SNSPDs.



Requirements for Ytterbium ion trap SNSPDs:

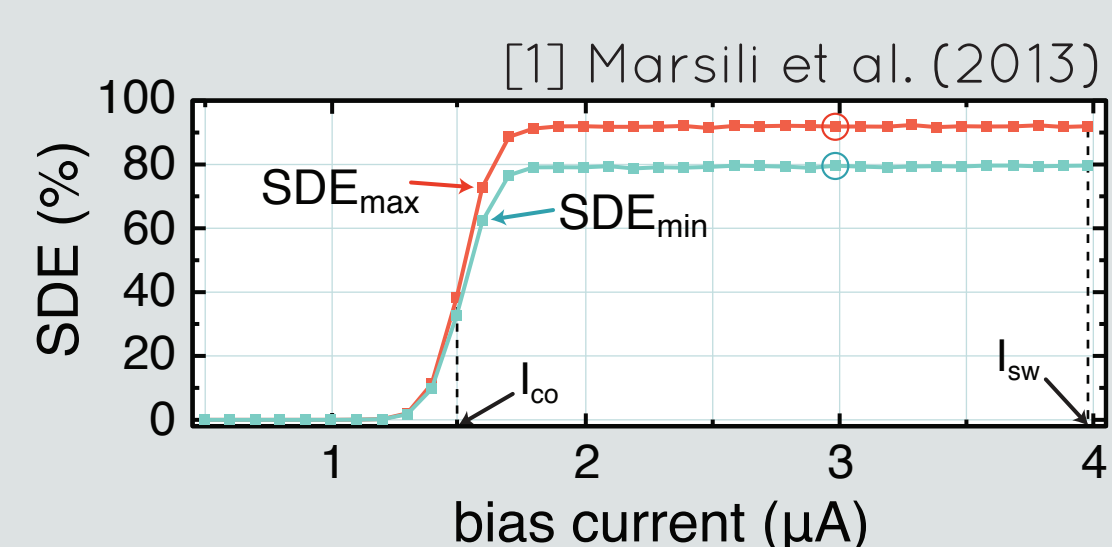
- High efficiency at 370 nm
- Low dark count rates
- Compatible with cryocoolers running above 3 K

## WHAT IS AN SNSPD?



after [1] Gol'tsman et al. (2001)

## WHY SNSPDS?

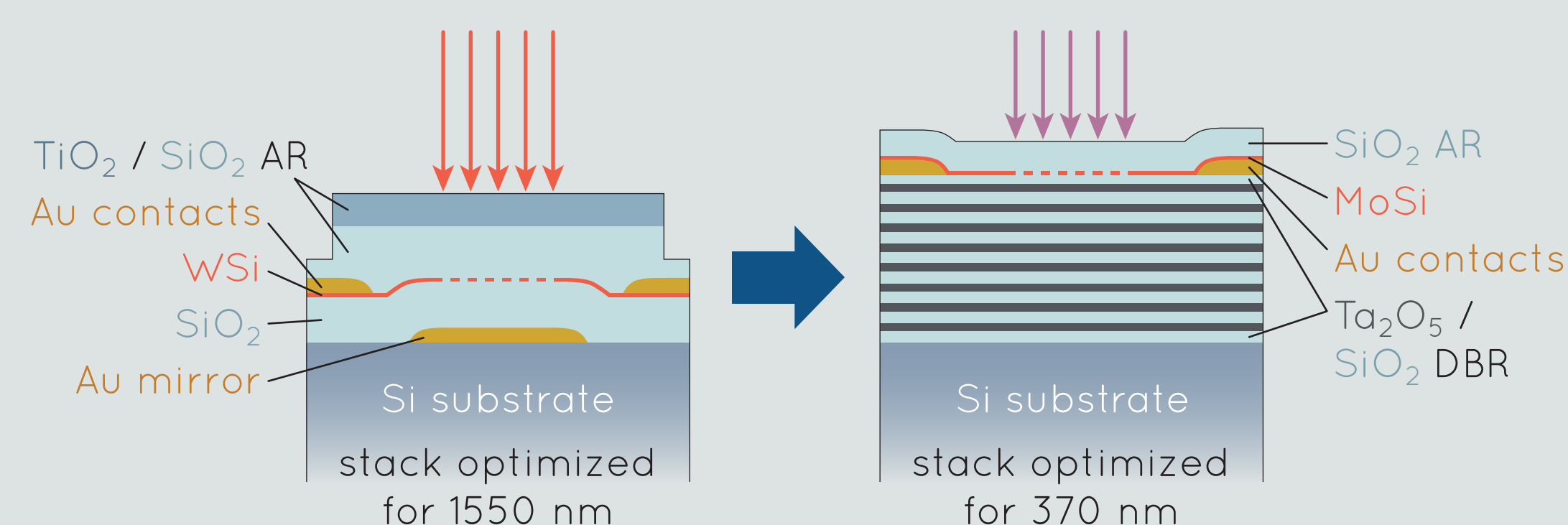


### JPL/NIST near-IR SNSPD capabilities

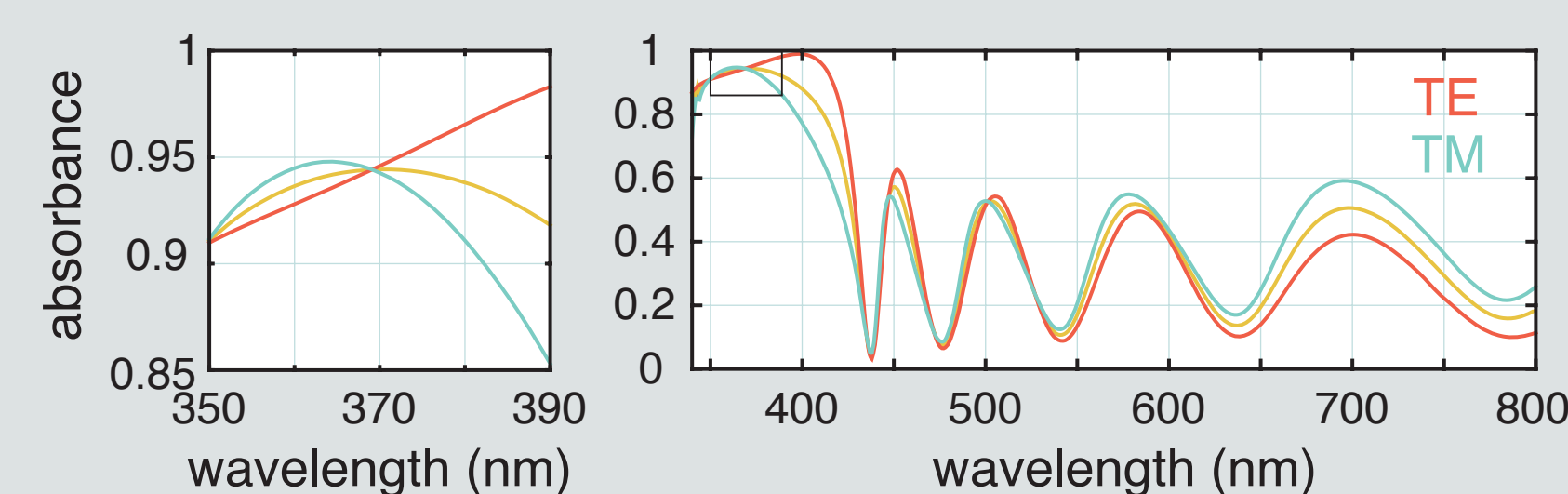
- 93% system detection efficiency at 1550 nm using WSi in an optical cavity
- Intrinsic dark count rate < 1 Hz
- ~100 ps timing jitter
- 40 ns reset time

SNSPDs should work well in the UV, but they are untested below 400nm.

## DESIGN & FABRICATION



Instead of a TiO<sub>2</sub> anti-reflection (AR) layer and gold back mirror, which both absorb light below 400 nm, we use a SiO<sub>2</sub> AR layer and a distributed Bragg reflector (DBR). We also use MoSi instead of WSi, because WSi's low critical temperature restricts its operation to < 1 K.

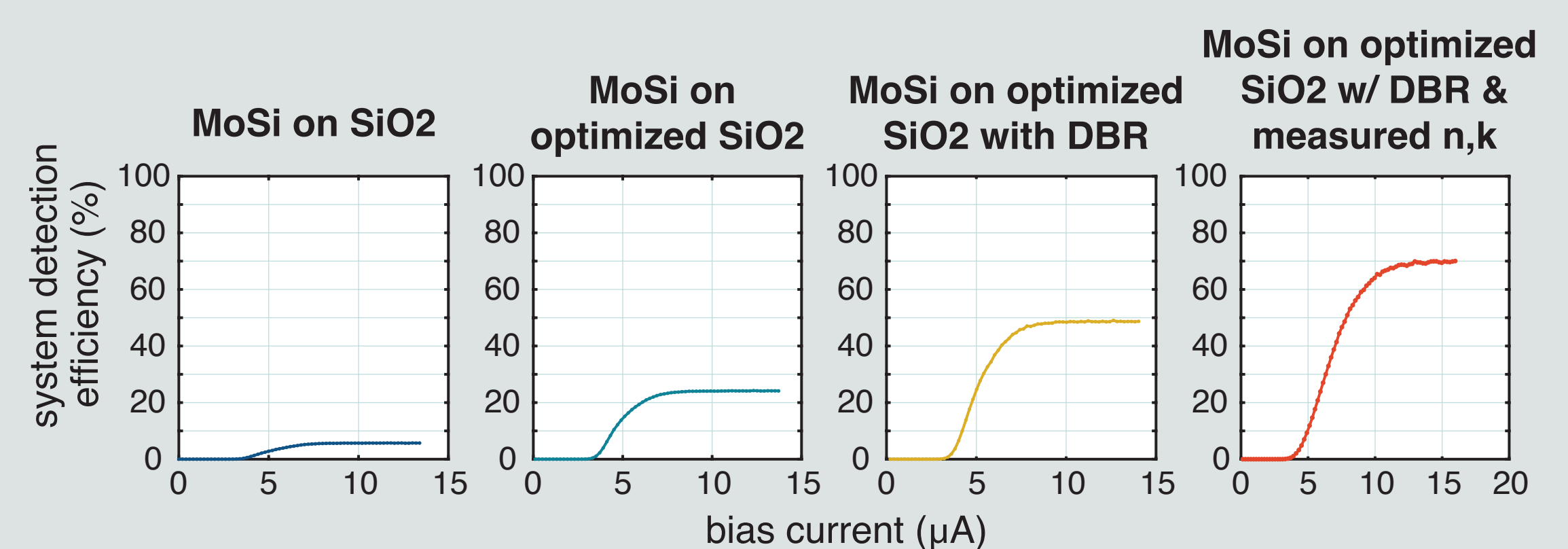


After optimizing the layer thicknesses, over 90% of light at 370 nm is predicted to couple into the nanowire layer.

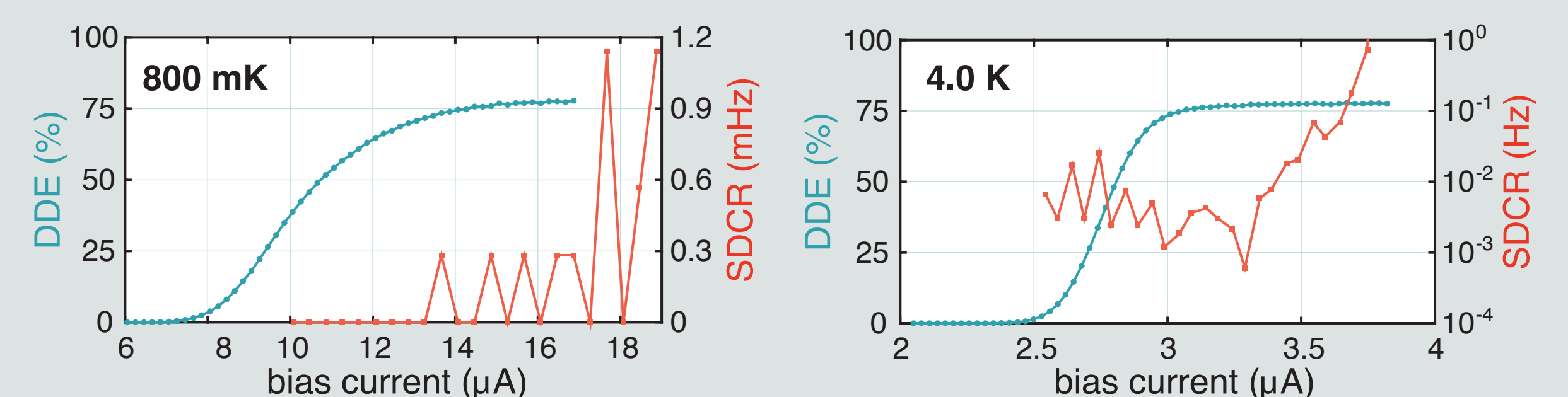


False-color SEM of the nanowire pattern. The active area (gray) is designed for coupling to a 10 μm core multimode fiber. Wire width, thickness, and pitch have been experimentally optimized for high detection efficiency and operation at high temperatures.

## PERFORMANCE



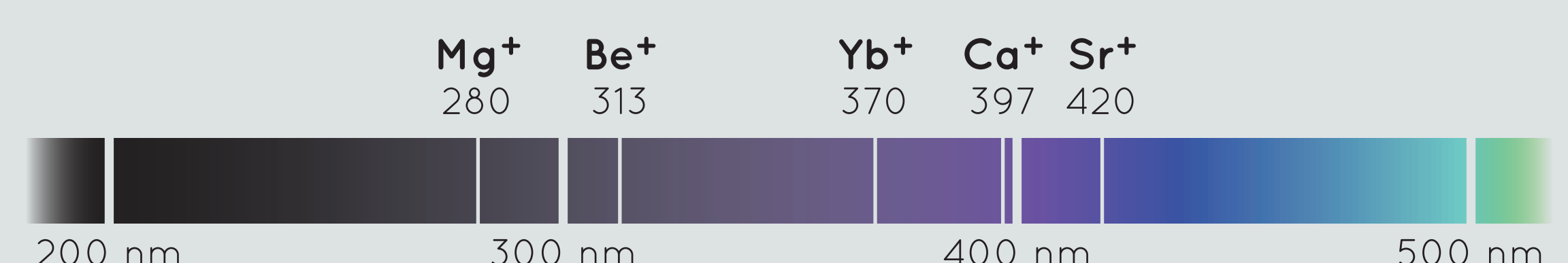
Initial devices without an optical stack were less than 10% efficient. After optimizing the stack using measured optical constants for all materials, the latest version has ~70% system detection efficiency. The fiber transmission in our system is < 90%, so the detection efficiency of the device (DDE) should be ~80%.



Below 1 K, we measure a system dark count rate (SDCR) of < 1 count per hour. This rate is measured with the detector connected to room-temperature optics, and without any filtering of blackbody radiation. At 4 K, the dark count rate increases to ~10 mHz.

## SUMMARY

- We designed, fabricated, and measured SNSPDs with ~70% system efficiency for 370 nm light at 4 K, with a dark count rate < 10 mHz.
- Using early, less-efficient JPL devices, Duke University has already improved their qubit readout time by a factor of 2.
- We are exploring shorter wavelengths for operation with other ion qubits.



## REFERENCES

- [1] Gol'tsman et al., "Picosecond superconducting single-photon optical detector," *Appl. Phys. Lett.* **79**, 705-707 (2001).  
[2] Marsili et al., "Detecting single infrared photons with 93% system efficiency," *Nat. Photonics* **7**, 210-214 (2013).

## ACKNOWLEDGEMENTS

This work is part of the EPICS collaboration in coordination with Jungsang Kim at Duke University and Christian Arrington and Peter Maunz at Sandia National Laboratories.

# YBCO kinetic-inductance bolometers (KIBs) for outer solar system missions

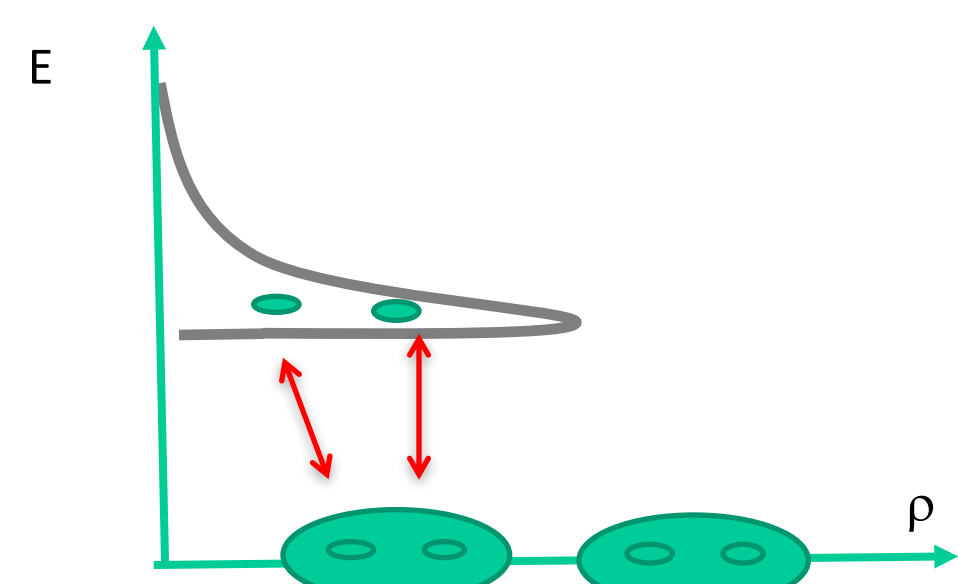
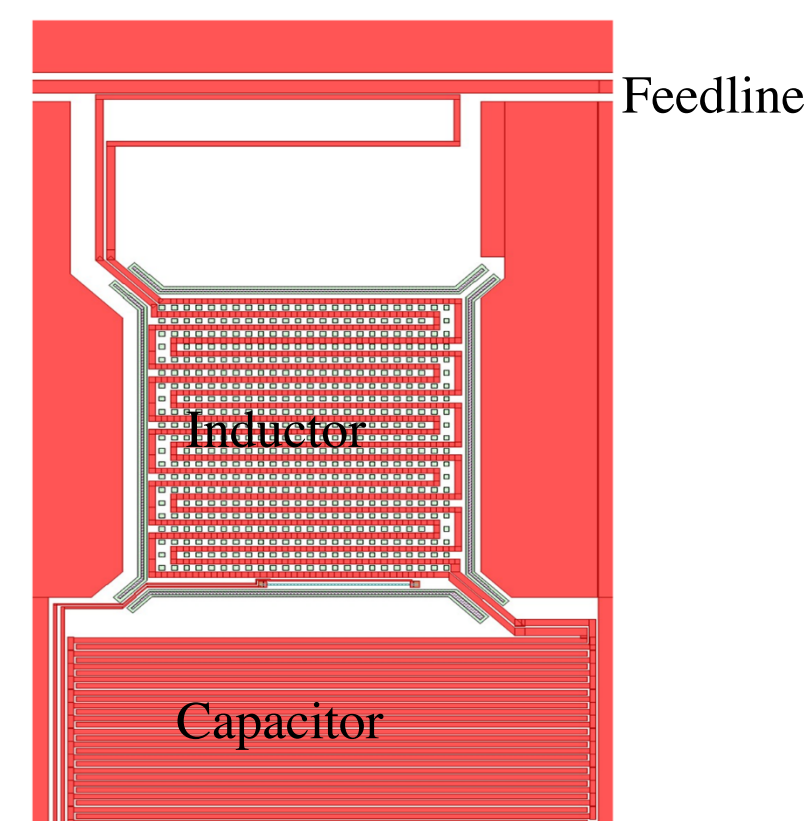
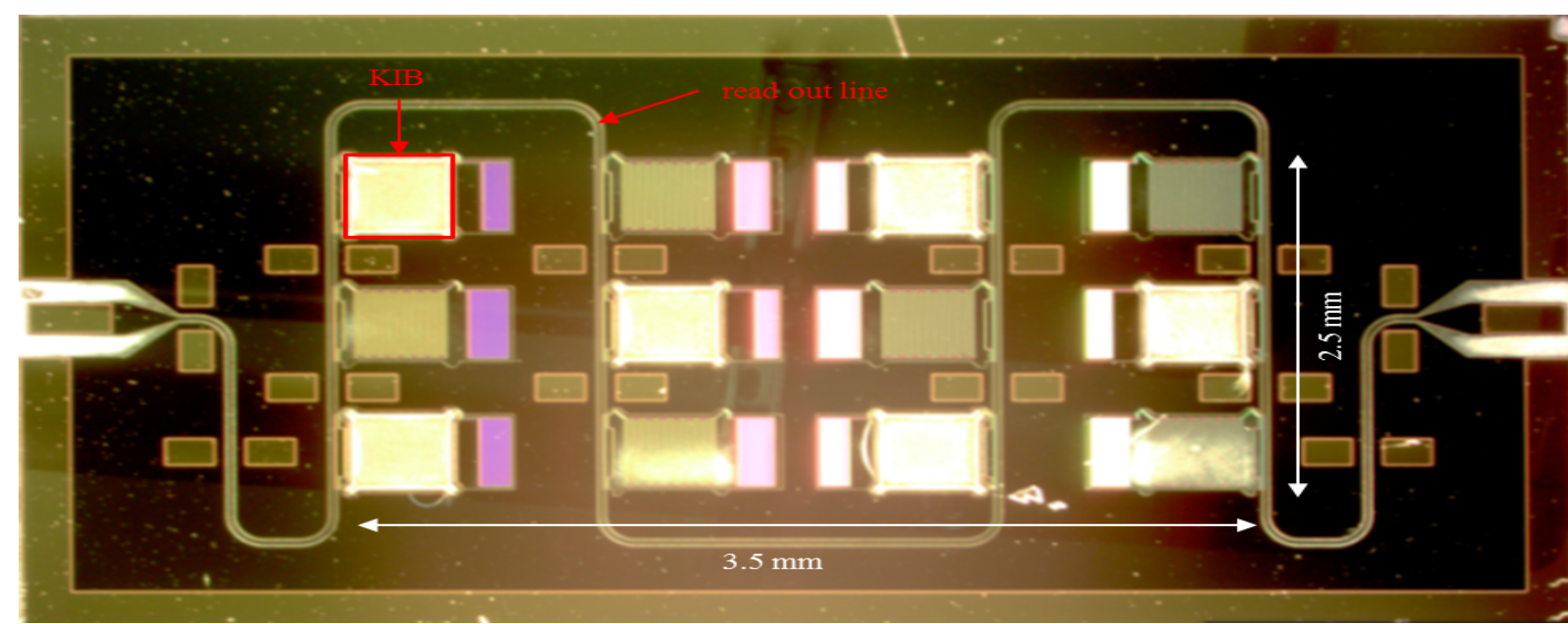
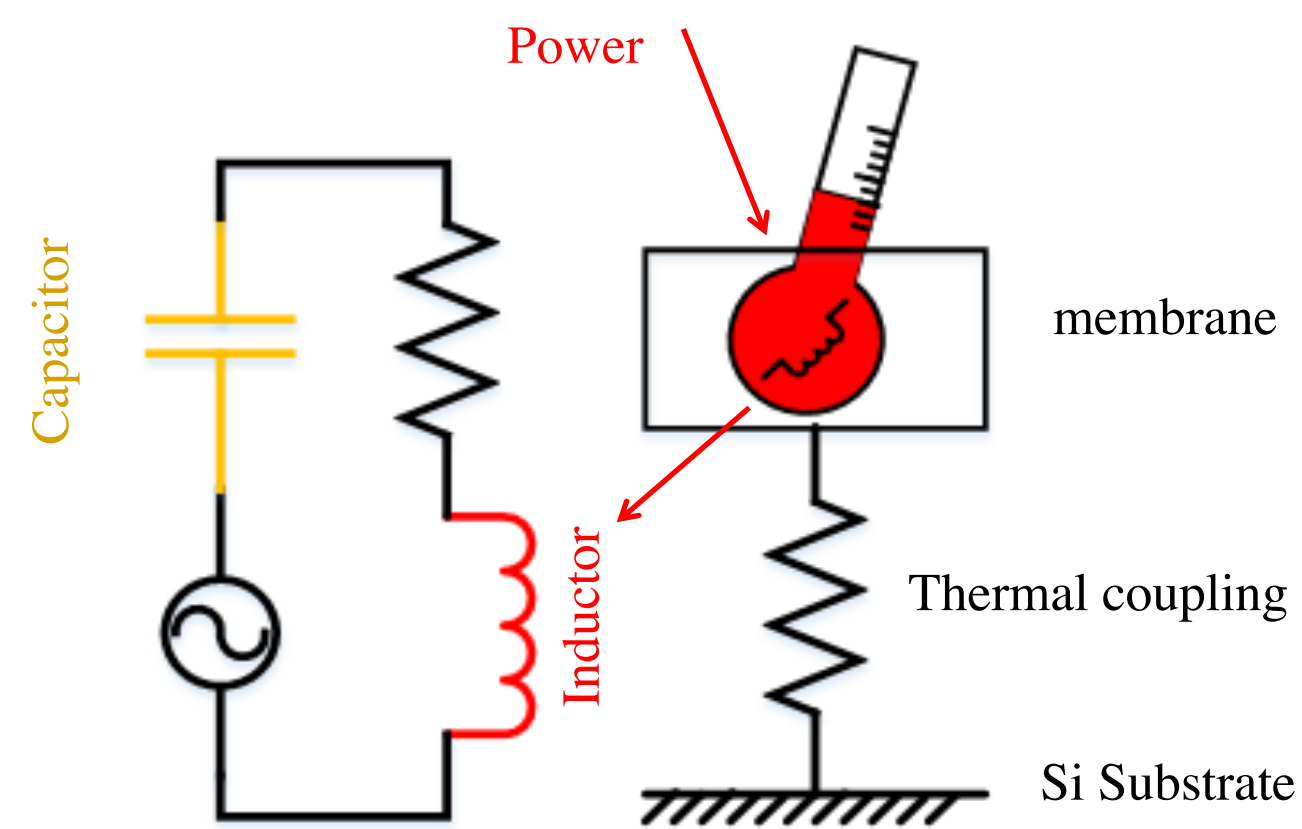
Ayan Chakrabarty (389)

M. A. Lindeman (382), B. Bumble (389), F. Marsili (389), E. C. Brageot (382),  
A. W. Kleinsasser (389), W. A. Holmes (389)

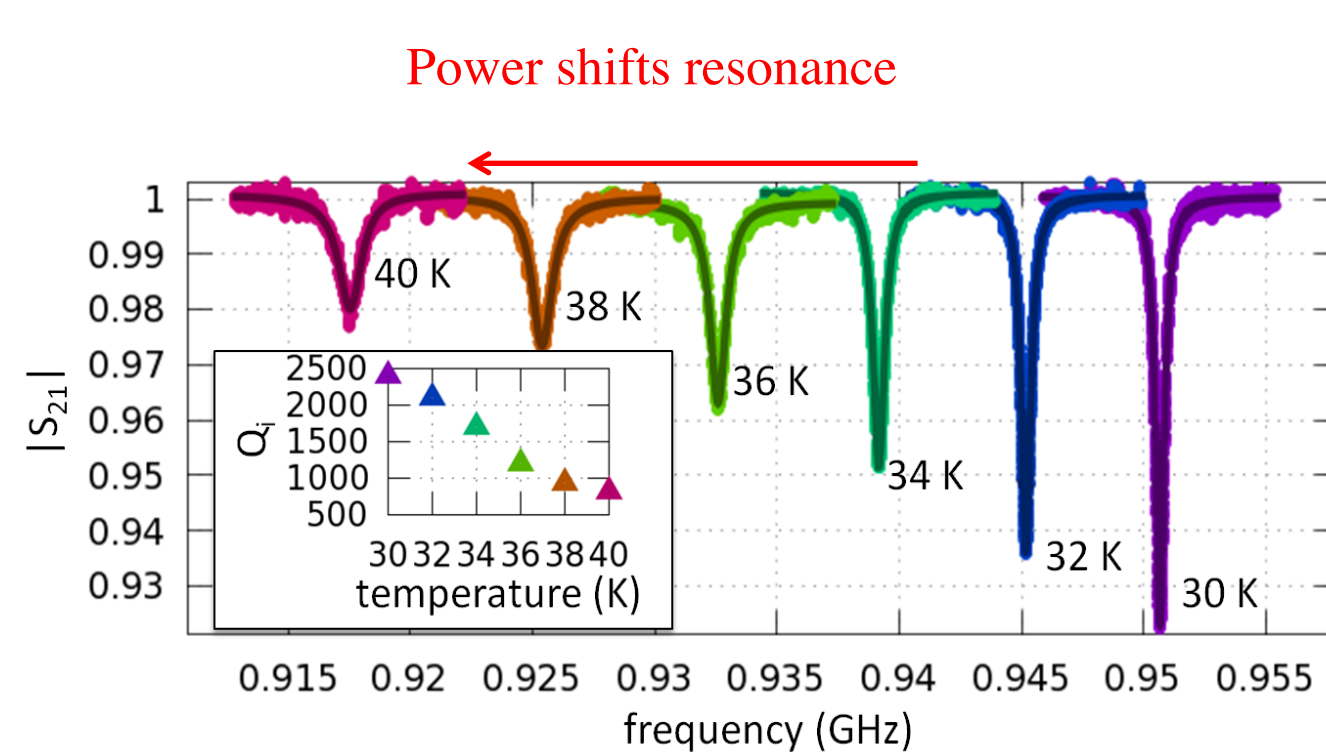
## Kinetic Inductance Bolometers (KIB)

### Kinetic Inductance Device (KID)

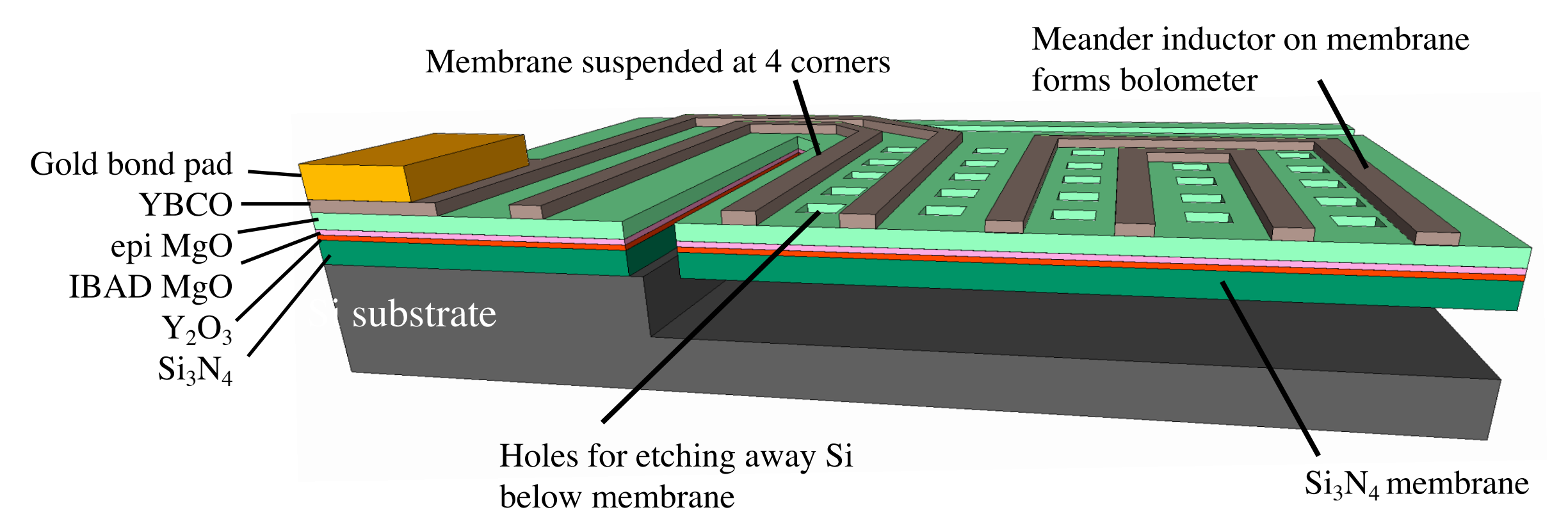
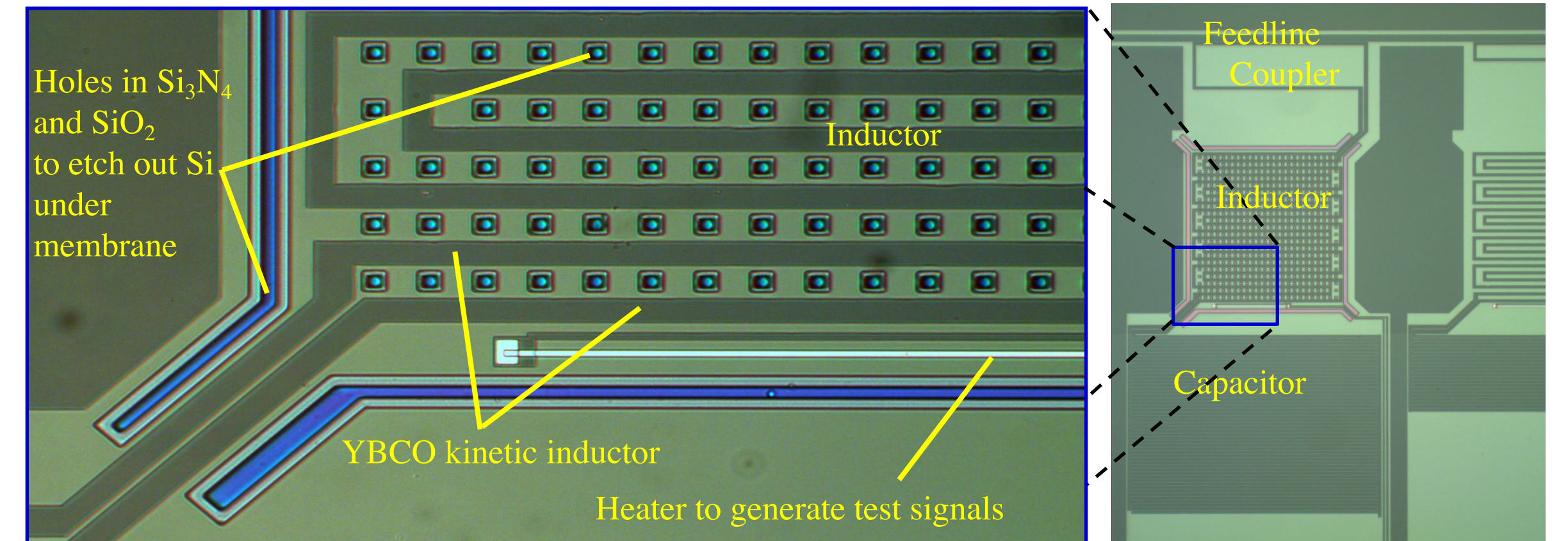
- Absorption of radiant energy warms membrane and inductor
- Kinetic inductance increases with temperature
- L-C resonance frequency of circuit decreases
- Resonator coupled to feedline for detector read out



- Quasiparticles responsible for inductance change
- In bolometer:**
  - KID is thermally isolated on membrane
  - Absorbed energy is thermalized
  - KID measures temperature
  - Heat slowly leaks out through weak thermal link
- Resonance moves significantly with temperature compared to width of resonance
- Or Equivalently: Reactance changes significantly compared to resistance in resonator
- 100 × More sensitive than other broadband detector technology.

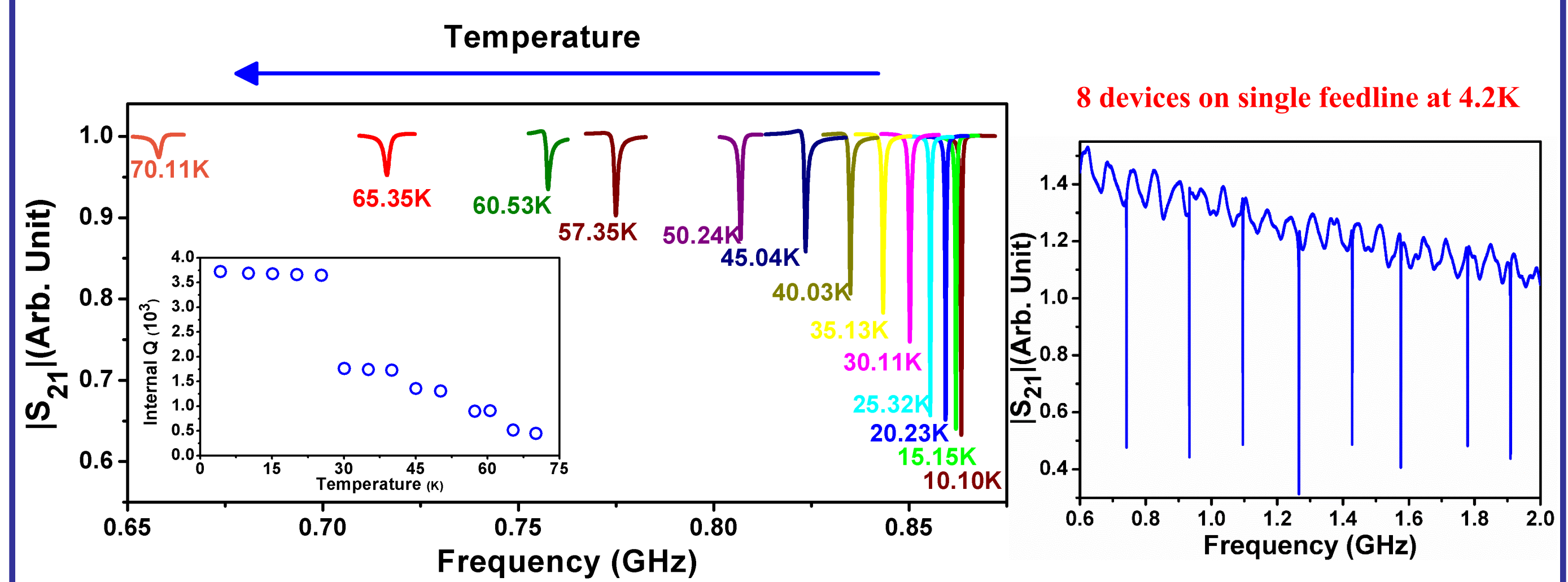


## YBCO KIB Design



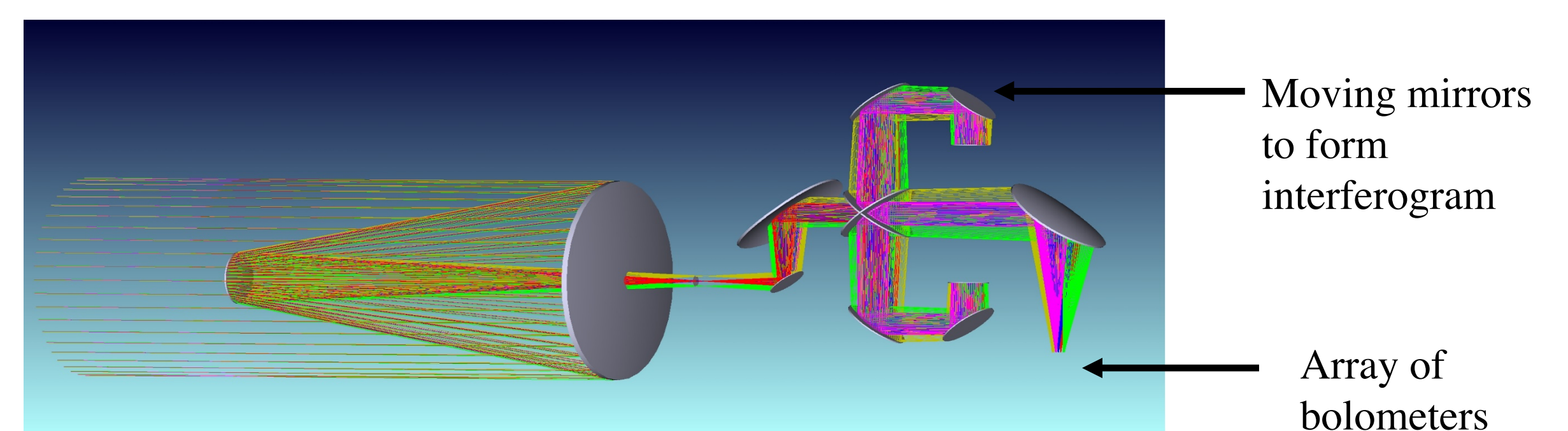
### Device performance

- Achieved working devices at target temperature of 55 K
- Will aim for higher Q at high temperatures
- Device redesign enabled significant progress.



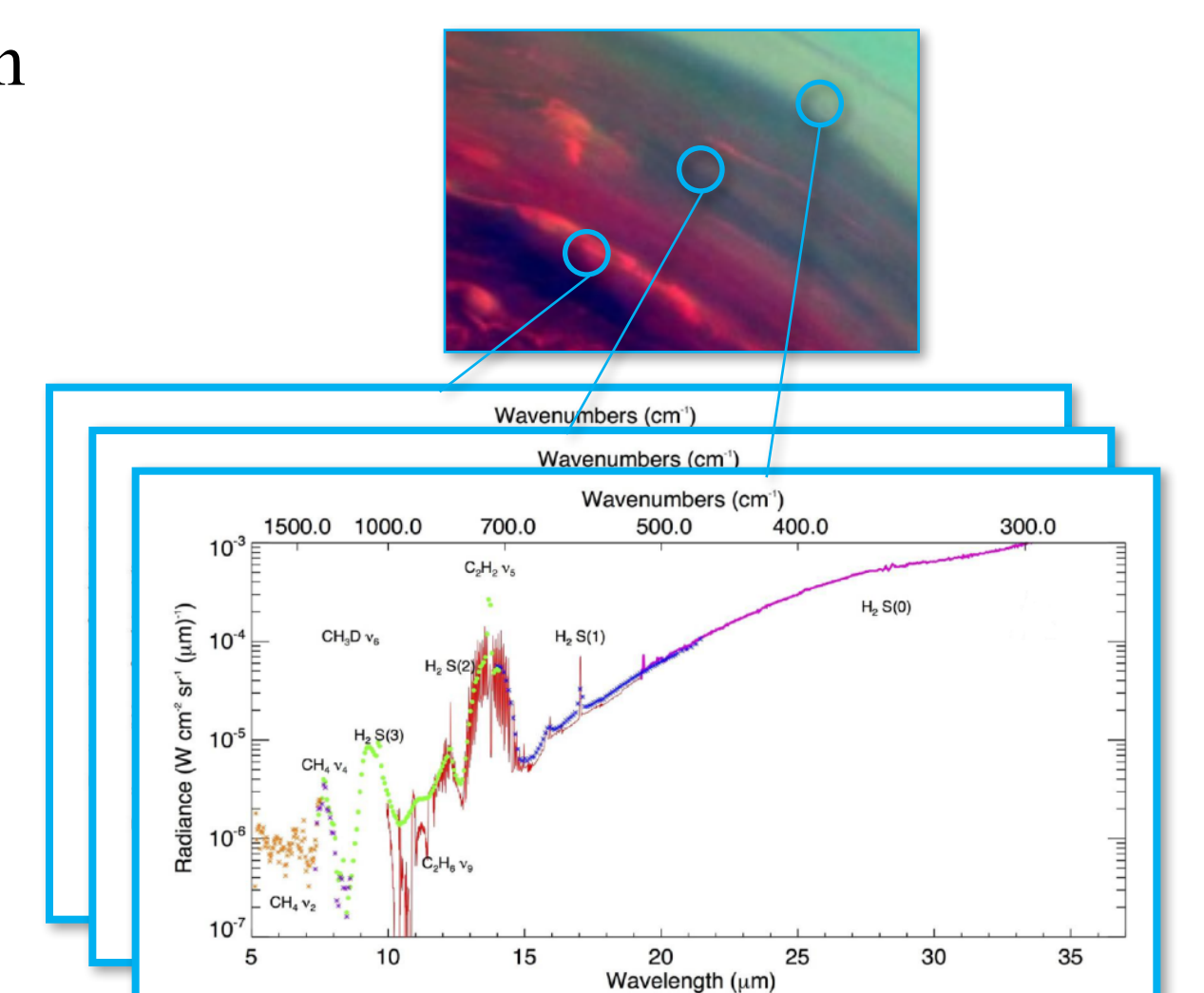
## Instrument Design

### Imaging Fourier Transform Infrared spectrometer



## Science Goals

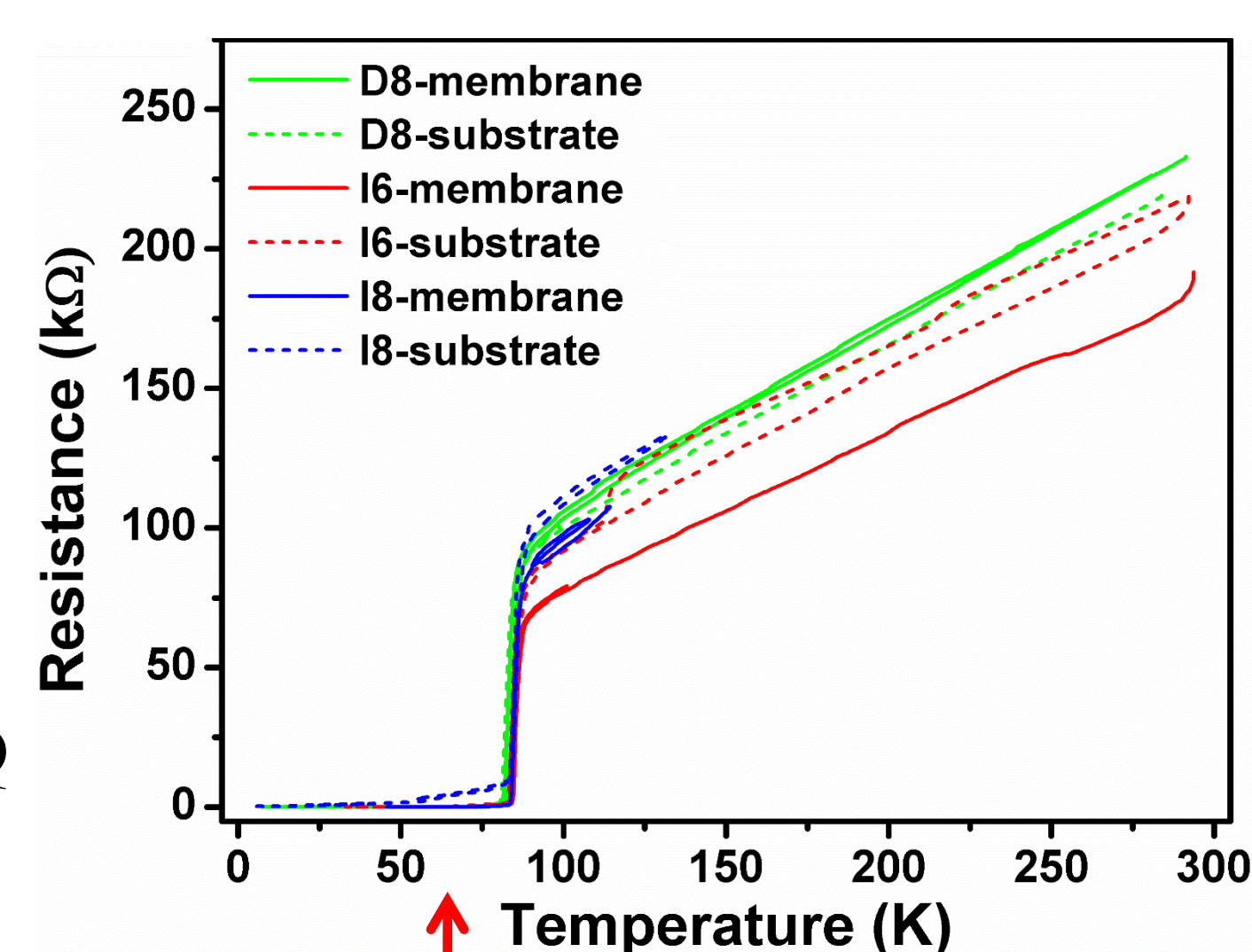
- Obtain high resolution spectra from each image pixel in minutes
- Gas giants
  - Dynamic phenomena
  - Atmospheric composition
  - Elemental Isotopic abundances
- Titan
  - Hydrocarbon cycle
  - Windows to surface
- Icy bodies
  - Thermophysical properties



## Why YBCO KIBs ?

### High performance, low cost

- Want to operate at 55 K for using passive cooler
- Proven cooling technology on Cassini VIMS instrument 1:
  - 55 K focal plane
  - Passively cooled by radiator
  - Optics cooled to 120 K
- Want to operate superconducting resonators well below Tc for high Q resonators
- Use high temperature superconductor YBCO (Yttrium barium copper oxide) with Tc of ~85K



operate at ~55 K

# In-situ liquid extraction and analysis platform for Mars and icy ocean worlds

F. Kehl (389K), D. Wu (389K), E. Tavares Da Costa (389K), M. F. Mora (389K), J. Creamer (389K), P. A. Willis (389K)

## ABSTRACT

Mars, Europa, Enceladus and Titan are the most auspicious worlds to search for signatures of past or present alien life in our Solar System. Here we present a compact, integrated sample extractor and analysis unit that could be used to support robotic missions seeking these chemical signatures of life. This wet chemistry instrument addresses habitability and the potential to preserve biosignatures by characterizing the local geochemical environment. In a first step, inorganic and putative organic compounds are automatically extracted from 1cm<sup>3</sup> of regolith or ice/soil mixtures by subcritical water extraction (SCWE) at 175 - 200°C and elevated pressures. Inline, miniaturized electrochemical probes quantify the eluate's pH, redox potential and electrical conductivity to better understand the ice or soil chemistry and mineralogy. Colorimetric measurements by flow injection analysis (FIA) in a fully integrated mesofluidic manifold furthermore allow additional assessment of the soil's ionic composition. Besides the evaluation of the potential for past or present biology, this system can be employed as a front-end instrument for subsequent, more sophisticated organic analyzers such as capillary electrophoresis (CE) or mass spectrometer (MS) units, to put these down-stream measurements in context.

## Subcritical Water Extractor

**WHY?** Subcritical water extraction (SCWE) uses liquid water as extractant at temperatures above the atmospheric boiling point of water (273 K, 0.1 MPa), but below the critical point of water (647 K, 22.1 MPa). At elevated temperatures, the permittivity, viscosity, ionization constant and surface tension of water are decreased, whereas its diffusion rate increases, making it a powerful solvent for both polar and non-polar compounds.

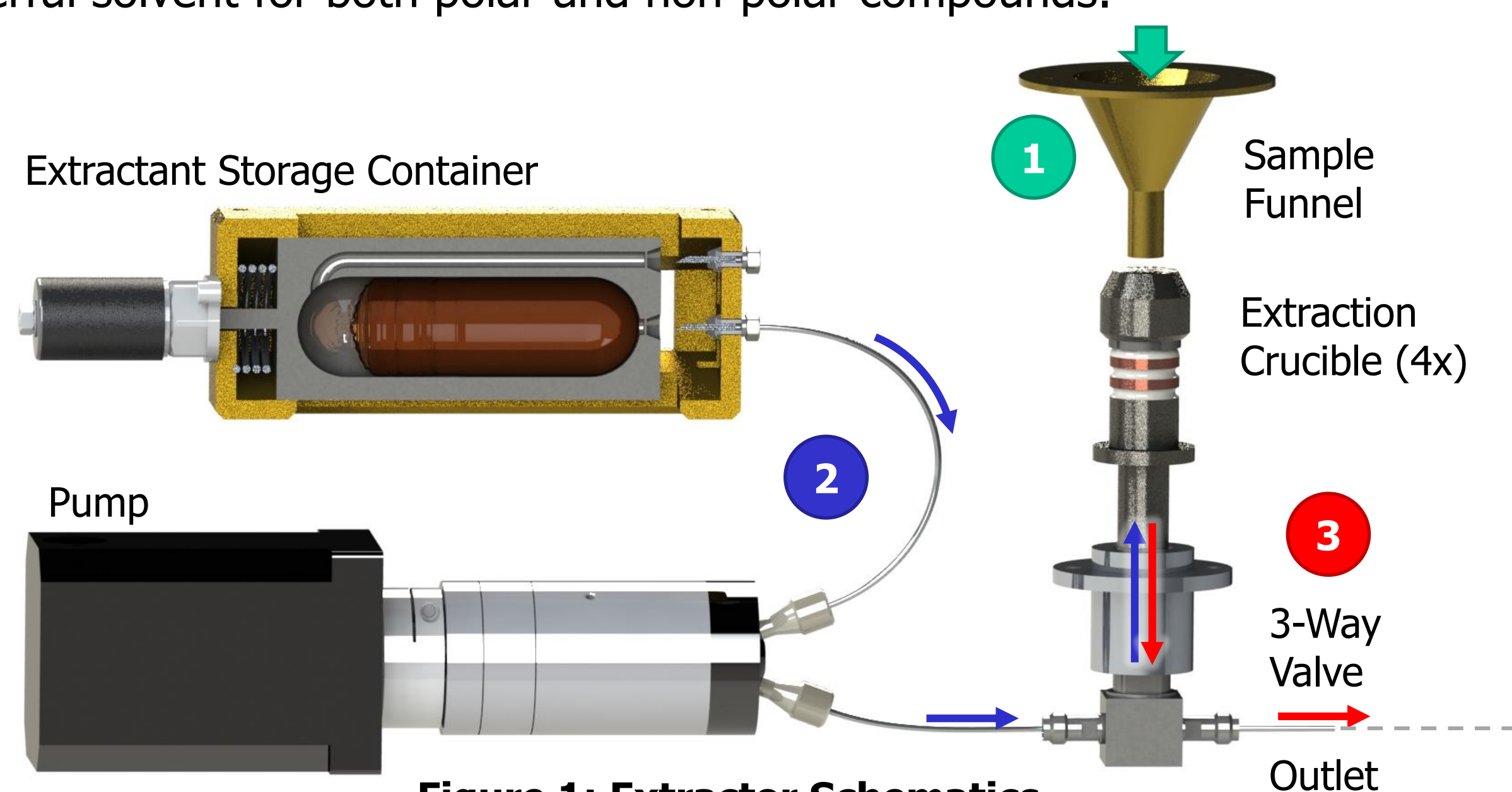


Figure 1: Extractor Schematics

**HOW?** Figure 1: The solids enter one of the four extraction crucibles through the sample funnel (1). Thereafter, the crucible is hermetically sealed by a linear motor and pre-pressurized with the extractant by a high pressure pump (2). Subsequently, the temperature of the crucible is increased to 200°C by an internal resistive heater, initiating the extraction of the compounds. The extraction is concluded by releasing the eluate via a 3-way valve (3).

**RESULTS:** The presented SCWE system (Figure 2) allows for four independent extractions. The crucibles are mounted on a rotary holder and automatically moved by a stepper motor to four positions: 1. sample loading, 2. crucible capping via linear motor, 3. liquid interface, 4. heater.

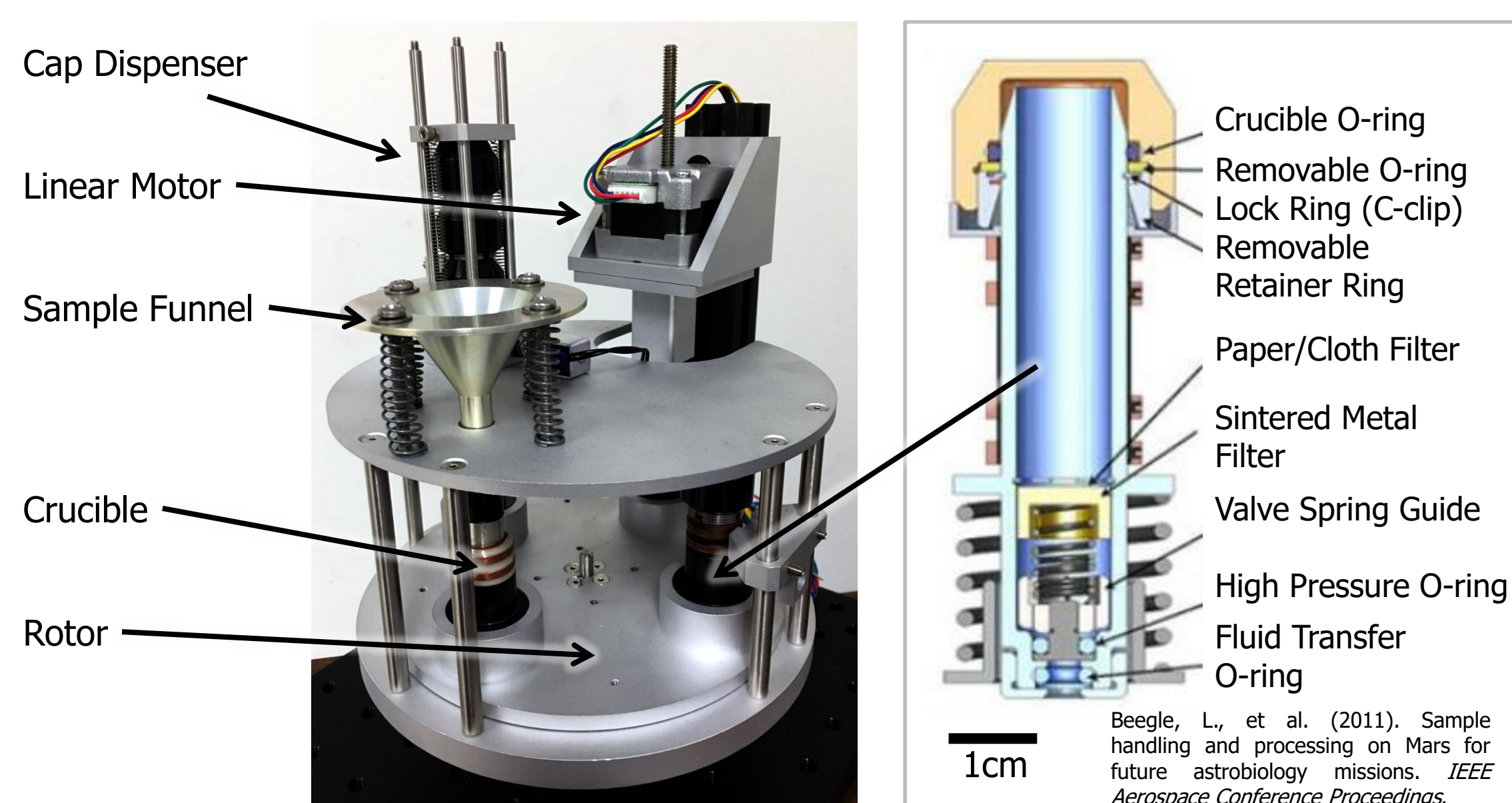


Figure 2: Realization of Automated SCWE System

## Flow Injection Analysis (FIA)

**WHY?** FIA is a technique where a liquid sample is injected into a moving carrier stream. The two liquids form a reaction plug, which is transported toward a detector that continuously measures changes in e.g. absorbance and electrode potential. FIA is a powerful but simple tool to measure ion concentrations, pH, ORP and electrical conductivity of a liquid sample.

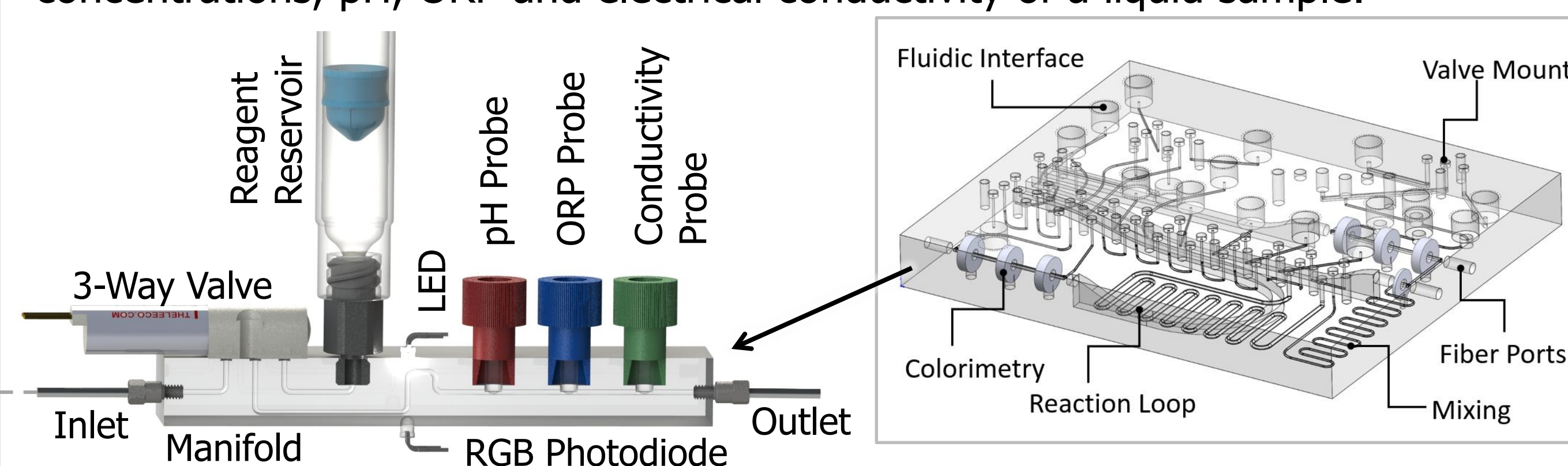


Figure 3: General FIA Concept. Inset: FIA Manifold

**HOW?** Figure 3: The liquid sample enters the FIA manifold and is routed via various 3-way valves. A liquid plug of reagent is injected into the carrier stream by switching one of the 3-way valves, accessing the reagent reservoir. The sample and reagent mix and react, leading to an absorbance change depending on the reagent and the concentration of the analyte of interest in the sample. These colorimetric changes and therefore the analyte concentration can be determined by a RGB LED and photodiode. Custom-made, miniaturized electrochemical sensors additionally measure pH, Oxidation Reduction Potential (ORP), temperature and electrical conductivity of the liquid sample.

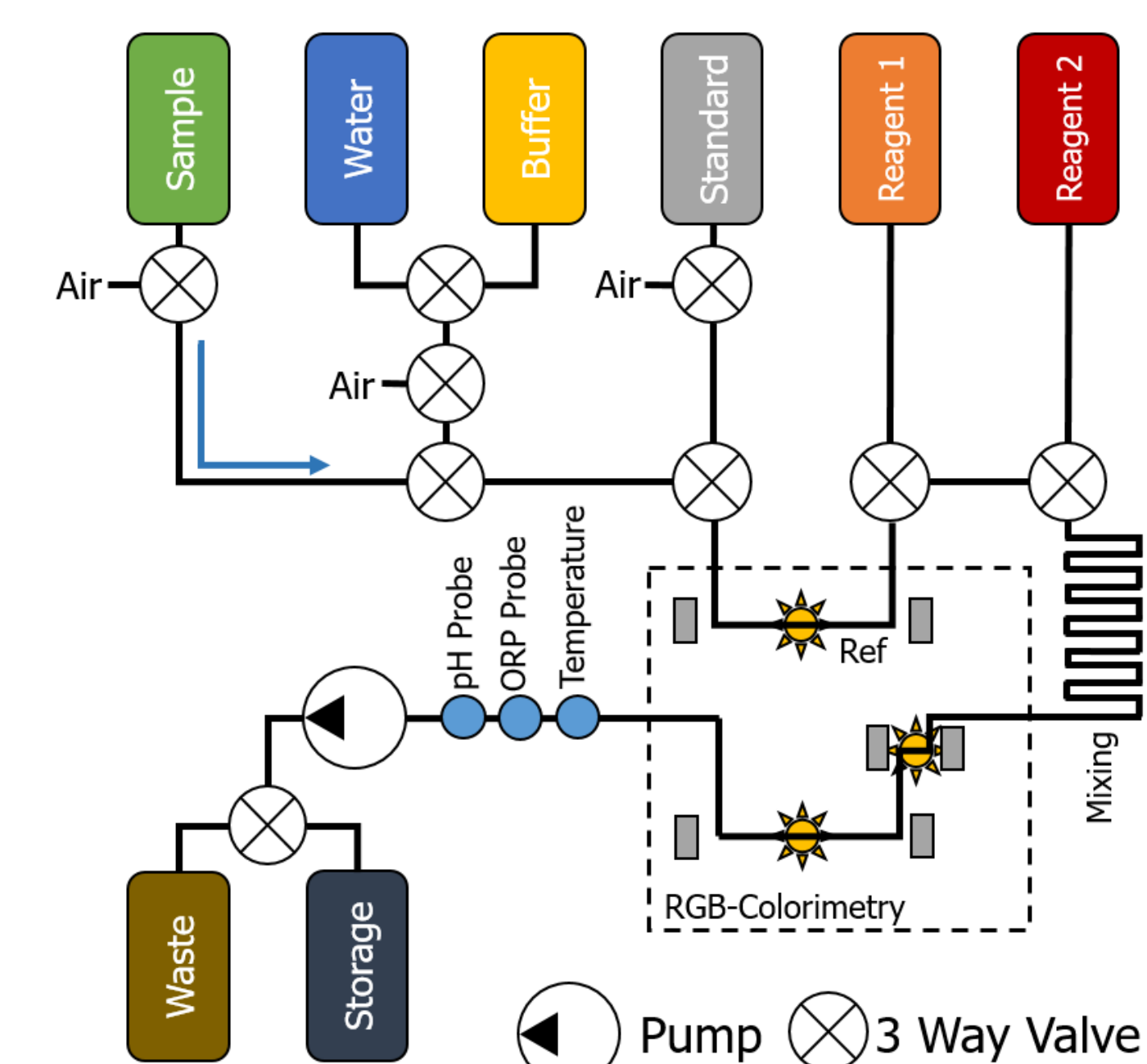


Figure 4: FIA Schematics

**RESULTS:** The presented, fully automated FIA system (Figure 5) allows to quantify up to six different analytes (such as, but not limited to, Mg<sup>2+</sup>, PO<sub>4</sub><sup>3-</sup>, Cu<sup>2+</sup>, NH<sub>3</sub>-N, H<sup>+</sup>, Formaldehyde) by colorimetry and pH and ORP by electrochemical sensors.

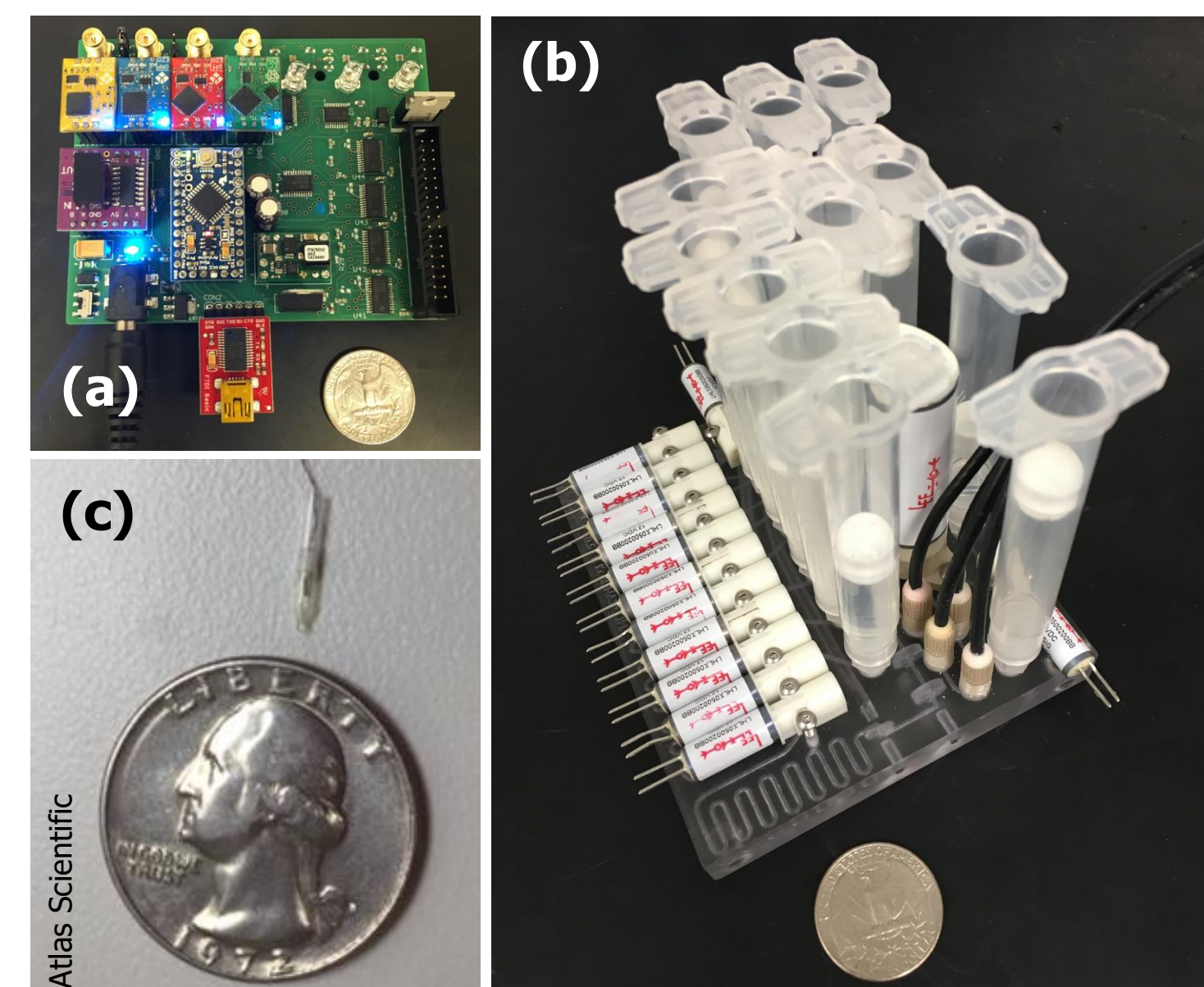


Figure 5: (a) FIA Electronics, (b) FIA System, (c) Miniature pH Half-Cell

**OUTLOOK** After the engineering effort and successful technology demonstration, extended measurement campaigns are planned to evaluate both efficiency of the extractor as well as limit of detection of the FIA system. In the near future, the two system will be combined for an end-to-end analysis of Mars analogue samples. In 2017, a fully-integrated version will be installed on the K-Rex Rover (NASA Ames) for in-situ measurements in the Atacama Desert (Chile).



# Improving Chiral Resolution of Amino Acid Biomarkers by Capillary Electrophoresis with Laser Induced Fluorescence Detection

Jessica S. Creamer (389K)

Maria F. Mora (389K) and Peter A. Willis (389K)

## Objective

To develop a capillary electrophoresis method capable of measuring the chiral distribution of low levels (parts per billion) of amino acids in soil, water, or ice samples

## Background

- The search for life in our Solar System is one of the highest priorities at NASA
- Amino acids are both necessary building blocks of life and ubiquitous byproducts of abiotic reactions

- To distinguish biotic amino acids from those produced abiotically it is possible to look at three distinct biosignatures

### 1) Which amino acids are present

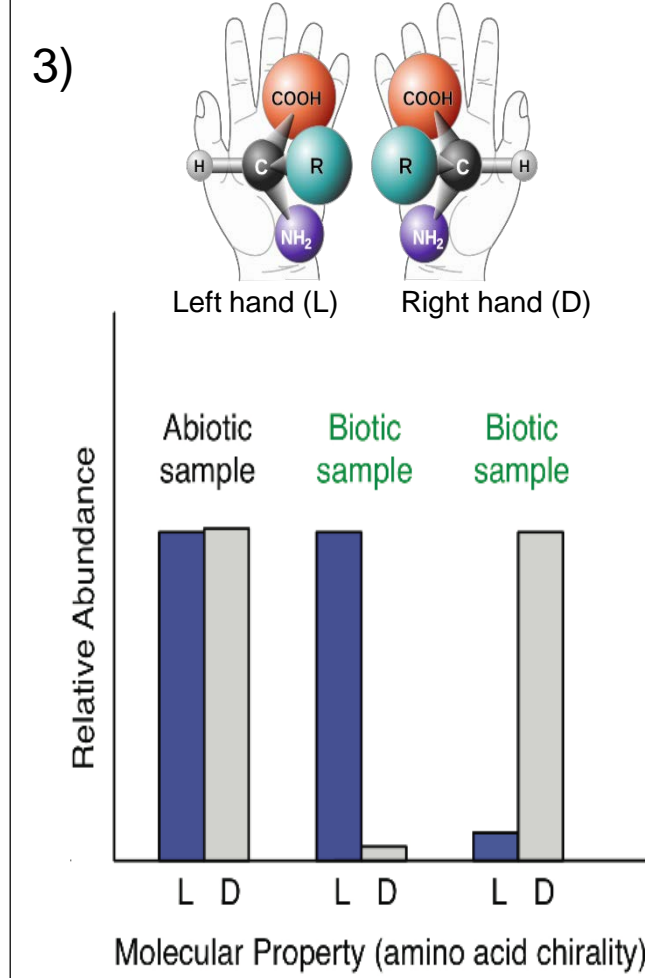
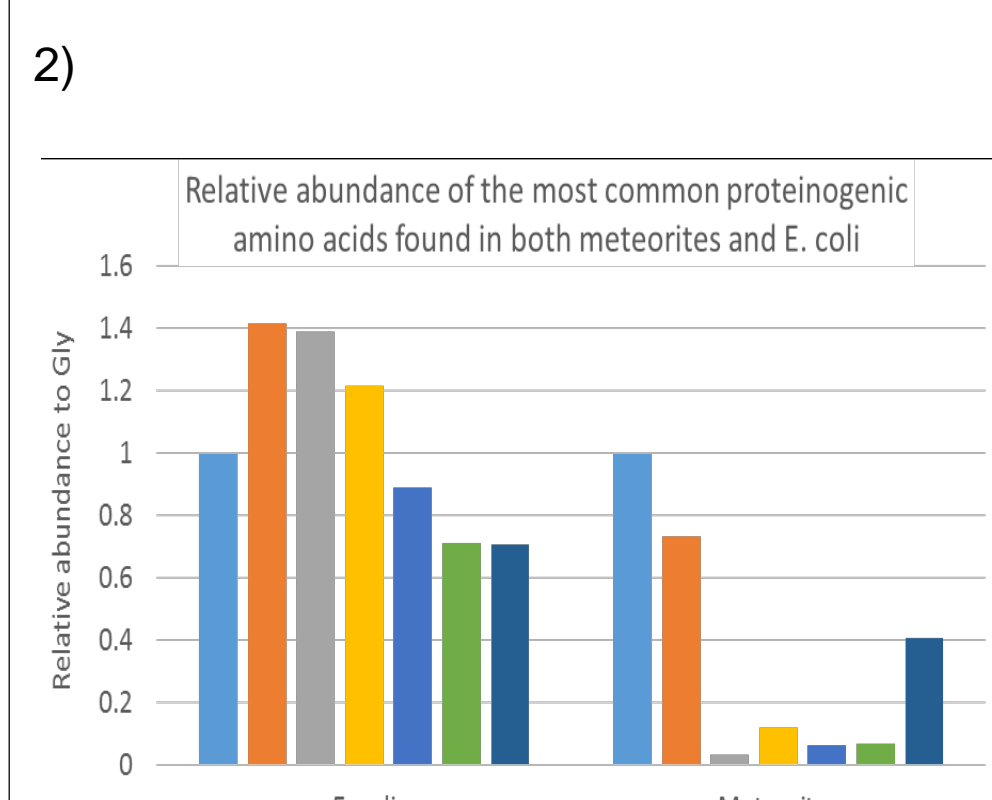
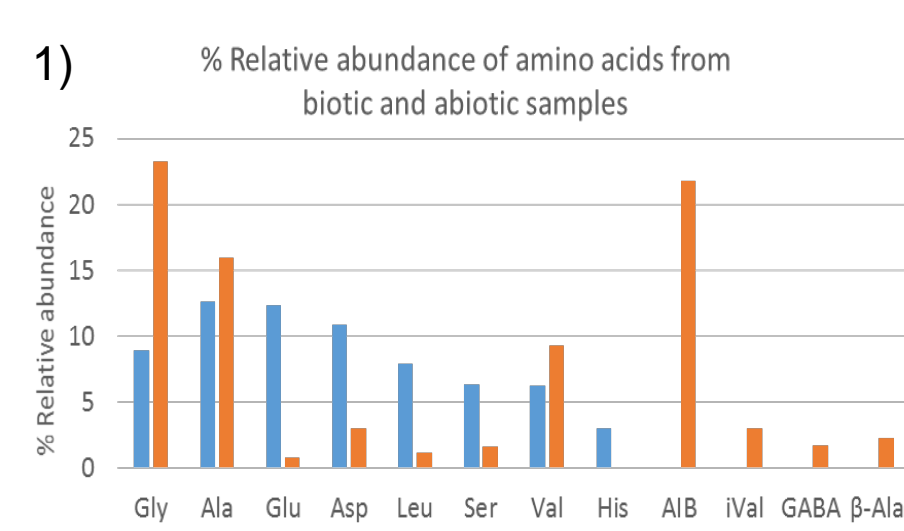
Do they correspond with the abiotic, biotic, or proteinogenic classifications found here on Earth?

### 2) The relative abundance of those amino acids to glycine

Biotic samples contain higher abundances of the larger molecular weight amino acids

### 3) The presence of a chiral excess

Chiral molecules are non-superimposable mirror images, like your hands. Abiotic amino acids are generated as a 50:50 mixture of both left- and right-handed mirror images while life on Earth uses only the left-handed amino acids to create proteins

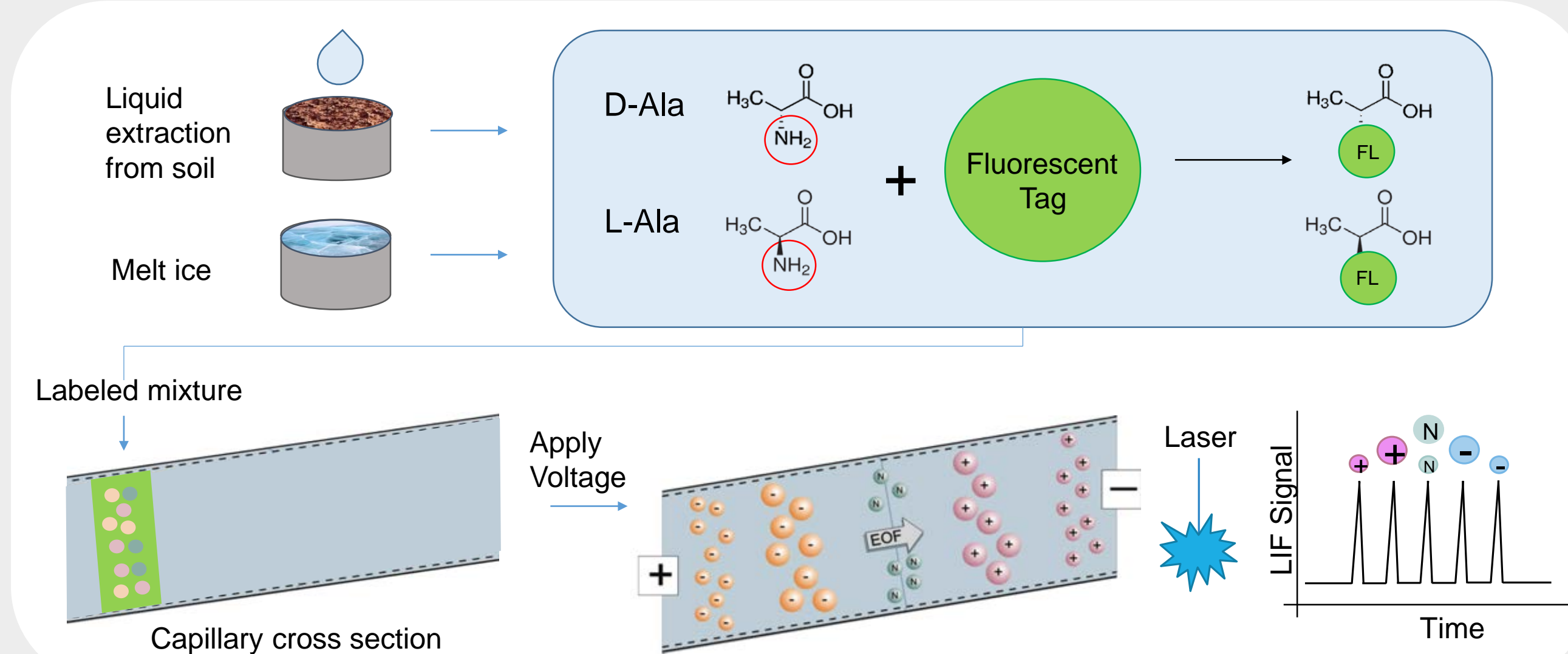


- We have identified the 17 amino acids found in the highest abundances in both abiotic and biotic samples
  - 7 chiral pairs (left- and right-handed species) – Ala, Asp, Glu, His, Leu, Ser, and Val
  - 3 achiral amino acids – Gly,  $\beta$ -Ala, and GABA
- Method development focused on the simultaneous separation and high sensitivity detection of mixtures containing these 17 species

## Methods

Capillary electrophoresis (CE) with laser induced fluorescence detection (LIF) allows for high sensitive analysis of polar organics in the aqueous phase

- Liquid extraction is used to liberate amino acids from samples
- Amino acids are labeled with fluorescent tag for high-sensitivity LIF detection
- Labeled sample is delivered directly to the capillary where voltage is applied
- Analytes are separated in CE based on their mobility ( $\mu$ ) which is proportional to their mass-to-charge ratio
- At the end of the capillary a laser excites the fluorescent tag and the data is collected as a signal vs time plot



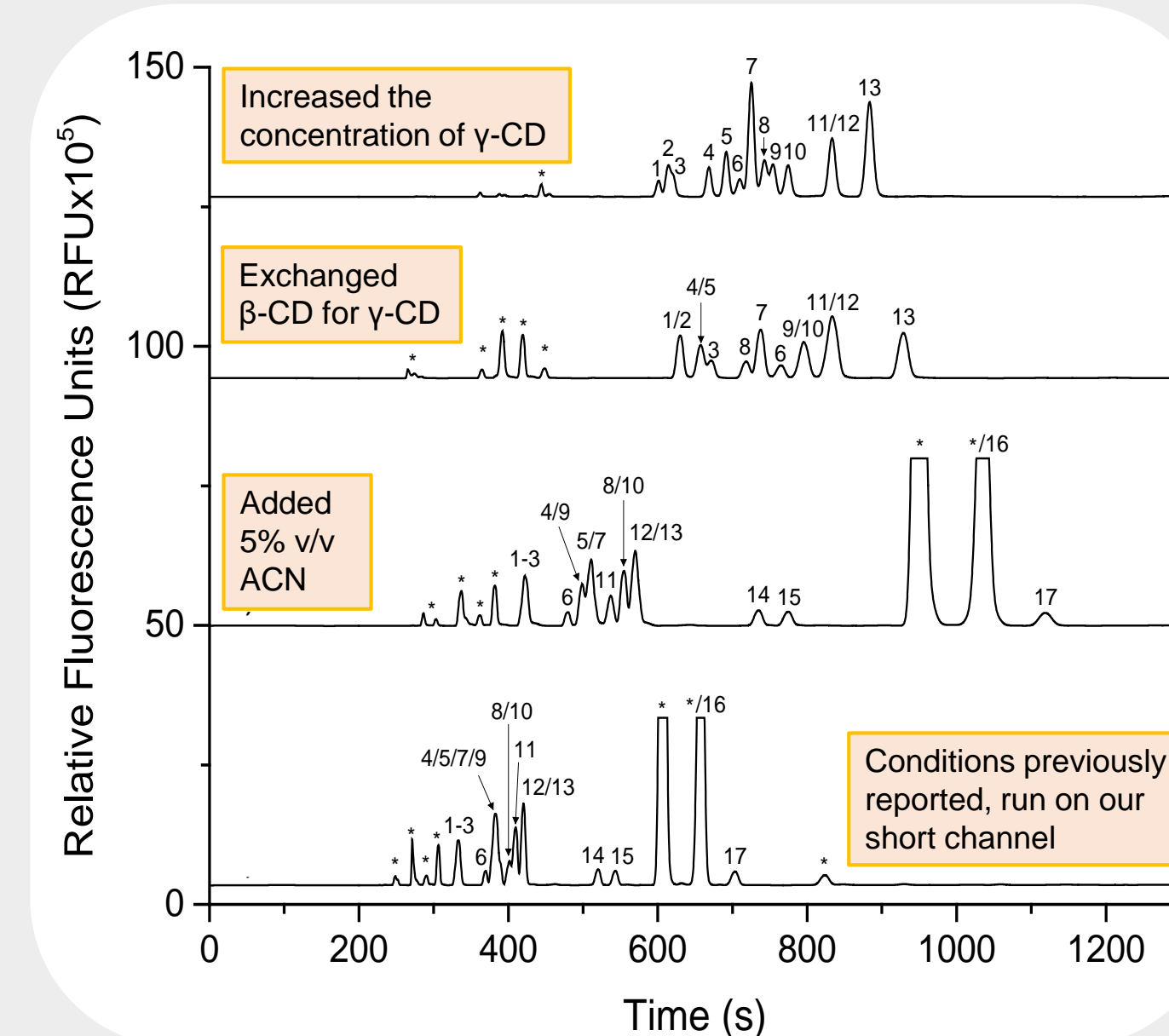
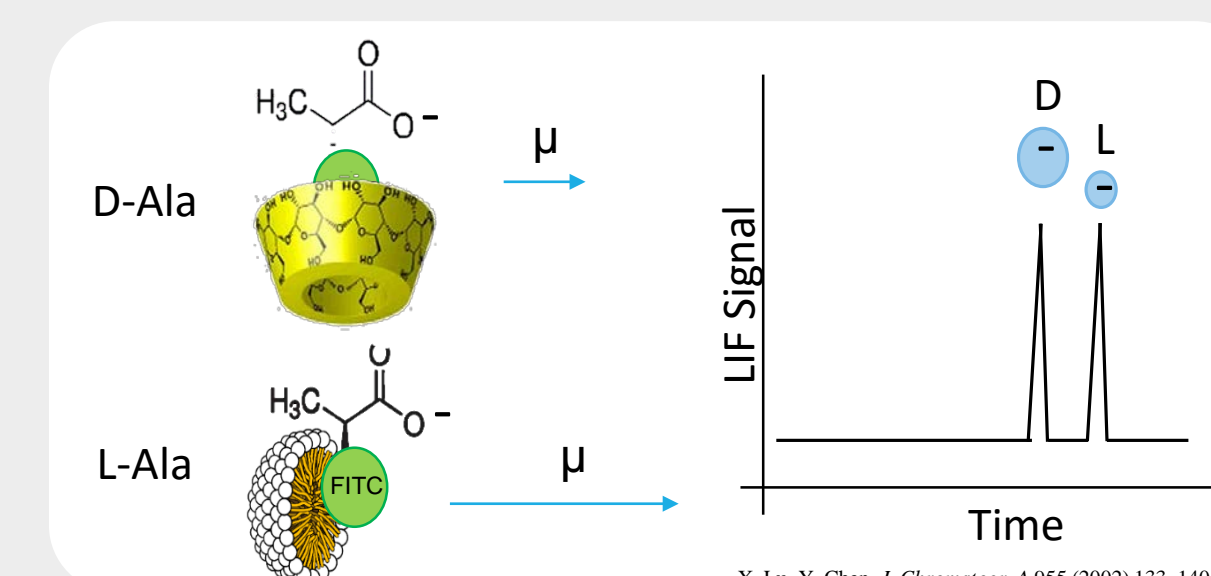
## The Challenge

The separation of these species on a short channel is difficult because they have very similar electrophoretic mobilities ( $\mu$ ), particularly after derivatization with a large fluorescent tag

## Results

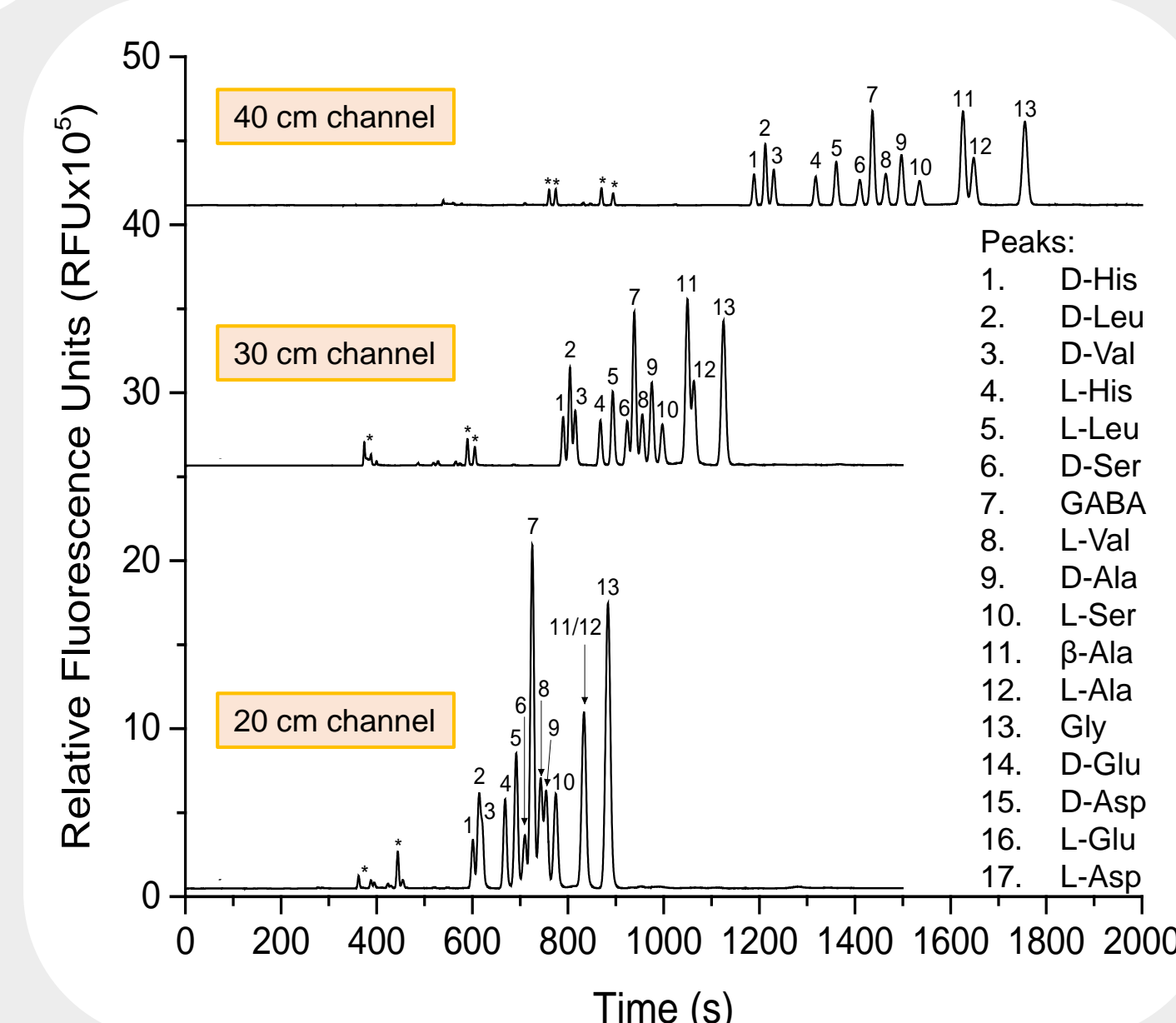
Previous work by Lu et al. determined a cooperative effect between chiral selectors  $\beta$ -cyclodextrin ( $\beta$ -CD) and sodium taurocholate (STC) for individual chiral pairs

- $\beta$ -CD - Interaction with D-amino acids
- STC - Interaction with L-amino acids



- Further optimization was needed to be able to resolve several chiral pairs simultaneously
- Acetonitrile was added to slow the EOF and allow the amino acids extra time in the capillary
- $\beta$ -CD was exchanged for  $\gamma$ -CD which has a larger cavity that better accommodates the large fluorescent tag

- Finally, the constraint of the 20 cm capillary was chosen because of the design of the current portable system
- By increasing the capillary length we see greatly improved resolution between the neutral amino acids
- As we move forward we will need to consider redesigning the system for the next prototype to allow for a longer channel



## Conclusions

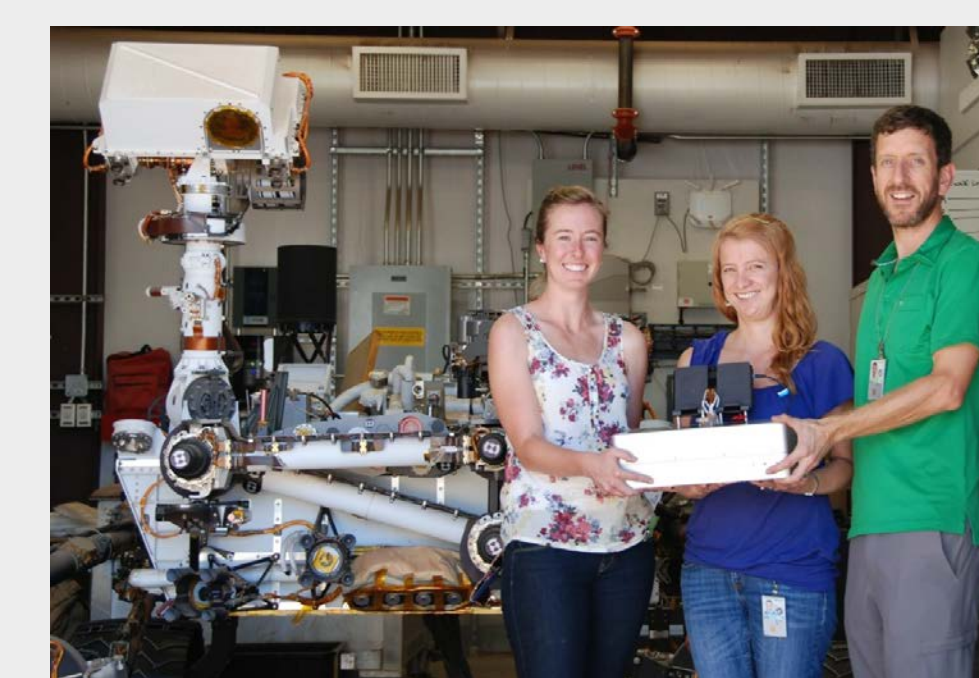
- On a short channel it was possible to partially resolve the 13 neutral amino acids
- By increasing the channel length to 40 cm all 13 neutral species were fully resolved, this change in channel length will inform the design of the next portable system prototype developed in our lab
- This improves upon our previous work in which 5 enantiomer pairs were resolved using two methods

## Future directions

- Create a second method for analysis of acidic amino acids
- In-lab analysis of Europa and Mars analog samples
- Transfer the method to the Chemical Laptop, a portable instrument developed by the Willis group that houses the electronics and optics needed to perform sample handling and analysis

## Acknowledgements

- The Peter Willis Group
- The NASA-PICASSO Program funding for the "Microfluidic Life Analyzer" project
- The NASA Postdoctoral Program
- This work was carried out at the Jet Propulsion Laboratory, California Institute of Technology, under contract with NASA.



# Science Standardised Embedded Data infrastructure for Drones (SSEDD)

Jane Wyngaard (398M)

Lindsay Barbieri (University of Vermont doctoral candidate)

## Context

In response to a growing interest in the use of low cost small unmanned aerial systems (sUAS) in the sciences, the authors formed an Earth Science Information Partners Federation (ESIP) Drones Cluster in 2015. The purpose of such being to work towards overcoming some of the immediate barriers to such and to seek community use of relevant good data stewardship practices given the domain's nascent state..

While there are currently various challenges around using sUAS for science, the existing and anticipated advantages mean that the domain is swelling with innovation and sUAS are expected to become a standard piece of field equipment for scientist within the near future. As "an open, networked community that brings together science, data and information technology practitioners" ESIP is an ideal forum from within which to address some of these challenges. The work presented here is one component of the cluster's initial work regarding such. (See our Open Science Frameworks page for other activities: <https://osf.io/nuvem/>)

## Conclusions and Future Work

This short test campaign provided too little data to draw definitive conclusions as regards the scientific value and potential of sUAS based GHG monitoring. However, results were sufficiently promising to see further testing scheduled for later this year. Similarly, ESIP Testbed funding has been awarded to see further development and tests of SSEDD on a hexacopter operating a range of additional sensors. This funding will also enable migration from ROS to ROS2 and mavlink to Mavlink2, and see the release of a first beta version for public review and use.

A secondary outcome to this work includes a discussion paper to be presented at SciDataCon (Q4 2016). As noted there are a number of challenges that remain before sUAS will be ubiquitous in the sciences, or before their data value is fully realised. This paper discusses such and offers a strawman for community discussion regarding adopting common standard protocols and guidelines so as to achieve maximal value by ensuring sUAS data provenance, interoperability, and discoverability.

## SSEDD Design:

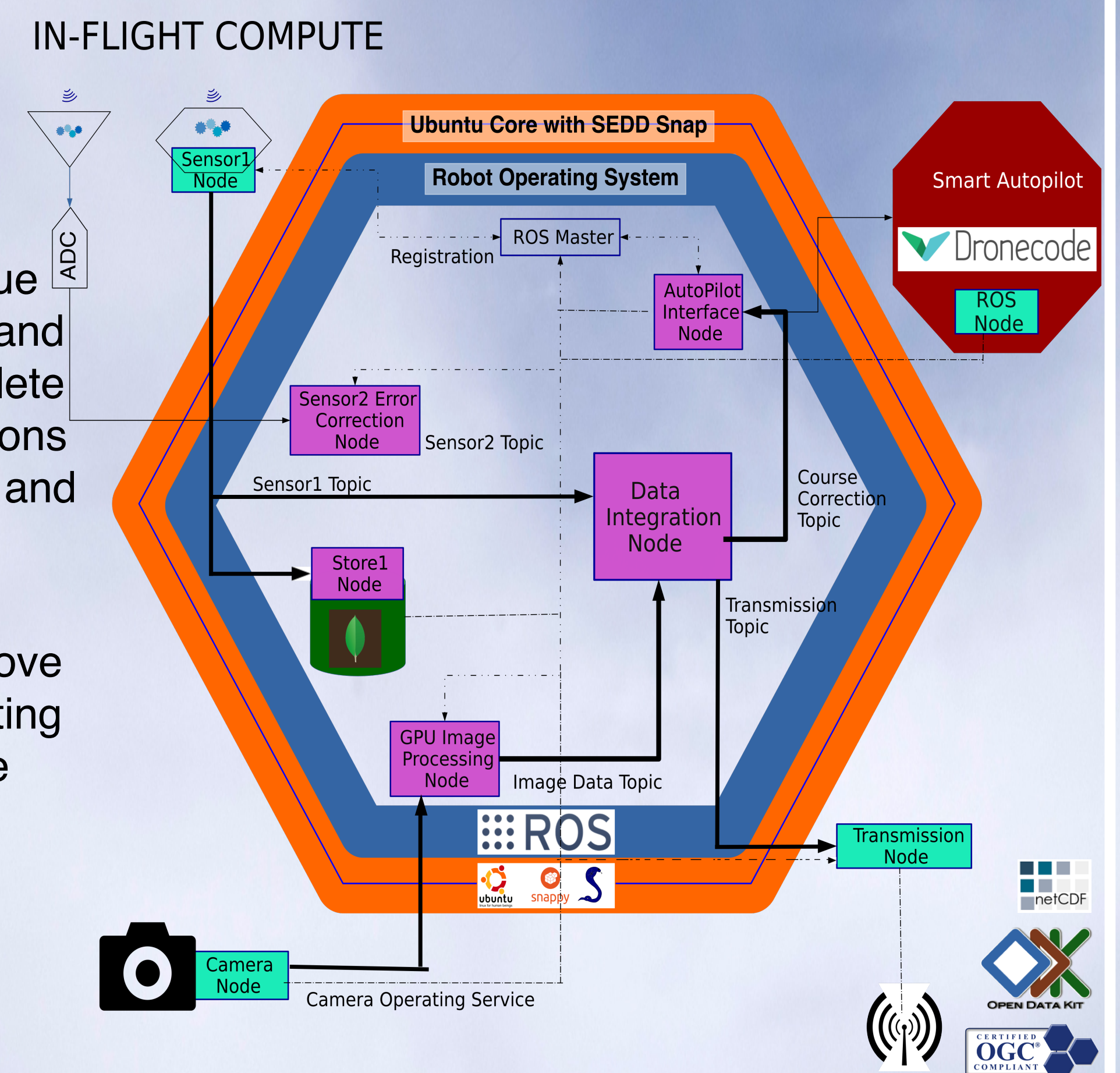
For multiple reasons there is a notable need for a flexible, complete, science capable, sUAS ecosystem such as is currently unavailable. While the hobbyist sUAS community have successfully build a mature and sophisticated sUAS stack, including multiple autopilots, communication protocols, component and system simulators, sensor integrations, and ground stations (many of which involve both hardware and software), there remains an missing enabler as regards carrying out scientific data capture missions. SSEDD is intended to be this enabler, utilising these existing open mature projects so as to:

- (1) Make small scale low cost sUAS more readily accessible to Earth Scientists by automating and generalising many of the 'engineering' stages required for flexible innovative experimental work.
- (2) Lower the learning curve required to use sUAS by offering platform and system independence alongside qualified systems.

- (3) Provide a degree of data qualification and procedure automation.

- (4) Provide an alternative to commercial offerings that prevents the loss of data value through proprietary formats and contracts and ensures complete freedom of scientific innovations by providing largely platform and sensor agnostics tools.

SSEDD accomplishes the above goals by utilising multiple existing mature open source tools (see representative diagram) that enable sophisticated sUAS operation and standards adherence, while still offering platform independence.



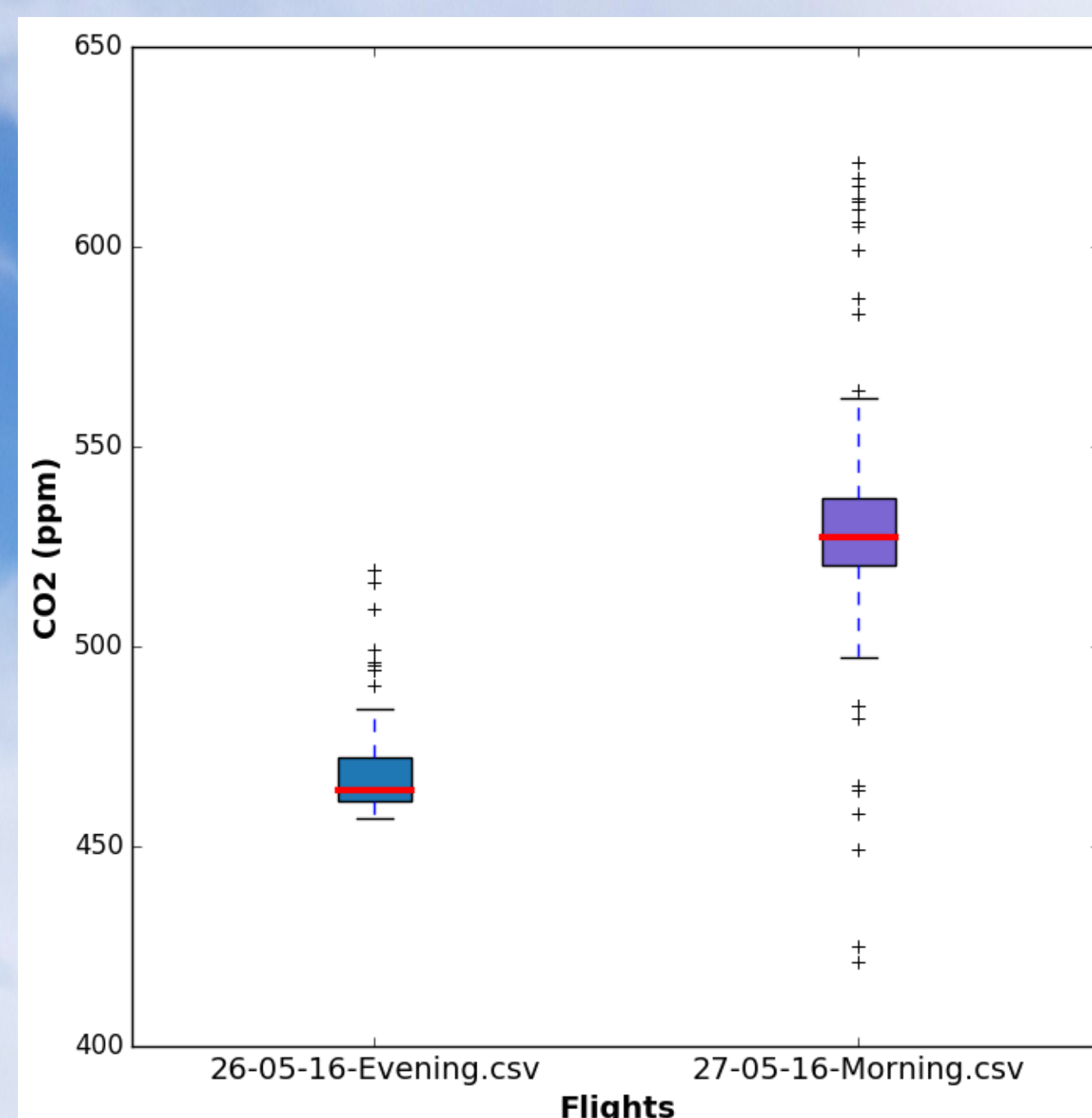
## Test Campaign1

Using Funding awarded at ESIP *FundingFriday* 2015 a low cost off-the-shelf (OTS) yet 90% open source sUAS was purchased to explore the design space and functionality of SSEDD thus far. As a coincidentally created hypothesis, the target use case for testing was to explore the viability of enabling efficient agricultural green house gas (GHG) emissions monitoring for the purposes of mitigation measure assessment, using a low cost sUAS.

- Preliminary results shown alongside provide highlights:
- Sensor and profile flights were sensitive enough to detect distinct concentration differences at different time of the day.
  - Data capture took 1/10th of the time of science user's current practice (ground based field testing)
  - All data processing was carried out using fully open source tools including: OpenDroneMap (for generating (3D mesh and geotagged orthomosaics) MeshLab (for visualising mesh), and QGIS (for survey map and overlays)
- (For detailed results see the report available on <https://osf.io/nuvem/>)



**NIR 3D field model (above):** Near Infrared (NIR) 3D model



**Box plot (above):** Comparison of CO2 concentration densities over 2 vertical profile flights undertaken at approximately 5pm and 9am on consecutive days. Notable is the jump in concentrations in the morning, indicative of what is to be expected given overnight CO2 pooling.

- 1 week
- 6 flights
- 3 crashes

- 1 OTS quadcopter
- 3 Instruments
- 5 repairs

**Iris+** (opposite): Low cost Iris+ (~\$1600 from 3DRobotics) carrying Raspberry Pi2 (\$45) and K30 1% CO2meter (\$85 from CO2meter)



**Drone Balloon (behind):** Kristian Brevik monitoring a gas sample cable during a vertical profile test involving both ground based and drone mounted CO2meters. Site: Burlington Vermont, 21/05/16.

**NIR orthomosaic composite (above):** Orthomosaic (captured with hacked Canon S100, \$100) overlaid on Google maps base layer. Geotagged CO2 values are overlaid on top. Increasing intensity of blue indicates higher value bins (~420-650ppm) approximately correlating with lower altitudes (5-10m)